Water management practices and anthropogenic carbon sources alter the patterns of CH_4 and CO_2 emissions from inland waters

Zeyad Alshboul

Accepted Dissertation thesis for the partial fulfillment of the requirements for a

Doctor of Natural Sciences

Fachbereich 7: Natur- und Umweltwissenschaften

Universität Koblenz-Landau

Thesis examiners:

Prof. Dr. Andreas Lorke, University of Koblenz-Landau

Prof. Dr. Hermann Jungkunst, University of Koblenz-Landau

Date of the oral examination: [23 March 2016]

Declaration

I herewith declare that I independently carried out the PhD dissertation entitled "Water management practices and anthropogenic carbon sources alter the patterns of CH_4 and CO_2 emissions from inland water systems". I certify that this work contains no material which has been used for the award of any other degree under my name, in any university or other tertiary institution, except where due reference has been made in the text. I certify that no part of this work will be used in future in a submission under my name for any other degree in any other territory or institution without prior approval of the University of Koblenz-Landau and where applicable, any other Partner institution responsible for the joint-award of this degree. All assistance from others has been declared and the contributions of those involved are clearly indicated.

This work is based on the following manuscripts:

1- **Alshboul, Z.**, and A. Lorke. 2015. Carbon Dioxide Emissions from Reservoirs in the Lower Jordan Watershed. PLoS One 10: e0143381. (Published in **Plos One**)

2- **Alshboul, Zeyad**, Fernández, Jorge, Hofmann, Hilmar, Lorke, Andreas, Export of dissolved methane and carbon dioxide with effluents from municipal wastewater treatment plants, Environmental science and technology, 2015. (under review in **Environmental Science and Technology**)

3- **Alshboul, Zeyad**, Celia Somlai-Haase, Christoph Bors, Andreas Lorke, Simple approaches to measure the diffusive flux of carbon dioxide and the rate of bubble release in shallow aquatic systems, Limnology and Oceanography, 2015. (submitted to **Limnology and Oceanography-Methods**)

4- Jeremy Wilkinson, Andreas Maeck, **Zeyad Alshboul**, and Andreas Lorke, Continuous seasonal river ebullition measurements linked to sediment methane formation, *Environmental Science & Technology*, DOI: 10.1021/acs.est.5b01525. (published in **Environmental Science and Technology**)

Landau, 11 April 2016 Zeyad Alshboul ……...

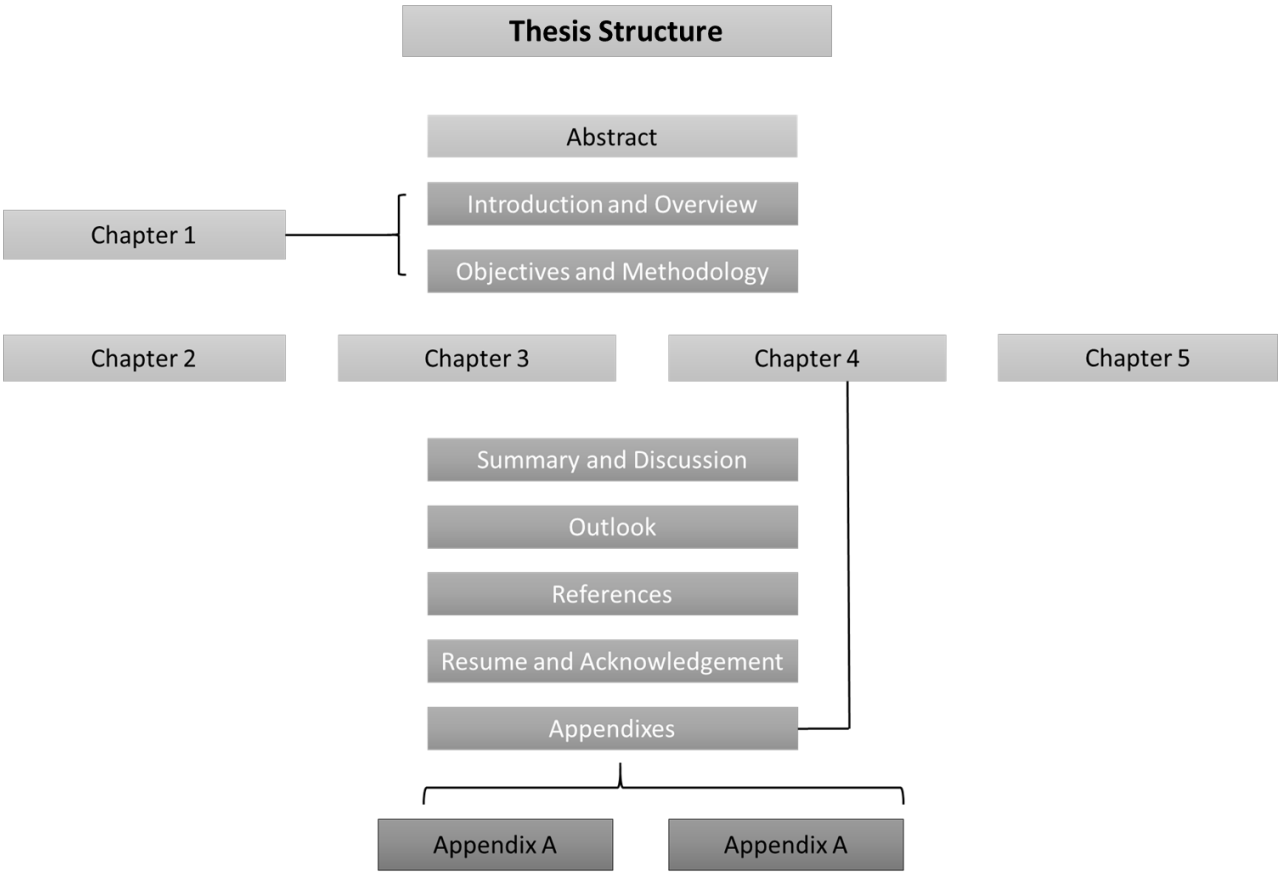
Thesis Structure
Abstract
Introduction and Overview
Chapter 1
Objectives and Methodology
Chapter 2
Chapter 3
Chapter 4
Chapter 5
Summary and Discussion
Outlook
References
Resume and Acknowledgement
Appendixes
Appendix A
Appendix A

Abstract (English)

Recent estimates have confirmed that inland waters emit a considerable amount of CH_4 and CO_2 to the atmosphere at the regional and global scale. But these estimates are based on extrapolated measured data and lack of data from inland waters in arid and semi-arid regions and carbon sources from wastewater treatment plants (WWTPs) as well insufficient resolution of the spatiotemporal variability of these emissions. Through this study, we analyzed monthly hydrological, meteorological and water quality data from three irrigation and drinking water reservoirs in the lower Jordan River basin and estimated the atmospheric emission rates of CO_2. We investigated the effect of WWTPs on surrounding aquatic systems in term of CH_4 and CO_2 emission by presenting seasonally resolved data for dissolved concentrations of both gases in the effluents and in the receiving streams at nine WWTPs in Germany. We investigated spatiotemporal variability of CH_4 and CO_2 emission from aquatic ecosystems by using of simple low-cost tools for measuring CO_2 flux and bubble release rate from freshwater systems. Our estimates showed that reservoirs in semi-arid regions are oversaturated with CO_2 and acted as net sources to the atmosphere. The magnitude of observed fluxes at the three water reservoirs in Jordan is comparable to those from tropical reservoirs (3.3 g CO_2 m^{-2} d^{-1}). The CO_2 emission rate from these reservoirs is linked to changes of water surface area, which is the result of water management practices. WWTPs have been shown to discharge a considerable amount of CH_4 (30.9±40.7 kg yr^{-1}) and CO_2 (0.06±0.05 Gg yr^{-1}) to their surrounding streams, and emission rates of CH_4 and CO_2 from these streams are significantly enhanced by effluents of WWTPs up to 1.2 and 8.6 times, respectively. Our results showed that both diffusive flux and bubble release rate varied in time and space, and both of emission pathways should be included and variability

should be resolved adequately in further sampling and measuring strategies. We conclude that future emission measurements and estimates from inland waters may consider water management practices, carbon sources from WWTPs as well spatial and temporal variability of emission.

Abstract (German)

Aktuelle Schätzungen bestätigten, dass Binnengewässer eine erhebliche Menge Methan (CH_4) und Kohlendioxid (CO_2) sowohl auf regionaler Ebene, als auch global freisetzen. Jedoch basieren diese Schätzungen auf extrapolierten gemessenen Daten, ungenügender Auflösung der räumlich-zeitlichen Variabilität und es mangelt an Daten aus ariden und semi-ariden Gebieten, sowie den Kohlestoffquellen aus Kläranlagen.

Für die hier vorliegende Studie analysierten wir monatliche hydrologische und meteorologische Daten sowie Daten zur Wasserqualität von drei Stauseen aus dem Gebiet des unteren Jordans, die zur Trinkwassergewinnung und zur Bewässerung genutzt werden, und schätzten damit deren Emissionsrate an CO_2 ab. Wir untersuchten den Effekt von Kläranlagen auf die umliegenden Gewässer im Hinblick auf CH_4 und CO_2-Emissionen indem wir saisonal aufgelöste Daten der Konzentration der beiden gelösten Gase in Kläranlagenauslässen und in Vorflutern von neun Kläranlagen in Deutschland analysierten. Mithilfe von Low-Cost-Methoden die die CO_2-Transportrate und die Ausgasungsrate über Gasblasen messen, untersuchten wir die räumliche und zeitliche Variabilität der CH_4 und CO_2-Emissionen von aquatischen Süßwasser-Ökosystemen.

Unsere Schätzungen zeigen, dass Stauseen in semi-ariden Regionen CO_2 übersättigt sind und somit CO_2 an die Atmosphäre abgeben, also eine Netto-Quelle sind. Die Größenordnung der beobachteten Transportraten der drei jordanischen Stauseen ist vergleichbar mit denen von tropischen Stauseen (3,3 g CO_2 m^{-2} Tag^{-1}). Die CO_2-Emissionsrate ist abhängig von Änderungen der Wasseroberfläche, welche durch den Betrieb der Stauseen verursacht sind. Kläranlagen entlassen eine beachtlichen Menge an CH_4 (30.9±40.7 kg $Jahr^{-1}$) und CO_2 (0.06±0.05 Gg $Jahr^{-1}$)

in ihre umgebenden Flüsse und Bäche. Deren Emissionsraten sind durch diese Einleitung der Kläranlagen um 1,2-fach für CH_4 oder 8,6-fach für CO_2 erhöht. Unsere Ergebnisse zeigen, dass sowohl die diffusive als auch die Gasblasenemissionsrate räumlich und zeitlich variabel ist, weshalb beide Emissionsraten bei zukünftigen Studien auch in der nötigen Auflösung gemessen werden sollten.

Wir schlussfolgern, dass bei zukünftigen Emissionsmessungen und –schätzungen von Binnengewässern auch die Gewässerbewirtschaftung, die Kohlenstoffquelle von Kläranlagen und die räumliche und zeitliche Variabilität der Emissionen beachtet werden sollten.

Table of Contents

Chapter 1: General Introduction

1.1. Overview

The presence of greenhouse gases (GHGs) in the atmosphere, e.g. water vapor, methane (CH_4), carbon dioxide (CO_2) and nitrous oxide (N_2O), keep our planet habitable. These gases raised the global mean surface temperature from -18 °C in the absence of an atmosphere (Mitchell 1989) to 15 °C (NOAA, 2015). The atmospheric concentrations of CH_4, CO_2 and N_2O in 2011 exceeded the pre-industrial level (by about 150%, 40% and 20%) 1.803 ppm, 391 ppm and 0.324 ppm, respectively. Increasing in the atmospheric well-mixed GHGs resulting in 7.5% increase in the radiative forcing (*RF*)[1] from 2005 to 2011, and CO_2 is contributing 80% of the *RF* (IPCC 2013) (Box 1). The combined *RF* resulting from increase of anthropogenic and non-anthropogenic concentrations of long-lived GHGs (CO_2, CH_4, N_2O, halocarbons and Sulphur hexafluoride) is 2.63 Wm^{-2} (±0.26). The global mean concentrations of CH_4 and CO_2 alone cause to an *RF* of 0.84 (±0.05) and 1.66 (±0.17) W m^{-2}, respectively (Forster et al. 2007; IPCC 2007).

Box 1: Radiative forcing

RF is quantified at the tropopause and defined as a concept used for quantitative the difference of insolation absorbed by the Earth and energy radiated back to space. *RF* caused by changes in insolation and the concentrations of GHGs. Anthropogenic *RF* has estimated to be 1.6 W m^{-2}, this is likely to be at least five times higher than that due to solar irradiance changes. However, this indicates a substantial warming influenced by human since the industrial Era (Forster et al. 2007).

CH_4 is about 34 times more potential that CO_2 on mass basis over 100-year horizon. CH_4 emissions have four indirect radiative effects by enhances its own lifetime through changes in the OH concentrations. This lead to changes in tropospheric ozone enhances stratospheric water vapor levels and produces CO_2. The indirect radiative effect is denoting to the direct effect of degradation production or radiative effects of changes in concentrations of GHGs caused by the presence of an emitted gas or its degradation products (Forster et al. 2007; IPCC 2013).

[1] RF: is the radiative forcing (measured in Watt m^{-2}), which is quantifies the change in energy fluxes caused by natural and anthropogenic substances and processes that alter the Earth's energy budget.

The sources of global atmospheric CH_4 are determined by many terrestrial and aquatic surface sources, balanced with one atmospheric sink, and can be broadly grouped into biogenic, thermogenic and pyrogenic categories (Kirschke et al. 2013). 90% of atmospheric CH_4 is oxidized by hydroxyl radical and the rest is consumed by methanotrophic bacteria in aerated soil (~6%), reaction with Cl and O in the stratosphere (~3%) and reactions with Cl radicals from sea salt in the marine boundary layer (~3%) (Curry 2007; Kirschke et al. 2013; Zhuang et al. 2004). However, atmospheric CH_4 has increased 2.5 times since 1750, due mainly to anthropogenic emissions. For instance, the dominant anthropogenic CH_4 sources are emissions from fossil fuel, landfills, rice paddies, waste and growing number of ruminants. The average growth rate of atmospheric CH_4 has increased form 0.5 ppb yr^{-1} to 6 ppb yr^{-1} for the periods of 1999-2006 and 2007-2011, respectively (IPCC 2013).

The accumulated anthropogenic CO_2 emission has been reported to be 555 gigatons of carbon (GTC) from 1750 to 2011 originating from land-use changes (e.g. deforestation) equivalent to 180 (ranging from 100 to 260) GTC and fossil fuel and cement production of 375 (ranged from 345 to 405) GTC (IPCC 2013). Around ~43% of the combined anthropogenic CO_2 emissions have accumulated in the atmosphere, and the reminder have been assigned to marine sequestration (~28%) and accumulated in natural terrestrial ecosystems (~29%) (IPCC 2013). Atmospheric CO_2 concentrations have steadily increased from a rate of 1.9 to 2.1 ppm yr^{-1} during 2002-2011. However, the CO_2 growth rate varies from year to year as it is driven by small changes in the balance between photosynthesis and respiration on land. The location of the continental carbon sinks remain uncertain (Heimann and Reichstein 2008) but they are assumed to lie within the terrestrial biosphere (Battin et al. 2009).

Box 2: aquatic ecosystems in global C context

The role of aquatic ecosystems in terms of their involvement in lateral C fluxes has been known for a long time (Sarmiento and Sundquist 1992), but was considered as a natural loop in the global C cycling unaffected by anthropogenic perturbation (Regnier et al. 2013). However, the magnitude of anthropogenic perturbation has recently become apparent (Battin et al. 2009; Cole et al. 2007; Regnier et al. 2013). The increase of atmospheric concentration of CO_2, land-use change, sewage discharges, damming, freshwater withdrawal and agricultural activity have impacted the outgassing and burial rate of C since the pre-industrial Era, resulting in a 0.1 Pg C yr^{-1} anthropogenic perturbation flux. 50% of this flux is respired back to the atmosphere, while the rest is buried and exported to estuaries.

Inland waters (e.g. lakes, reservoirs, streams, rivers and wetlands) form about 1% of the Earth's surface and often shape the Earth's landscapes. Recent studies have highlighted the role of inland waters in the sequestrations, transport and mineralization of organic carbon, revealing the significant contribution of the inland waters to global carbon fluxes relative to terrestrial and marine ecosystems (Battin et al. 2009; Cole et al. 2007; Downing et al. 2006; Richey et al. 1988). Human activities such as land use change, damming, water management and sewage-water production have potentially modified the carbon and nutrient cycle (e.g. the exchange of carbon between atmosphere, freshwaters and open ocean) (Regnier et al. 2013) (Box 2). However, global estimates of CH_4 and CO_2 emissions from inland waters prone to uncertainties in the drivers that control CH_4 and CO_2 evasion; e.g. the amount of CH_4 and CO_2 present in the water, global surface area of inland waters and the gas exchange velocity (Lauerwald et al. 2015; Raymond et al. 2013).

CO_2 exchange between surface water and atmosphere occur strictly by diffusion (Bastviken et al. 2004). The diffusive flux is driven by the difference in gas partial pressure between the air and the water and the gas exchange velocity. Gas exchange velocity is controlled by the near-surface turbulence dissipation rate at the air-water interface (Vachon et al. 2010; Zappa et al. 2003) and can be modeled based on the physical characteristics of a specific system

that correlate with turbulence (Bastviken et al. 2004; Raymond et al. 2012; Wanninkhof and Bliven 1991; Wanninkhof and McGillis 1999). For instance, the gas exchange velocity has been found to be driven by wind speed (Crusius and Wanninkhof 2003; Wanninkhof and Bliven 1991; Wanninkhof and McGillis 1999), rainfall (Ho et al. 2007), thermal convection (Schladow et al. 2002), size of system (Bastviken et al. 2004; Read et al. 2012) and discharge (Raymond et al. 2012). Moreover, CO_2 diffusive exchange can be chemically enhanced under low turbulence conditions and high pH values due to the hydration reactions of CO_2 with hydroxide ions and water molecules in the boundary layer (Wanninkhof and Knox 1996). See Box 3. On the other hand, about ~90% of CH_4 exchange at the air-water interface occurs via diffusion and ebullition, and the rest exchanges via plant-mediated transport (Bastviken et al. 2004; Bastviken et al. 2011; Prairie and del Giorgio 2013) (Figure 1-1). CH_4 emission by ebullition in aquatic ecosystems is an important and plausible mode of transport because of the low solubility of CH_4, and is strongly driven by the production rate, physico-chemical and hydrological characteristic of aquatic ecosystem (Bastviken et al. 2004; Baulch et al. 2011; Hoffmann et al. 2015a; Hope et al. 2001).

Box 3: chemical enhancement of CO_2

CO_2 can react in water through two hydration reactions. First, CO_2 reacts with water and produces carbonic acid, and the second is the reaction with the hydroxide to produce bicarbonate. The rate of the reactions is a function of temperature, pH and ionic strength. However, the fraction of the CO_2 reacted within the boundary layer is a function of the boundary layer thickness, pH and the reaction rate constant (is a function of temperature and ionic strength). Therefore, the gas exchange of CO_2 at air-water interface is presented as a product of enhancement factor and gas exchange velocity of a nonreactive gas (e.g. CH_4) (Cole et al. 2001; Wanninkhof and Knox 1996).

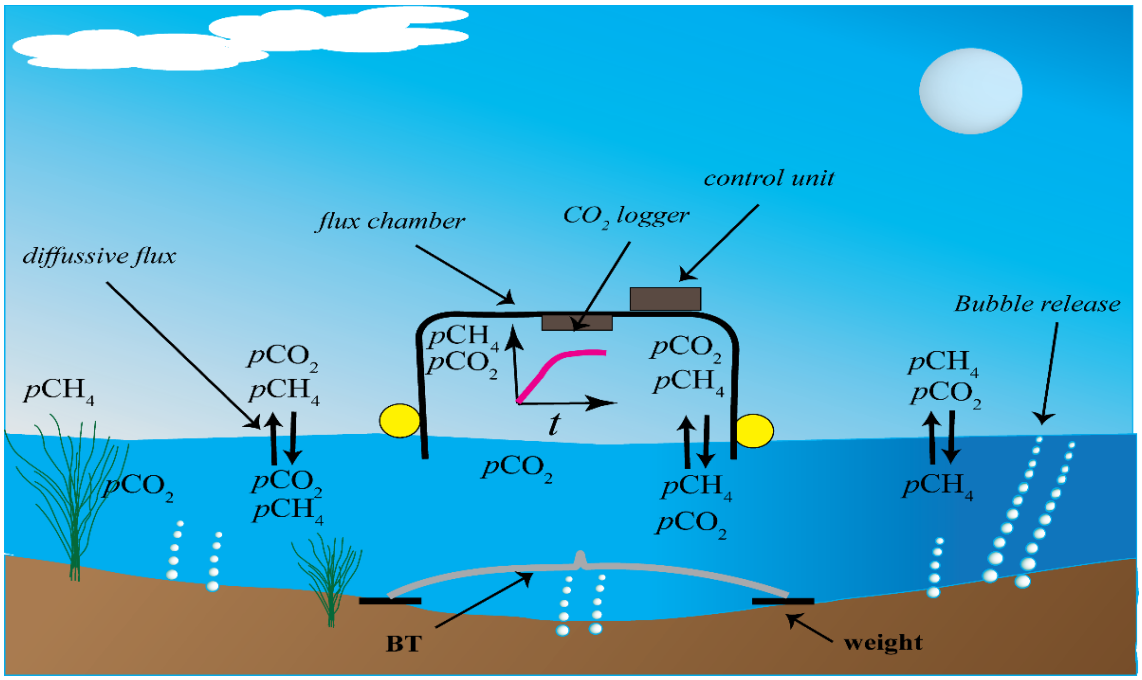

Figure. 1-1: conceptual diagram of CH_4 and CO_2 emission pathways in aquatic ecosystems. This figure shows the deployment of automated flux chamber and bubble trap (BT).

Current global estimates of CO_2 emissions form reservoirs are based on limited field measurements and are from regions where surface water is rather abundant (e.g. boreal and tropical zones) (Barros et al. 2011; Raymond et al. 2013; St. Louis et al. 2000). However, CO_2 emissions from inland water from areas suffering from water shortage and increasing in water demand (e.g. arid and semi-arid regions) are limited. Hydrological characteristics of aquatic systems, e.g. residence time, water level, discharge and freshwater withdrawal rate, as well as, discharges of treated wastewater shown to be key factors altering carbon cycling, and thus CH_4 and CO_2 emission rates (Casper et al. 2000; Deshmukh et al. 2014; Duarte et al. 2008; Guérin et al. 2007). While water management practices and operational regime may rapidly change the hydrological characteristics of inland waters (e.g. water level of drinking water reservoirs), substantial changes in CH_4 and CO_2 exchange rate are expected (Read et al. 2012). Neglecting the effects of water management practices and anthropogenic carbon sources in inland waters can lead to a large uncertainty of the estimated CH_4 and CO_2 gross emissions. Further, large

uncertainty in the quantification of emission rates of CH_4 and CO_2 of aquatic systems at the local and global scales can be caused by spatial and temporal variability of CH_4 and CO_2 fluxes.

However, recent estimates of CH_4 and CO_2 emission from inland water systems do not sufficiently resolve the spatial and temporal variability, and are based on extrapolated data of field measurements (Bastviken et al. 2004; Cole et al. 2007; Lauerwald et al. 2015; Raymond et al. 2013). Constraining diffusive flux from inland waters to the atmosphere poses a significant challenge due to the uncertainty in water surface area and variability of dissolved gases and the gas exchange velocity, resulting in significant uncertainties in lumped regional and global emission estimates (Aufdenkampe et al. 2011; Borges et al. 2015; Lauerwald et al. 2015; Raymond et al. 2013; Regnier et al. 2013). Moreover, quantifying CH_4 emission by ebullition is arguably even more challenging due to the episodic emission mode, high variability in time and space and a lack in straight-forward sampling technique (Crawford et al. 2014b). It is crucial to quantify and measure CH_4 and CO_2 flux via a high resolution spatiotemporal sampling mode, and finding linkages to underlying processes (e.g. this can be accomplished with a correlation analysis between flux regimes and biogeochemical, physico-chemical and hydrological variables) is not less important.

1.2. Objectives and methodology

1- *Although previous estimates reported that human-made reservoirs emit substantial amount of carbon per year, it has not been considered the arid and semi-arid reservoirs and temporal variation of emission that resulted from water management practices.*

In *chapter 2*, we have analyzed monthly hydrological, metrological and water quality data from three drinking and irrigation water reservoirs in the lower Jordan River basin (between 2006 and 2013), and estimated atmospheric emission of CO_2. In this chapter, we compare CO_2 emissions from reservoirs in semi-arid regions with current estimates of CO_2 emissions from reservoirs and natural lakes in similar and different climatic zones. We have assessed the contribution of chemical enhancement on the diffusive CO_2 flux for the three reservoirs as well as the uncertainty related to the measured input parameters. One of the studied reservoirs receives its inflow from the surrounding tributaries and wastewater treatment plant, which can export additional organic and inorganic carbon to the receiving reservoir.

2- *Several syntheses indicated that anthropogenic carbon sources, e.g. effluent of WWTPs, can affect the carbon cycle of inland waters, but these sources are remaining to be evaluated* and *quantitatively assessed*.

While terrestrially derived organic and inorganic carbon has been identified as the main source of CH_4 and CO_2 emissions from inland waters, anthropogenic inputs have rarely been considered. Treated wastewater

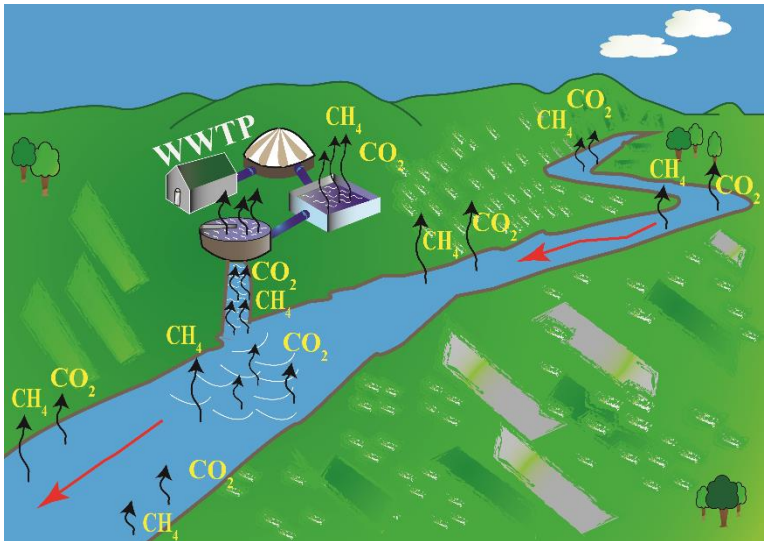

Figure 1-2: conceptual diagram of CH_4 and CO_2 exported via effluent to the surrounding river.

(effluent) from municipal wastewater treatment plants can be an additional anthropogenic source of carbon when it is discharge to surrounding water systems (e.g. streams) (Figure 1-2, Box 4). This in role can potentially alter the atmospheric emissions of both gases directly by the export of an additional dissolved CH_4 and CO_2 load, and indirectly by changing the physical, chemical and hydrological characteristics of the receiving water system. Discharged CH_4 and CO_2 with effluents have not directly been measured, and such effluents thus represent unknown sinks and sources in wastewater treatment plant and inland water carbon budgets, respectively.

Box 4: CH_4 and CO_2 emission from WWTPs

CH_4 can be generated and emitted from wastewater when treated (or disposed) anaerobically. Besides CH_4, CO_2 and N_2O have been reported to be emitted and discharged during wastewater treatment processes and effluent discharge (Czepiel et al. 1995; Czepiel et al. 1993; Daelman et al. 2012; El-Fadel and Massoud 2001; Guisasola et al. 2008; Law et al. 2012). While CO_2 emissions from WWTPs have not been considered in national total emission budgets because it is of biogenic origin (IPCC 2007), Law et al. (2013) reported that 4-14% of sewage influent organic carbon originates from fossil derived compounds. When this carbon ends up in the atmosphere as CO_2, it contributes to increasing atmospheric CO_2 concentrations, and should be considered as an anthropogenic C source and thus treated and quantified separately.

In *chapter 3*, we present monthly resolved data of dissolved CH_4 and CO_2 concentrations and their fluxes in effluents from nine WWTPs in Germany with differing design capacities, and two of which were not equipped with energy recovery systems. We estimated the exported CH_4 and CO_2 residence time at two selected receiving streams. Per capita CH_4 and CO_2 export in the effluents has been estimated and compared with per capita gross emission from the WWTPs. Continuous dissolved CH_4 and CO_2 concentration was also measured to obtain the diel variation of both gases at the effluent waters for two selected WWTPS and to resolve the uncertainty related to the strict daytime sampling. See also chapter 4.

3- *Flux estimates are often subject to uncertainty caused by a lack of high spatiotemporal measurements resolution. Providing simple and low-cost CO_2 flux measurement techniques that able to cover large spatial and temporal scales can reduce the uncertainty margin*.

Diffusive flux of CH_4 and CO_2 across the air-water surface often rely on flux chamber measurements and calculated based on the change of both gases over time. This is conceptually a straight–forward measurements technique where the targeted area is covered by a sealed chamber and the accumulation rate of both gasses is measured (Bastviken et al. 2015). Besides floating chambers, CH_4 flux by ebullition can also be measured volumetrically using inverted funnel-type bubble traps, and the volume and partial pressure of the trapped gas is used to obtain CH_4 flux by ebullition (Bastviken et al. 2015; Baulch et al. 2011; Duc et al. 2013; Hoffmann et al. 2015b) (Figure 1-3). Flux estimates of CH_4 and CO_2 are often subject to uncertainty resulting from high variability in time and space, and performing high spatial and temporal resolution flux measurements is time and cost consuming. On the other hand, volumetric measurements of ebullition rate in a continuous time series in deep waters is possible (Maeck et al. 2014), but this is not applicable for shallow waters due to the large size of the instrumentation. To our

Figure 1-3: automated chamber (upper panel) and bubble trap (lower panel)

knowledge, there were no volumetric measurements of CH_4 emission by ebullition for shallow waters where the water depth is less than 15 cm.

In *chapter 4*, we present two simple and low cost tools to measure (i) continuous diffusive flux of CO_2 and (ii) bubble release rate for shallow water systems. The first tool is an automated flux chamber and can measure continuous CO_2 flux for specified measurement interval. The automated flux chamber is consisted of three main unites: (i) floating chamber, (ii) control unit and (iii) CO_2 logger. The CO_2 logger measures the partial pressure of CO_2, temperature and relative humidity. The basic principle of the *AFC* is venting the headspace zone after specific time period using external air pump, which is controlled by a microcontroller. The second tool is a bubble trap and it designed to measure bubble release rate for shallow waters. The bubble trap is made of plastic material and narrowed at the top into a gas bag. We measured hourly CO_2 flux at two sampling points for six weeks as well as bubble release rates at 5 sampling points. The measurements were performed for a shallow pond (<40 cm) at Eusserthal Research Station, and dissolved oxygen, water temperature and water level were measured. We used transparent and non-transparent plastic materials for the automated flux chamber and the bubble trap designs in order to investigate the effect of transparency on diffusive flux of CO_2, bubble release rate and sediment temperature. See chapter 5.

4- *Temperature has been shown to be a key driver for sediment CH_4 production in various aquatic ecosystems explaining the seasonal dynamics of CH_4 ebullition.*

Quantifying and model CH_4 ebullition from deep and shallow water ecosystems is challenging due to the spatiotemporal variability of ebullition. This variability is mainly originated from the multiple controls over CH_4 production and release (e.g. total carbon quality, sediment porosity, vegetation, atmospheric pressure and sediment temperature) (Bastviken et al.

2004; Duc et al. 2010; Wik et al. 2013; Wik et al. 2014). Temperature has been shown to be a key deriver for the sediment CH_4 formation and subsequent bubble release in various inland water ecosystems, at different sediment depths and climatic zones, (Duc et al. 2010; Gudasz et al. 2010; Maeck et al. 2013; McDonald et al. 2013; Wik et al. 2013) by enhancing the rate of sediment methanogenesis (Boylen and Brock 1973; Zeikus and Winfrey 1976). However, the response of sediment CH_4 formation and ebullition to temperature changes varied between deep and shallow water sediments, and this can be linked to the difference in the rate of energy supporting primary production which contribute to organic substrate and in the rate of sediment warming which suitable for sufficient rates of CH_4 formation (Duc et al. 2010; Gudasz et al. 2010; Zeikus and Winfrey 1976).

CH_4 ebullition has been shown to primarily respond to heat gained by sediment, and solar radiation has been presented as a proxy for CH_4 ebullition in deep and shallow aquatic ecosystems (Wik et al. 2014). Darken the water column above sediment surface, e.g. due to increase in dissolved carbon, water color and any non-transparent media, would decrease light penetration and causing a reduction in sediment temperature (Houser 2006; Wik et al. 2014). However, using non-transparent materials for measuring CH_4 flux for aquatic ecosystems may bias the gross emission estimates.

In *Chapter 5*, we measured CH_4 production rate for sediment subsamples from the Saar River, Germany at different depths and temperatures by performing laboratory sediment incubation. Sediment cores were collected and subsampled at up to four depths and incubated at five temperatures. CH_4 production rate has been calculated based on a weekly measured concentration in the incubation flasks over a period of 21 days.

Chapter 2 : Carbon dioxide emissions from reservoirs in the lower Jordan watershed

Zeyad Alshboul[*,‖], *Andreas Lorke*[‖]

*zeyad@uni-landau.de

[‖]University of Koblenz-Landau, Institute for Environmental Sciences, Fortstr.7, 76829 Landau, Germany.

Published in **Plos One,** 2015, DOI: 10.1371/journal.pone.0143381

This chapter is based on the following journal publication (Alshboul and Lorke 2015).

Alshboul, Z., and A. Lorke. 2015. Carbon Dioxide Emissions from Reservoirs in the Lower Jordan Watershed. PLoS One 10: e0143381.

Author contribution

Alshboul, Zeyad: Date collection - Data analysis – Writing the manuscript

The readers are kindly asked to read the published paper following this link:

http://journals.plos.org/plosone/article?id=10.1371/journal.pone.0143381

Abstract

We have analyzed monthly hydrological, meteorological and water quality data from three irrigation and drinking water reservoirs in the lower Jordan River basin and estimated the atmospheric emission rates of CO_2. The data were collected between 2006 and 2013 and show that the reservoirs, which differ in size and age, were net sources of CO_2. The estimated surface fluxes were comparable in magnitude to those reported for hydroelectric reservoirs in the tropical and sub-tropical zones. Highest emission rates were observed for a newly established reservoir, which was initially filled during the sampling period. In the two older reservoirs, CO_2 partial pressures and fluxes were significantly decreasing during the observation period, which could be related to simultaneously occurring temporal trends in water residence time and chemical composition of the water. The results indicate a strong influence of water and reservoir management (e.g. water consumption) on CO_2 emission rates, which is affected by the increasing anthropogenic pressure on the limited water resources in the study area. The low wind speed and relatively high pH favored chemical enhancement of the CO_2 gas exchange at the reservoir surfaces, which caused on average a four-fold enhancement of the fluxes. A sensitivity analysis indicates that the uncertainty of the estimated fluxes is, besides pH, mainly affected by the poorly resolved wind speed and resulting uncertainty of the chemical enhancement factor.

Keywords:

Aquatic metabolism; reservoirs; carbon dioxide; greenhouse gas; Jordan River

2.1. Introduction

Inland waters represent an important component of terrestrial landscapes, playing an ecological and biogeochemical role that is largely disproportional to their areal extent (Aufdenkampe et al. 2011; Williamson et al. 2008). Only recently it has been recognized that the amount of terrestrial carbon, which is processed and eventually emitted into the atmosphere as CO_2 from inland waters is similar in magnitude than current estimates of global net terrestrial ecosystem production (Aufdenkampe et al. 2011; Cole et al. 2007; Raymond et al. 2013). Quantifying the role of freshwater systems in terms of carbon sinks and sources is fundamental for improving the balance approach of regional and global carbon budgets. The role of inland waters for global and regional carbon cycling is strongly affected by human activities (Regnier et al. 2013; Tranvik et al. 2009). On the basis of the limited available data, it was suggested that man-made reservoirs, as a rather small part of the inland water systems, are potentially an important source of greenhouse gases to the atmosphere, with CO_2 emission rates exceeding those of natural lakes (Barros et al. 2011; St. Louis et al. 2000; Tortajada et al. 2012). The current estimates of CO_2 emissions from inland waters are either based on syntheses and spatial upscaling of (i) few direct CO_2 partial pressure measurements and direct flux measurements, e.g., obtained using head space technique and floating chambers (Barros et al. 2011; Tortajada et al. 2012), or (ii) estimates of CO_2 partial pressures and CO_2 fluxes calculated from pH, alkalinity, temperature and wind speed data that are available from water quality monitoring programs and climatological stations (Butman and Raymond 2011; Duarte et al. 2008; Raymond et al. 2013).

Most studies on which current knowledge on reservoir greenhouse gas emissions is based on, are from regions where surface water is rather abundant, e.g. from the boreal and tropical zones (Barros et al. 2011; St. Louis et al. 2000). Representative flux measurements from

reservoirs in arid and semi-arid regions, where the anthropogenic pressure on surface waters can be expected to be highest due to extensive water usage, are limited (but see (López et al. 2011; Morales-Pineda et al. 2014)). The lower Jordan River basin, located between Lake Tiberias and the Dead Sea, and its tributaries can be considered as an example for such systems. Surface waters in this region are expected to be highly vulnerable to climatic change (Evans 2009). About 83% of the population of Jordan and the majority of the country's irrigated agriculture and water resources are located within the lower Jordan River basin (Gunkel and Lange 2012). The scarce water resources in Jordan are subject to salinization (Farber et al. 2004), which can result in chemical enhancement of water-atmosphere CO_2 fluxes (Duarte et al. 2008). Further, high loading with organic carbon from treated and untreated waste water (Shatanawi and Fayyad 1996) and high sediment yield from intense agricultural land use (Al-Sheriadeh and Al-Hamdan 1999) provide favorable conditions for aerobic and anaerobic C-degradation and comparably high atmospheric emission rates of CO_2.

The objective of this study is to estimate the CO_2 fluxes from irrigation and drinking water reservoirs in the lower Jordan River basin. We use water quality and meteorological data from three reservoirs for the time period 2006 to 2013 to estimate the CO_2 partial pressures and the wind-speed dependent gas exchange velocities. The resulting fluxes were analyzed statistically to identify potential temporal trends and correlations to available hydrological data. We relate our findings to the current estimates of CO_2 emissions rates from hydropower reservoirs and natural lakes in different climatic zones and discuss potential regional-specific drivers for flux variations.

2.2. Materials and methods

2.2.1. Study sites

We analyzed data from three main reservoirs located in the northern part of the lower Jordan watershed: King Talal Dam, Al-Wihdeh Dam and Wadi Al-Arab Dam (Figure 2-1). The reservoirs differ in surface area, catchment size, water quality, and outflow rate. The main characteristics of these reservoirs are summarized in Table 2-1 and briefly described below.

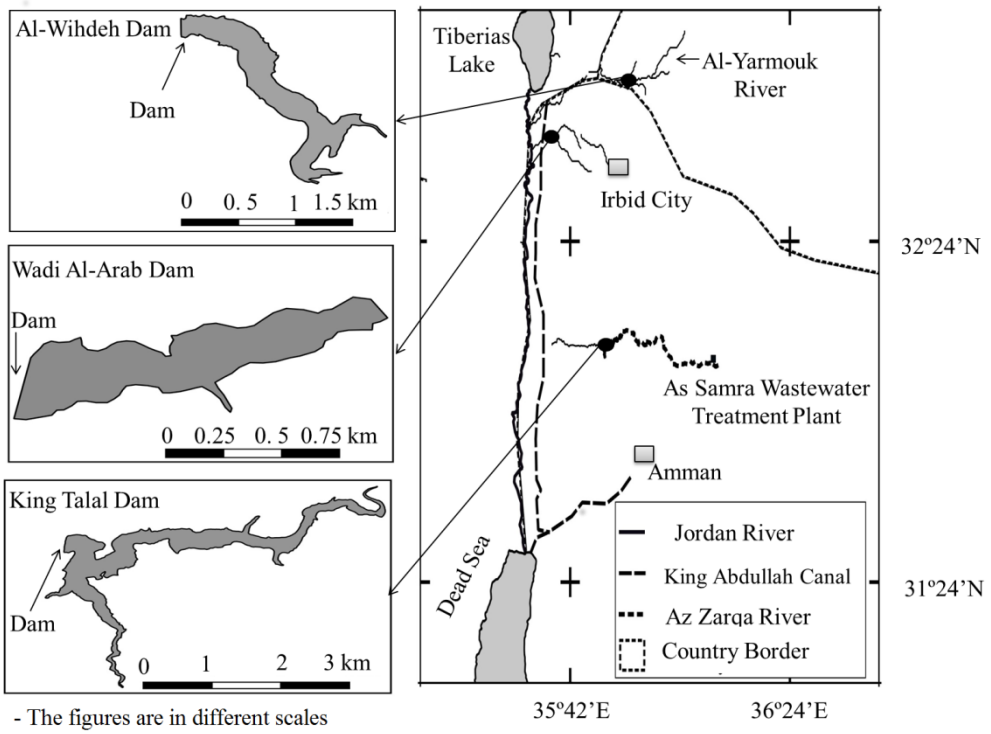

Figure 2-1. The map on the right shows the location of the three reservoirs (King Talal Dam, Al-Wihdeh Dam and Wadi Al-Arab Dam) within the lower Jordan watershed between Lake Tiberias and the Dead Sea. The morphological characteristics of the reservoirs are shown in the detailed maps on the left at different scales.

Table 2-1. The main physical characteristics of the three reservoirs. Numbers are provided as mean±SD (standard deviation), if available.

	Wadi Al-Arab Dam	King Talal Dam	Al-Wihdeh Dam
Surface area (km^2)	0.56±0.1	1.6±0.26	0.82±0.44
Total capacity (10^6 m^3)	16.9	74	110
Dam height (m)	83.5	108	87
Main tributaries	- King Abdullah Canal - Al-Yarmouk River	- Az Zarqa River - Effluent of As-Samra WWTP	- Al-Yarmouk River
Outflow (10^6 m^3 y^{-1})	11.4±1.8	98.5±8.9	14.9±4.5
Year of construction	1987	1986	2006
Usage	Agriculture, industrial and domestic	Agriculture	Agriculture and domestic

King Talal Dam is the largest reservoir in the northern part of Jordan and it is designed to supply water for irrigation in the Jordan valley (Shatanawi and Fayyad 1996). The reservoir receives its inflow from the surrounding tributaries and from the As Samra Wastewater treatment plant. The tributaries include the winter floods and the effluent of the Az Zarga River desalination plant, which is governed by the Jordanian Ministry of Water and Irrigation. The desalination plant is fed by the surrounding ground waters and started to operate in 2008. As Samra Wastewater treatment plant was constructed in 1985 and was expanded between 2006 and 2010 to treat 79% of all wastewater generated in Jordan (Al-Ghazawi and Abdulla 2008). Its effluents are discharged in the Az Zarqa River, which receives its water from the springs of Amman City.

Al-Wihdeh Dam is located in the trans-boundary basin of the Al-Yarmouk River, between Jordan and Syria. The dam began to receive water in 2006, while the construction was

completed in 2009. Al-Wihdeh Dam is mainly fed by the winter floods and available base flow from the upstream located catchment of the Al-Yarmouk River including groundwater (Al-Taani 2013).

Wadi Al-Arab Dam is located in the northern part of Jordan, 10 km south of Lake Tiberias. The reservoir mainly receives waters from the King Abdullah Canal and surrounding tributaries (Saadoun et al. 2008b). The reservoir waters are used for irrigation and during periods of water shortage also for human consumption. More information on water quality and physico-chemical features of Wadi Al-Arab Dam can be found elsewhere (Saadoun et al. 2010).

2.2.2. Data

Water temperature, pH, alkalinity, specific conductance and the concentrations of calcium, magnesium, potassium, sodium and chloride, were obtained for all three reservoirs from monthly measurements conducted by the Water Authority of Jordan (Dataset: Physico-chemical and hydrological parameters of the three studied reservoirs: http://journals.plos.org/plosone/article?id=10.1371/journal.pone.0143381.). The water samples were collected below the surface at the outflow of the reservoirs. pH, specific conductivity and water temperature measurements were conducted using a portable pH/conductivity/temperature meter (Hanna, Hannainst, USA: pH: 0-14 ±0.05; conductivity: 0-3999 μScm^{-1} ±1 μScm^{-1}; temperature: 0-60 °C ± 0.1˚C). The meter was weekly calibrated following the instructions of the manufacturer using standard buffers for pH (4.01, 7.01 and 10.01) and conductivity (1413 μScm^{-1}). Water samples were titrated for alkalinity measurements with sulfuric acid to an equivalent point of pH 4.5 (±0.018 mmol l^{-1}). The major ions were analyzed with ion chromatograph (Dionex, USA), equipped with an analytical column (CS12, 4×250mm), a guard

column (CS12, 4×50mm) and a self-regenerating suppressor (CSRS- II,mm) for cations, and an analytical column (Ionpac® anion AS4A-SC, 4×250mm), a guard column (AG4A-SC, 4×50mm) and a self-generating suppressor (ASRS-I, 4mm) for ions. The water chemistry data of King Talal Dam and Al-Wihdeh Dam are available from August 2006 to April 2013 and the data for Wadi Al-Arab Dam are available from April 2007 to April 2013.

Hourly values of wind speed at 10-meter height (U_{10}) at King Talal Dam and Al-Wihdeh Dam were obtained from the metrological stations located at the dams and operated by the Jordan Valley Authority. The U_{10} data for Wadi Al-Arab Dam were obtained from the National Oceanic and Atmospheric Administration (NOAA, http://www.noaa.gov/index.html) as the mean value of three hours measured at Irbid and Ghor Safi climatological stations. The mean U_{10} value between the water sampling dates was used in our calculations.

The daily mean of the outflow, inflow, water level, water volume and the water surface area as a function of water levels, for all three reservoirs were obtained from the database of Jordan Valley Authority (JVA, http://www.jva.gov.jo/sites/en-us/default.aspx). (See also on-line supporting information, Dataset: Physico-chemical and hydrological parameters of the three studied reservoirs: http://journals.plos.org/plosone/article?id=10.1371/journal.pone.0143381. Available at:

http://journals.plos.org/plosone/article?id=10.1371/journal.pone.0143381)

2.2.3. Calculations and Analyses

The concentration of dissolved gaseous CO_2 (mol l^{-1}) was calculated from the available data for alkalinity, pH, water temperature and ion concentrations by assuming chemical

equilibrium conditions using the software PHREEQC v3 (Parkhurst and Appelo 2013). The concentration of CO_2 was converted to partial pressure pCO_2 using the temperature dependent Henry constant $K_H\left(\text{mol l}^{-1}\ \text{atm}^{-1}\right)$ provided by *Wanninkhof* [1992].

The atmospheric flux of CO_2 (mol m^{-2} d^{-1}) at the reservoirs surface was estimated following Wanninkhof and Knox (1996)

$$Flux = k'_{CO_2}\ \alpha\ K_H\left(pCO_{2,aq} - pCO_{2,\text{air}}\right) \qquad (2.1)$$

where k'_{CO_2} is the gas exchange velocity (m d^{-1}) for CO_2, α describes the chemical enhancement of the CO_2 flux, K_H is the Henry constant (mol l^{-1} atm^{-1}), $pCO_{2,aq}$ and $pCO_{2,\text{air}}$ (µatm) are the partial pressures of CO_2 in water and the atmosphere, respectively. The atmospheric partial pressure $pCO_{2,\text{air}}$ was considered to be constant (396 µatm), corresponding to the global mean value in March 2013 (http:\\esrl.noaa.gov).

The gas exchange velocity k'_{CO_2} was estimated from the wind-speed dependent exchange velocity at a Schmidt number of 600 (k'_{600}) and the temperature-dependent Schmidt number of CO_2 (Sc_{600}) (Crusius and Wanninkhof 2003)

$$k'_{CO_2} = k'_{600}\left(\frac{600}{Sc_{600}}\right)^n \qquad (2.2)$$

We used a Schmidt number exponent n of 2/3 and 1/2 for U_{10} below and above 3.7 m s^{-1}, respectively (Wanninkhof 1992). k'_{600} was calculated as a function of wind speed using the bilinear steady wind relationship according to Crusius and Wanninkhof (2003).

$$k'_{600}(\text{cm h}^{-1}) = \begin{cases} 0.72U_{10} & , U_{10} < 3.7 \text{ m s}^{-1} \\ 4.33U_{10} - 13.3 & , U_{10} \geq 3.7 \text{ m s}^{-1} \end{cases} \quad (2.3)$$

The exchange of CO_2 at the water surface can be enhanced in comparison to other gases by the dissociation of carbonic acid within the diffusive boundary layer (Wanninkhof and Knox 1996). The hydration reaction rates for CO_2 are functions of temperature, pH and ion concentrations. If the reaction time scales are the same order of magnitude as the residence time of the CO_2 molecules in the aqueous boundary layer, both chemical reaction and diffusion are important for CO_2 exchange at the air-water interface (Wanninkhof and Knox 1996). The chemical enhancement factor α was calculated using the model of Hoover and Berkshire (1969). The calculations include the first and second apparent dissociation constants for carbonic acid according to Dickson and Millero (1987) and the hydration rate constant of carbonic acid and bicarbonate according to Johnson (1982). The model further includes water salinity, which was calculated from specific conductance using the empirical approximation provided by Duarte et al. (2008).

The annual mean retention time (d) for each reservoir was estimated by dividing the annual mean water volume (m^3) by the mean outflow rate ($m^3\ d^{-1}$). The daily mean of the water surface area was calculated from the daily mean water level, using linear regressions of the measured water surface area and water level for the three reservoirs at different dates. The emission rate of CO_2 was multiplied by the daily mean surface area of the reservoirs to estimate the total mean emission rates from the three reservoirs (g CO_2 yr^{-1}).

The relative importance of the variations of the input variables alkalinity, pH, temperature and salinity for the estimated variations of pCO_2 and CO_2 flux was evaluated by performing additional calculations using the constant mean values of the respective variables.

The same analysis was conducted for evaluating the effect of dissolved ions by comparing the estimates of pCO_2 and flux with estimates for which ions were omitted in the chemical equilibrium calculations. The relative importance of variations of wind speed for the estimated variations of the CO_2 flux was evaluated by using a constant mean wind speed instead of measured time series.

Most of the parameters involved in our calculations violate normality assumptions. Thus, the nonparametric Spearman's rank correlation coefficient (ρ) was used and the correlations among measured and estimated variables were considered at the significance level of $p<0.05$, unless stated otherwise. Temporal trends were estimated by linear regression at a significance level of $p<0.05$. The temporal trends of the variables were analyzed for years with complete data coverage, i.e. between 2007 and 2012 for King Talal Dam and Al-Wihdeh Dam, and between 2008 and 2012 for Wadi Al-Arab Dam.

2.3. Results

2.3.1. Physico-chemical characteristics

The daily mean of water surface area varied between 1.2 and 2.4 km^2, 0.37 and 0.76 km^2, and 0.18 and 2.16 km^2 in King Talal Dam, Wadi Al-Arab Dam and Al-Wihdeh Dam, respectively (Figure 2-2a). The surface area varied seasonally due to changes in water volume. Maximum and minimum storage volumes were registered in April and in November, respectively. The storage volume varied also inter-annually with maximum water volumes registered in April 2013 with 13.4 $\times 10^6$ m^3 for Wadi Al-Arab Dam, 62.7×10^6 m^3 for King Talal Dam and 52.6×10^6 m^3 for Al-Wihdeh Dam (Figure 2-2b). The annual mean water volume stored in the reservoirs was continuously decreasing in King Talal Dam (-13×10^6 m^3 y^{-1}) and Wadi Al-Arab Dam (-0.9 $m^3\times10^6$ y^{-1}) and increasing in Al-Wihdeh Dam (0.6×10^6 m^3 y^{-1}). The available

data for King Talal Dam showed that this reservoir received 89% of its inflow from the Az Zarqa River, which is fed by the As Samra Wastewater treatment plant, and from the springs of Amman City. The remaining inflow was from the surrounding tributaries including the flood waters and the discharges of the Az Zarqa desalination plant. The annual mean outflow rate from the reservoirs increased throughout the observation period at King Talal Dam (15330 m^3 y^{-1}) and at Al-Wihdeh Dam (4380 m^3 y^{-1}), while significant changes in water inflow were not observed at both sites. Contrary, the inflow was decreasing (-2190 m^3 y^{-1}) without significant changes of water outflow at Wadi Al-Arab Dam. The resulting water retention times decreased in all three reservoirs (King Talal Dam: -7 d y^{-1}, Al-Wihdeh dam: -25 d y^{-1} and Wadi Al-Arab Dam: -9 d y^{-1}). The mean water retention times in Al-Wihdeh Dam (247 ±57 d) and Wadi Al-Arab Dam (214 ±57 d) were two times higher than in King Talal Dam (115 ±16 d) (Table 2-2).

In contrast to Wadi Al-Arab and Al-Wihdeh Dam, we did not observe clear seasonal patterns of the outflow rate at King Talal Dam, although the water inflow rate varied seasonally. Highest and lowest inflow rates for King Talal Dam were registered in March and July-August, respectively. A similar pattern was observed for the inflowing water at Al-Wihdeh Dam. The outflow rate was varied over growing seasons in Wadi Al-Arab Dam and Al-Wihdeh Dam with highest and lowest values in late August and late March, respectively.

Water surface temperature varied seasonally with maximum values of 27 °C at the beginning of August and minimum values around 8 °C in February (Figure 2-2c). The mean water temperatures and ranges of variation were of comparable magnitude in all three reservoirs. Salinity in King Talal Dam was nearly twice as high as in the other two reservoirs (Table 2-2) and decreased significantly in all three reservoirs during the observation period (Al-Wihdeh

Dam: -0.005 ppt y^{-1}, Wadi Al-Arab: -0.04 ppt y^{-1}, King Talal Dam: -0.07 ppt y^{-1}). Seasonal variations of salinity were not observed.

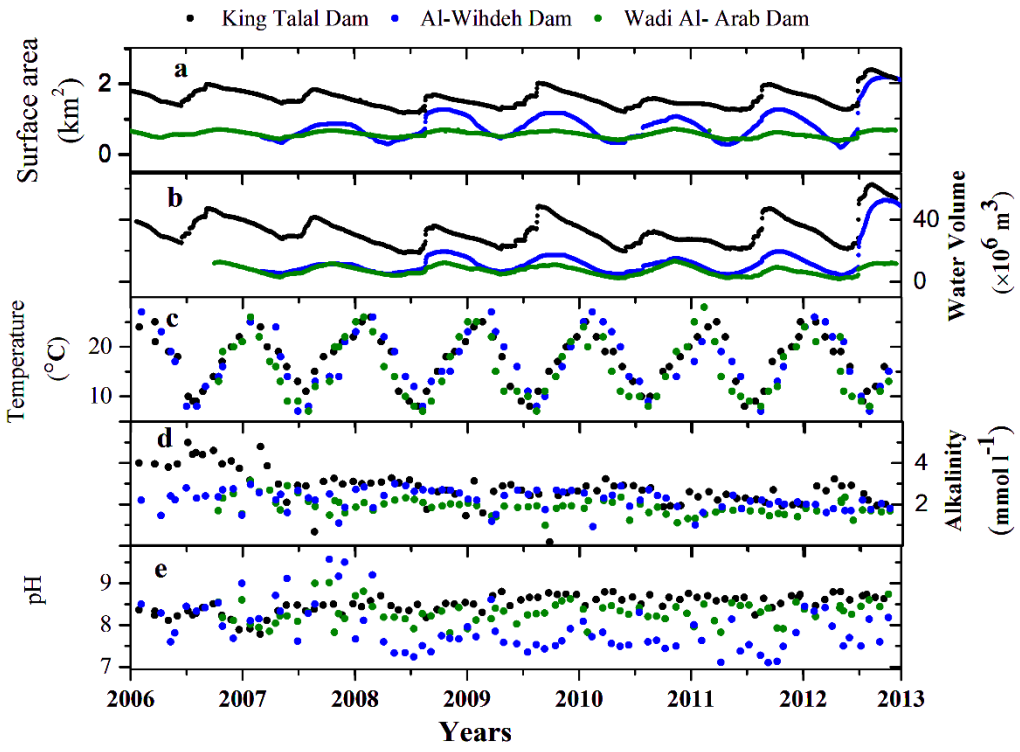

Figure 2-2. Time series of the physico-chemical parameters in three reservoirs King Talal Dam (black), Wadi Al-Arab (green) and Al-Wihdeh (blue): (a) Daily mean surface area, (b) daily mean water volume, (c) water surface temperature, (d) alkalinity, and (e) pH.

Measured alkalinity varied between 0.97 and 3.13 mmol l^{-1} in Wadi Al-Arab Dam, 0.67and 5.0 mmol l^{-1} in King Talal Dam and between 0.92 mmol l^{-1} and 3.0 mmol l^{-1} in Al-Wihdeh Dam (Figure 2-2d). Exceptionally high alkalinity (>0.4 mmol l^{-1}) was measured in 2006 and 2007 in King Talal Dam, which however dropped to values which were comparable to the other two reservoirs in November 2008. After this period, a significant decrease in alkalinity was observed in King Talal Dam (-0.26 mmol l^{-1} $y^{-1)}$ and in Wadi Al-Arab Dam (-0.15 mmol l^{-1} y^{-1}).

Alkalinity was significantly correlated with salinity in King Talal and Wadi Al-Arab Dams (Table 2-3).

Table 2-2. Summary of the measured and estimated physico-chemical variables and CO_2 fluxes for the three reservoirs. *n* indicates the number of available water chemistry samples. All numbers are given as mean±SD. The arrows in parentheses indicate significant linear temporal trends (↑ increasing, ↓ decreasing, - not significant for $p<0.05$).

	King Talal Dam	Wadi Al-Arab Dam	Al-Wihdeh Dam
	n = 83	*n* = 75	*n* = 78
pH	8.55±0.20 (↑)	8.29±0.26 (-)	7.85±0.0.51(↓)
Alkalinity (mmol l^{-1})	2.85±0.78 (↓)	1.87± 0.4 (↓)	2.28±0.48 (-)
Temperature (ºC)	17±5 (-)	15.5±6 (-)	16.4±6 (-)
Salinity (ppt)	1.4±0.3 (↓)	0.8±0.1 (↓)	0.7±0.1 (↓)
Water volume ($\times 10^6$ m^3)	32±9 (↓)	7±3 (↓)	13±10 (↑)
Retention time (d)	115±16 (↓)	214±57 (↓)	247±57 (↓)
pCO_2 ($\times 10^3$ µatm)	1.0±0.87(↓)	1.1±0.86 (↓)	5.4±4.2 (↑)
Chemical enhancement	8.0±3.1	2.8±1.23	1.6±0.8
k'_{600} (m d^{-1})	0.62±2.0	0.83±0.42	0.61±0.5
Flux (g CO_2 m^{-2} d^{-1})	0.7±1.3 (↓)	1±1.6 (↓)	5.3±4.6 (↑)
Total annual emission ($\times 10^5$ g CO_2 d^{-1})	12±23	5.8± 9.6	45±21

The pH values in the three reservoirs varied between 7.10 and 9.81 (Figure 2-2e). The mean pH in King Talal Dam (8.50) was consistently higher than the mean pH in Al-Wihdeh (7.85) and Wadi Al-Arab Dam (8.29) (Table 2-2). Exceptionally high pH values (pH>9) were observed during the initial filling of Al-Wihdeh Dam in 2007 and 2008. In the years following the initial filling, the pH in Al-Wihdeh Dam was significantly lower than in the other two reservoirs. The pH increased during the observation period in King Talal Dam (0.07 y^{-1}) and decreased in Al-Wihdeh Dam (-0.1 y^{-1}).

Table 2-3. Cross-correlation coefficients for the selected parameters: pH, alkalinity (*Alk*) in mmol l^{-1}, salinity (*S*) in ppt, temperature (*T*) in ° C, pCO_2 in µatm, CO_2 flux (Flux) in mg CO_2 m^{-2} d^{-1}, water volume (*V*) in m^3, gas exchange velocity (k'_{600}) in m d^{-1} and chemical enhancement factor (α). For each combination of parameters, the three numbers are the cross-correlation coefficients observed for King Talal (upper), Wadi Al-Arab (middle) and Al-Wihdeh (lowest) dams. The most significant correlation coefficients ($p<0.05$) are marked bold, while $p<0.1$ for the remaining correlations. Not significant correlations are marked as x.

	pH	*Alk*	*S*	*T*	pCO_2	Flux	*V*	α
Alk	**-0.5**		**0.47**	x	**0.77**	**0.77**	0.32	x
	-0.28		**0.6**	x	**0.5**	**0.35**	x	x
	-0.23		x	x	**0.32**	**0.4**	-0.23	-0.31
S	-0.3	**0.47**		x	**0.4**	0.4	x	x
	-0.35	**0.6**		x	**0.5**	x	x	x
	x	x		x	x	x	x	x
T	x	x	x		x	x	0.3	**-0.68**
	x	x	x		x	0.38	x	**0.88**
	0.31	x	x		-0.22	x	x	**0.4**
pCO_2	**-0.89**	**0.77**	**0.4**	x		**0.98**	0.21	x
	-0.95	**0.5**	**0.5**	x		**0.83**	x	x
	-0.95	**0.32**	x	-0.22		**0.91**	x	x
Flux	**-0.86**	**0.77**	0.4	x	**0.98**		0.26	x
	-0.78	**0.35**	x	0.38	**0.83**		x	x
	-0.85	**0.4**	x	x	**0.91**		x	-0.29
V	x	0.32	x	0.3	0.21	0.26		x
	x	x	x	x	x	x		x
	x	-0.23	x	x	x	x		x
α	x	x	x	**-0.68**	x	x	x	
	x	x	x	**0.88**	x	x	x	
	x	-0.31	x	**0.4**	x	-0.29	x	
k'_{600}	x	x	-0.31	0.36	x	x	x	**-0.84**
	x	x	x	x	x	0.28	x	x
	0.28	x	x	x	-0.25	x	x	**-0.83**

2.3.2. CO_2 partial pressure

The three reservoirs were supersaturated with CO_2 with respect to the atmosphere for most of the time. 88% of the water samples from Wadi Al-Arab and Al-Wihdeh Dam, and 82% of the water samples from King Talal Dam had CO_2 partial pressures, which were exceeding the mean atmospheric value. The pCO_2 values in King Talal Dam ranged between 250 and 4900 µatm, in Wadi Al-Arab Dam between 121 and 3776 µatm, and in Al-Wihdeh Dam between 98 and 15616 µatm (Figure 2-3). The mean pCO_2 and its standard deviation was about five times higher in Al-Wihdeh Dam (5400±4200 µatm) than in the other two reservoirs, which had comparable mean CO_2 partial pressures of 1100 µatm (Table 2-2). While a clear seasonal pattern of pCO_2 could not be observed, it was continuously decreasing with time in King Talal Dam (-312 µatm y^{-1}) and in Wadi Al-Arab Dam (-186 µatm y^{-1}), while it was increasing at Al-Wihdeh Dam (879 µatm y^{-1}). The increasing trend in Al-Wihdeh Dam, however, was mainly caused by low CO_2 partial pressure during the initial filling period of the reservoirs until 2009. The pCO_2 in Al-Wihdeh Dam remained rather constant at high levels after the year 2010. pCO_2 was significantly correlated with pH and alkalinity in all three reservoirs and it was additionally correlated with salinity in King Talal and Wadi Al-Arab Dam (Table 2-3).

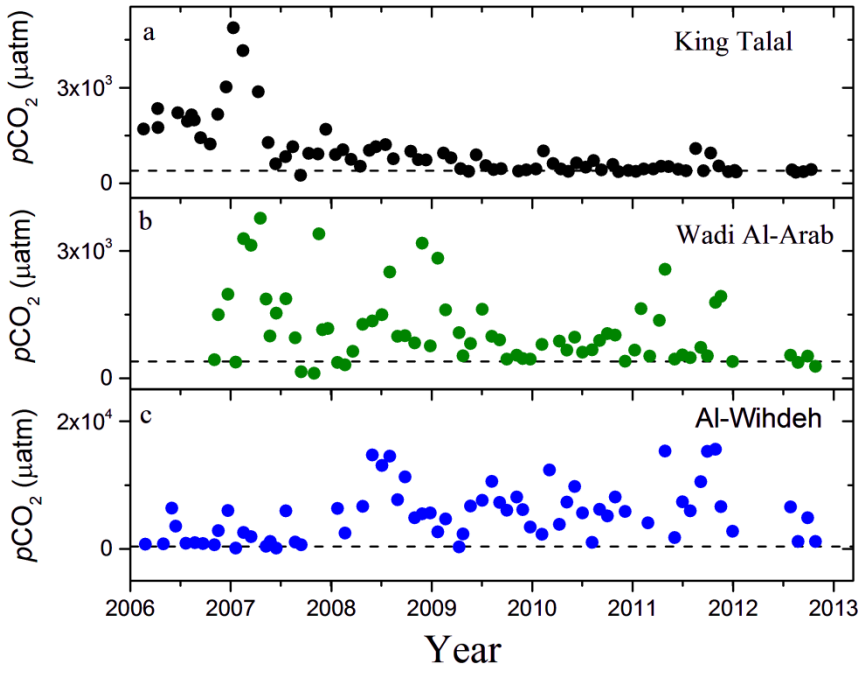

Figure 2-3. Time series of the monthly estimates of pCO_2 for (a) King Talal Dam (black), (b) Wadi Al-Arab Dam (green), and (c) Al-Wihdeh Dam (blue). The dashed lines show the mean atmospheric pCO_2 (396 µatm).

2.3.3. Fluxes

The wind-speed dependent gas exchange velocity k'_{600} was generally lower than 1 m d^{-1}, with 94 %, 86 % and 78 % of the values in King Talal, Al-Wihdeh and Wadi Al-Arab Dam, respectively (Figure 2-4a). The mean gas exchange velocity in Wadi Al-Arab Dam (0.83±0.42 m d^{-1}) was slightly higher than those in King Talal (0.62±2.2 m d^{-1}) and Al-Wihdeh (0.61±0.5 m d^{-1}) Dam (Table 2-2-2).

Chemical enhancement was an important process for CO_2 evasion in all three reservoirs and lead to an up to fourteen-fold increase of the gas exchange. The enhancement factors ranged between 1.4 and 6.9 in Wadi Al-Arab Dam, 1.0 and 14.4 in King Talal Dam and between 1.3 and 4.7 in Al-Wihdeh Dam (Figure 2-4b) and the mean enhancement factor was highest at King Talal

Dam (Table 2-2). Chemical enhancement was significantly correlated with water temperature, although the sign of the correlation coefficients differed among the three reservoirs (Table 2-3).

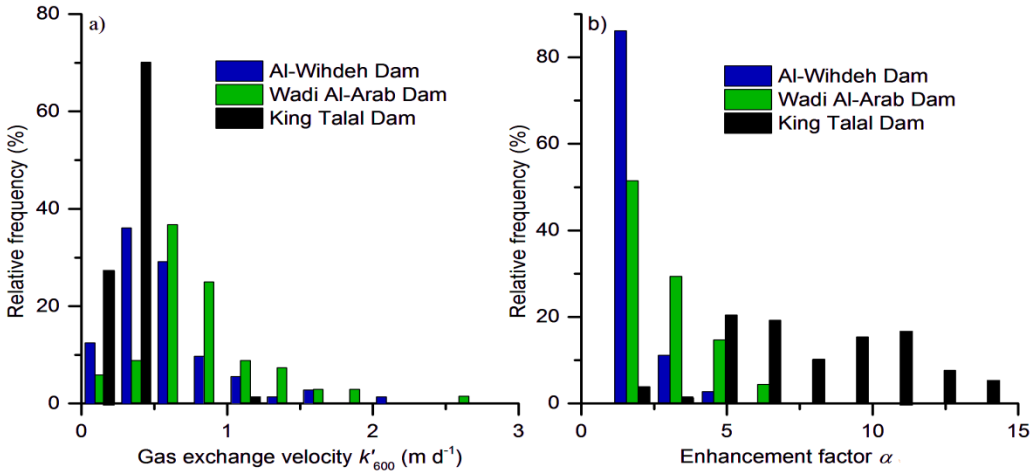

Figure 2-4. The frequency distribution of (a) gas exchange velocity and (b) chemical enhancement factor for the three reservoirs.

The CO_2 fluxes varied widely among the reservoirs and among sampling dates but except for the year 2013, where the available data did not cover the full year, annual mean fluxes were positive, i.e. the reservoirs were a net source for atmospheric CO_2 (Figure 2-5). Persistent seasonal patterns in the monthly flux estimates were not observed. The highest mean flux and range of variation were registered in Al-Wihdeh Dam with values between -1157 and 17440 mg CO_2 m^{-2}d^{-1}, where negative fluxes were mainly observed during the initial filling of the reservoir in 2007 and 2008. The estimated fluxes ranged between 448 and 8538 mg CO_2 m^{-2} d^{-1} in King Talal Dam and between -348 to 8657 mg CO_2 m-^{2} d^{-1} in Wadi AL-Arab Dam. The annual mean flux of CO_2 decreased significantly throughout the observation period in King Talal Dam (-686.5 mg CO_2 m-^{2}d^{-1} y^{-1}) and Wadi Al-Arab Dam (-264 mg CO_2 m^{-2}d^{-1} y^{-1}). The fluxes were significantly correlated with pH, alkalinity and pCO_2 in all three reservoirs (Table 2-3), although

pH can be considered as the most sensitive input parameter in our calculations (Figure 2-6). The resulting total emission rates were highest in Al-Wihdeh Dam (Table 2-2), which had the highest pCO_2.

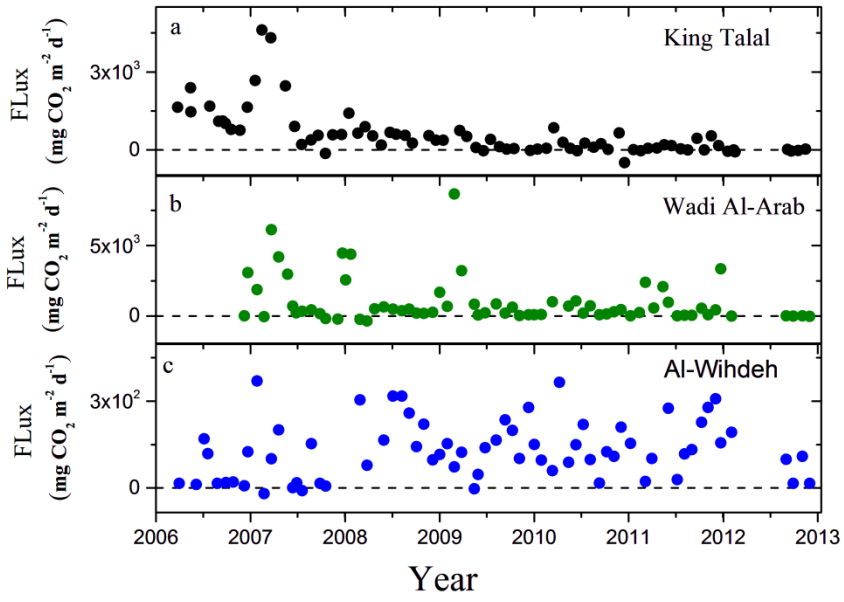

Figure 2-5. Time series of the CO_2 flux for the three reservoirs in (a) King Talal Dam (black), (b) Wadi Al-Arab Dam (green), and (c) Al-Wihdeh Dam (blue). The y-axes is in different scale and the dashed lines were fixed at zero.

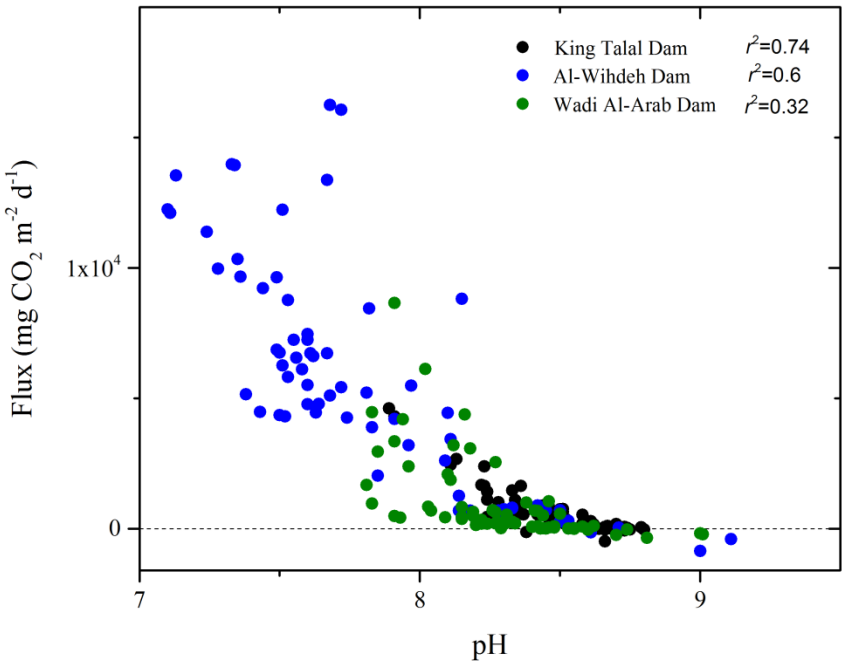

Figure 2-6. Atmospheric fluxes of CO_2 as a function of pH in the three reservoirs. r^2 denote to the linear regression.

2.3.4 Sensitivity analysis

To test the relative contributions of temporal variations of the different input data on the estimated mean values of CO_2 partial pressure and flux, we compared our results to corresponding estimates for which one variable was kept constant at its mean value. This sensitivity analysis indicates that variations in alkalinity, salinity and temperature had only minor effects on mean values of pCO_2 and fluxes (< 5%). Using a constant mean pH value for each reservoir resulted in an increase of estimated pCO_2 of up to 10 % for Al-Wihdeh and Wadi Al-Arab Dams, and 15 % for King Talal Dam. The pH affects not only the carbon equilibrium calculations but also the chemical enhancement factor. Thus, the sensitivity of the flux to variations in pH can be expected to be high. Whereas, excluding the measured ion concentrations in the chemical equilibrium calculations resulted in an overestimation of the mean pCO_2 by 10 %

in Al-Wihdeh, and 15 % in King Talal and Wadi Al-Arab Dam and corresponding increases of CO_2 fluxes.

The CO_2 fluxes were most sensitive to wind speed, which is affecting both the enhancement factor and the gas exchange velocity. Using a constant mean wind speed resulted in an increase of the mean flux by a factor of 3.4, 2.5 and 2.6 for King Talal, Al-Wihdeh and Wadi Al-Arab Dams, respectively.

2.4. Discussion

2.4.1. Uncertainties and chemical enhancement of the CO_2 flux

The flux estimates discussed above are subject to uncertainties caused by uncertainties of the measured input data, as well as by uncertainties arising from the limited spatial and temporal resolution of these data. The sensitivity analysis revealed that the nonlinear dependence of the estimated pCO_2 on alkalinity, pH, salinity, temperature and ion concentration caused only moderate uncertainties of the estimated fluxes of up to 10 to 15 %. In accordance with findings of Abril et al. (2015), these uncertainties cause an overestimation of the fluxes. An additional overestimation of comparable magnitude can occur in organic-rich and acidic waters, where organic acids make a significant contribution to the total alkalinity (Abril et al. 2005). However, there is no available data that can address the possible contribution of organic acids to the total alkalinity.

Much higher are the uncertainties of the flux estimates related to wind speed. While the gas exchange velocity was assumed to be linearly related to wind speed, its non-linear effect on the chemical enhancement factor can cause several-fold underestimations of the fluxes. The CO_2 exchange with the atmosphere for the three reservoirs was enhanced by up to fourteen fold, with

an average enhancement factor of four. This value is higher than that considered for natural lakes, where it was assumed to be three (Cole et al. 1994). Chemical enhancement was not considered in the most recent estimation of global CO_2 emissions from inland waters (Raymond et al. 2013). The importance of chemical enhancement has been addresses in lab experiments and in various aquatic ecosystems (Bade and Cole 2006; Cole et al. 1994; Wanninkhof and Knox 1996). The enhancement factor increases for increasing pH and temperature and is particularly high at low wind speeds, when the exchange velocity is low (Bade and Cole 2006). The relationship between the wind-speed dependent gas exchange velocity k'_{600} and the chemical enhancement factor is shown for a range of observed pH and temperatures in Figure 2-7. For pH≥8, the enhancement factor tends to become reciprocally related to k'_{600}, at small exchange velocities. This dependence results in a constant, i.e. wind-speed independent, enhanced exchange velocity ($k'_{600} \cdot \alpha$, cf. Eq. 2.1). Chemical enhancement thus provides a mechanism, which is capable to off-sets the decrease of the gas exchange velocity for decreasing wind speed.

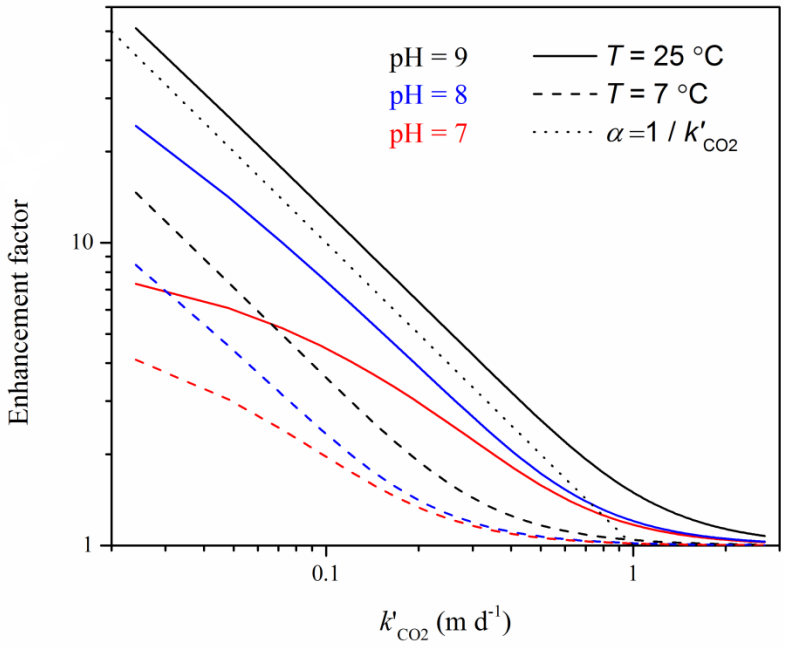

Figure 2-7. Chemical enhancement factor as a function of unenhanced gas exchange velocity k'$_{CO2}$ for three different pH values (color) and at two different temperatures (solid line: 25 °C, dashed line: 7 °C). The dotted line indicates a reciprocal relationship between both parameters and therewith a resulting exchange coefficient, which is independent of wind speed. Chemical enhancement further depends on salinity, which was fixed at a value of 0.8 ppt.

2.4.2. Variability of pCO_2 and fluxes

The observed seasonal patterns of water volume at the three reservoirs were mainly caused by the balance between the outflow and inflow rates. In contrary to King Talal Dam, the seasonal pattern of the water volume at Wadi Al-Arab Dam resulted from the seasonality of the inflowing water. On the other hand, decreasing outflow and increasing inflow rates at Al-Wihdeh Dam during March, and the opposite during July-August, caused the seasonal pattern of the

water volume in Al-Wihdeh Dam. However, the minimum and maximum values of inflow and outflow rates may refer mainly to the seasonality of precipitation and consumption rates, respectively.

The high salinity at King Talal Dam can be related to the water quality of the inflowing water, i.e. to the high amount of treated wastewater from the As Samra Wastewater treatment plant. Further studies should take into account the processes, which regulate the variability of the physico-chemical characteristics of the reservoirs. The significant correlation between salinity and alkalinity in King Talal Dam may explain the continuous decrease of the annual mean alkalinity during the observation period. The relationship between water salinity and alkalinity can be linked to the removal of freshwater, i.e. the decreasing contribution of spring waters, which is reflected by salinity changes (Jiang et al. 2014; Lee et al. 2006; Millero et al. 1998). The long term decrease of the annual mean pCO_2 and CO_2 flux that was observed in Wadi Al-Arab Dam and at King Talal Dam was mainly caused by decreasing alkalinity. Mean gas exchange velocity in King Talal dam was lower than in the other reservoirs (Table 2-2), which resulted in the highest enhancement factor in King Talal Dam (Figure 2-4b). The negative relationship between the chemical enhancement factor and the gas exchange velocity (Figure 2-7) was proposed by the model of Hoover and Berkshire (1969). Chemical enhancement varied strongly among the three reservoirs under study, indicating that using the fixed default value which was proposed by Cole et al. (1994) can result in a high degree of uncertainty of the flux estimates.

The observed change in surface area for the three reservoirs over the growing seasons resulted a substantial change in the total emission. Therefore, the variability in the hydrological characteristics for the three reservoirs, which was causing the change in surface area, is strongly linked to the water management practice, i.e. the balance between inflow and outflow. The

emerged sediments in the seasonally varying dry belts can be additional, potentially strong sources of CO_2 emissions, which were not included in our estimates. von Schiller et al. (2014) found extraordinary high areal emission rates from Mediterranean rivers during temporary dry periods, which were exceeding the emission rates of both water surfaces and soil. Future studies, which aim at a complete greenhouse gas budget of reservoirs, should take these emissions into account.

2. 4.3. CO_2 fluxes in a global context

We estimated the atmospheric emission rates of CO_2 from three reservoirs located in the lower Jordan watershed using water quality monitoring data. The same methodological approach has been applied in the past to obtain regional to global scale estimates of CO_2 fluxes from reservoirs and other inland waters (Butman and Raymond 2011; Humborg et al. 2010; Raymond et al. 2013). The total mean CO_2 flux from the three reservoirs of 3.3 g CO_2 m^{-2} d^{-1} is in the range of fluxes reported for tropical and subtropical reservoirs in global assessments and corresponds to about 3-fold of the most recent mean flux from global lakes and reservoirs (The fluxes differed among the three reservoirs and while the mean values of the more than 20 year old reservoirs King Talal Dam and Wadi Al-Arab Dam are comparable to the global-mean estimate for lentic ecosystems of 1 g CO2 m-2 d-1 (Raymond et al. 2013), the emission rate from the newly established Al-Wihdeh Dam exceeds this value more than 5-fold. This relatively high emission rate is in the range of fluxes measured in other newly established reservoirs, both in the tropical as well as in the boreal zone (Teodoru et al. 2012) but is about 40 % higher than the global mean flux from reservoirs younger than 20 years estimated by Barros et al. (2011). In contrast to these studies, however, a significant decrease of the CO2 flux during the first years of operation was not observed in Al-Wihdeh Dam. Previous studies indicated that the main source

of carbon in the young reservoirs are originated flooded biomass (St. Louis et al. 2000; Teodoru et al. 2011), which was decomposed in the first three years (St. Louis et al. 2000). However, continuous increasing in the water volume in Al-Wihdeh dam indicates that the reservoir did not reach the first year of full filling and the biomass is still flooding. The fluxes from the two older dams decreased significantly during the observation period and with annual mean *pCO2* approaching atmospheric equilibrium the reservoirs appear to be a relatively weak source for atmospheric CO2 after about 25 years of operation in comparison to other inland waters (Raymond et al. 2013). While the declining fluxes with increasing reservoir age can potentially be caused by the declining availability of degradable carbon in the flooded biomass and soil organic matter (Barros et al. 2011), the simultaneously observed decreasing trends in water retention time and salinity suggest that also changes of water quality and water management contribute to the observed trends in CO2 fluxes from King Talal and Wadi Al-Arab Dam.

While previous studies have mainly focused on hydropower reservoirs, which are typically located in regions where water resources are more abundant (Abril et al. 2005; Barros et al. 2011; Teodoru et al. 2012), the irrigation and drinking water reservoirs studied here are subject to strong anthropogenic pressure on declining water resources. The fact that the studied reservoirs receive large fractions of their inflowing water as treated waste water suggests that besides reservoir age, also eutrophication and primary production can have strong effects on their carbon budgets. Primary production was measured in Wadi Al-Arab Dam in 2001 by Saadoun et al. (2008a) to be 92 mg C m-3 h-1. This rate corresponds to an areal CO2 uptake rate of ≈8 g CO2 m-2 d-1 only from production within the first meter of the water column, and therewith exceeds the estimated atmospheric emission rates. Changing nutrient concentration and water retention time, which affect the rate of primary production in reservoirs (Saadoun et al. 2008a),

can therefore be expected to also affect the amount of carbon emitted to the atmosphere. However, the high rates of the primary production in comparison to the observed CO2 flux suggest a strong diurnal variation of *pCO2* and CO2 flux, which can result in a substantial bias in the annual estimates of *pCO2* and exchange rate because the monthly sampling was restricted to day time. Diurnal variation of *pCO2* and exchange rate has been observed in various aquatic ecosystems (Crawford et al. 2014a; Morales-Pineda et al. 2014), which indicates the importance of high temporal resolution measurements for further studies.

The inorganic carbon, which is recycled within the reservoir by primary production can partly be stored in the sediments (Maeck et al. 2014) or it can be emitted during and after water usage either from soils after irrigation or during water treatment for drinking water production. A more complete analysis of the carbon and greenhouse gas budget of the reservoirs would therefore require the availability of data on organic and inorganic carbon burial within and export from the reservoirs (Tortajada et al. 2012). Data on sedimentation rates in the reservoirs are available for King-Talal Dam, where the mean annual sediment yield was estimated to be 0.63 106 m3 (Al-Sheriadeh and Al-Hamdan 1999). This sediment yield corresponds to a mean increase of sediment thickness of 0.3 m y-1. Such high sedimentation rates can be expected to lead to high production and emission rates of methane (Maeck et al. 2013). Therefore, further studies are needed to quantify and identify the total C released from these systems. The actual production rate of methane, however, depends strongly on the quantity and quality of organic carbon in the sediments, as well as on the physical characteristics. Predictors for methane emission rates, which are based on bulk water and sediment quality data require data for dissolved methane concentration in water (Bastviken et al. 2004), which are not readily available as the data required to estimate CO2 evasion.

Table 2-4). Moreover, the total mean CO_2 flux from the reservoirs exceeded those reported for reservoirs located in other semiarid regions (López et al. 2011; Morales-Pineda et al. 2014).

The fluxes differed among the three reservoirs and while the mean values of the more than 20 year old reservoirs King Talal Dam and Wadi Al-Arab Dam are comparable to the global-mean estimate for lentic ecosystems of 1 g CO_2 m^{-2} d^{-1} (Raymond et al. 2013), the emission rate from the newly established Al-Wihdeh Dam exceeds this value more than 5-fold. This relatively high emission rate is in the range of fluxes measured in other newly established reservoirs, both in the tropical as well as in the boreal zone (Teodoru et al. 2012) but is about 40 % higher than the global mean flux from reservoirs younger than 20 years estimated by Barros et al. (2011). In contrast to these studies, however, a significant decrease of the CO_2 flux during the first years of operation was not observed in Al-Wihdeh Dam. Previous studies indicated that the main source of carbon in the young reservoirs are originated flooded biomass (St. Louis et al. 2000; Teodoru et al. 2011), which was decomposed in the first three years (St. Louis et al. 2000). However, continuous increasing in the water volume in Al-Wihdeh dam indicates that the reservoir did not reach the first year of full filling and the biomass is still flooding. The fluxes from the two older dams decreased significantly during the observation period and with annual mean pCO_2 approaching atmospheric equilibrium the reservoirs appear to be a relatively weak source for atmospheric CO_2 after about 25 years of operation in comparison to other inland waters (Raymond et al. 2013). While the declining fluxes with increasing reservoir age can potentially be caused by the declining availability of degradable carbon in the flooded biomass and soil organic matter (Barros et al. 2011), the simultaneously observed decreasing trends in water retention time and salinity suggest that also changes of water quality and water

management contribute to the observed trends in CO_2 fluxes from King Talal and Wadi Al-Arab Dam.

While previous studies have mainly focused on hydropower reservoirs, which are typically located in regions where water resources are more abundant (Abril et al. 2005; Barros et al. 2011; Teodoru et al. 2012), the irrigation and drinking water reservoirs studied here are subject to strong anthropogenic pressure on declining water resources. The fact that the studied reservoirs receive large fractions of their inflowing water as treated waste water suggests that besides reservoir age, also eutrophication and primary production can have strong effects on their carbon budgets. Primary production was measured in Wadi Al-Arab Dam in 2001 by Saadoun et al. (2008a) to be 92 mg C m^{-3} h^{-1}. This rate corresponds to an areal CO_2 uptake rate of ≈8 g CO_2 m^{-2} d^{-1} only from production within the first meter of the water column, and therewith exceeds the estimated atmospheric emission rates. Changing nutrient concentration and water retention time, which affect the rate of primary production in reservoirs (Saadoun et al. 2008a), can therefore be expected to also affect the amount of carbon emitted to the atmosphere. However, the high rates of the primary production in comparison to the observed CO_2 flux suggest a strong diurnal variation of pCO_2 and CO_2 flux, which can result in a substantial bias in the annual estimates of pCO_2 and exchange rate because the monthly sampling was restricted to day time. Diurnal variation of pCO_2 and exchange rate has been observed in various aquatic ecosystems (Crawford et al. 2014a; Morales-Pineda et al. 2014), which indicates the importance of high temporal resolution measurements for further studies.

The inorganic carbon, which is recycled within the reservoir by primary production can partly be stored in the sediments (Maeck et al. 2014) or it can be emitted during and after water usage either from soils after irrigation or during water treatment for drinking water production. A

more complete analysis of the carbon and greenhouse gas budget of the reservoirs would therefore require the availability of data on organic and inorganic carbon burial within and export from the reservoirs (Tortajada et al. 2012). Data on sedimentation rates in the reservoirs are available for King-Talal Dam, where the mean annual sediment yield was estimated to be 0.63 10^6 m^3 (Al-Sheriadeh and Al-Hamdan 1999). This sediment yield corresponds to a mean increase of sediment thickness of 0.3 m y^{-1}. Such high sedimentation rates can be expected to lead to high production and emission rates of methane (Maeck et al. 2013). Therefore, further studies are needed to quantify and identify the total C released from these systems. The actual production rate of methane, however, depends strongly on the quantity and quality of organic carbon in the sediments, as well as on the physical characteristics. Predictors for methane emission rates, which are based on bulk water and sediment quality data require data for dissolved methane concentration in water (Bastviken et al. 2004), which are not readily available as the data required to estimate CO_2 evasion.

Table 2-4. Comparison of the estimated mean flux of CO_2 with zonal and global estimates from the recent literature.

	CO_2 flux ($g\ CO_2\ m^{-2}\ d^{-1}$)	Number of reservoirs	Reference
Global hydroelectric reservoirs	**1.5**		(Barros et al. 2011)
Temperate zone	0.4	85	
Tropical zone	3.1		
Younger than 20 years	3.7		
Older than 20 years	1.2		
Global reservoirs	**1.87**	**149**	(Tortajada et al. 2012)
Subtropical reservoirs	0.78	36	
Tropical reservoirs	4.0	20	
Global reservoirs	**1.8**	**22**	(St. Louis et al. 2000)
Temperate zone	1.4	17	
Tropical zone	3.5	5	
Global lakes and reservoirs	1.0	7939	(Raymond et al. 2013)
This study (subtropical reservoirs)	3.3	3	Table 2-2. (area-weighted average)

2.5. Conclusions

This study is providing estimates of CO_2 fluxes from reservoirs located in a semi-arid region from which a limited number of studies were addressing the magnitude CO_2 evasion rates. The magnitude of observed fluxes is most comparable to those from tropical reservoirs (López et al. 2011; Morales-Pineda et al. 2014; Tortajada et al. 2012) and generally agrees with estimates from larger-scale assessments. Moreover, our analysis revealed two important points: At first,

the relatively high fluxes were, to a large extent, controlled by chemical enhancement of gas transfer. Chemical enhancement becomes important at high pH and low wind speed, where this process is capable to off-set the linear dependence of the gas exchange velocity on wind speed. Nevertheless, the majority of recently published regional to global-scale flux estimates did not take chemical enhancement into account and potentially underestimate CO_2 emission rates from inland waters. Second, our analysis revealed pronounced temporal variations of the fluxes, which can be related to changes in water and reservoir management. While recent research has mainly been focusing on constraining regional and global scale flux estimates and carbon budgets, our results indicate an urgent need also for assessing temporal trends of the fluxes caused by anthropogenic activities. Potential effects of human activities on CO_2 emissions from inland waters has been reviewed by (Cole et al. 2007; Regnier et al. 2013), but mainly consider the construction of reservoirs and not water and reservoir management practices that also can affect the total emission.

Supporting information

Dataset: Physico-chemical and hydrological parameters of the three studied reservoirs:

http://journals.plos.org/plosone/article?id=10.1371/journal.pone.0143381.

Acknowledgements

The data for this paper are available in the supporting information. We thank the Ministry of Water and Irrigation (Water Authority of Jordan) for providing water quality data.

Chapter 3 : Export of dissolved methane and carbon dioxide with effluents from municipal wastewater treatment plants

Zeyad Alshboul,[⊥] *Jorge Encinas-Fernández,*[‡] *Hilmar Hofmann,*[‡] *Andreas Lorke,*[⊥]

*zeyad@uni-landau.de

[⊥] University of Koblenz-Landau, Institute for Environmental Sciences, Fortstr.7, 76829 Landau, Germany

[‡] Environmental Physics, Limnological Institute, University of Konstanz, Mainaustr. 252, D-78464 Konstanz, Germany

Author contribution

Alshboul, Zeyad: Date collection - Data analysis – Experimental part and field measurement – Writing the manuscript

Submitted to Environmental Science and Technology, 2015, under review.

Chapter 4: Simple approaches to measure the diffusive flux of carbon dioxide and the rate of bubble release in shallow aquatic systems.

Zeyad Alshboul,,⊥ Celia Somlai-Haase,⊥ Christoph Bors,⊥ Andreas Lorke⊥*

*zeyad@uni-landau.de

⊥University of Koblenz-Landau, Institute for Environmental Sciences, Fortstr.7, 76829 Landau, Germany

Author contribution

Alshboul, Zeyad: Data analysis – Experimental part and field measurement – Writing the manuscript

Submitted to Limnology and Oceanography - Methods, 2016, under review.

Abstract

The quantification of CH_4 and CO_2 emissions from aquatic ecosystems is essential for improving the current understanding of the role of inland waters in the global and in regional carbon cycles. Existing flux measurement techniques are very limited in spatial and temporal resolution and often inappropriate for application in small and shallow waters. Here we present two simple and low cost tools for continuous measurements of diffusive fluxes and bubbles release rates, that are specifically designed for shallow aquatic systems. The performance of an automated flux chamber, which uses a built-in CO_2 sensor and a pump for periodic headspace ventilation, was assessed under field conditions. The long-term stability of the CO_2 sensor was tested during longer-term chamber deployments in a small pond. Based on these measurements, we also tested the possibility to obtain time series not only of the fluxes, but also of the concentration of dissolved CO_2 and the gas exchange velocity, using exponential curve fitting of the headspace gas concentration. Time-integrated estimates of the ebullition rate of CH_4 were measured with simple shallow-water bubble traps, for which we provide detailed do-it-yourself construction instructions. We further assessed the effect of the transparency of the chambers and bubble traps on the flux measurements. The strong variations of CH_4 and CO_2 fluxes in our measurements, which were mainly associated with spatial scales of a few meters and with diurnal time scales, emphasized the need for replicable and continuous flux measurement tools and the practicability of the approaches presented here.

Keywords: gas exchange, flux chamber, shallow water, ebullition

4.1. Introduction

Aquatic ecosystems are a major component of the global carbon cycle and are net sources of the atmospheric greenhouse gases (GHG) carbon dioxide (CO_2) and methane (CH_4) (Bastviken et al. 2011; Battin et al. 2009; Cole et al. 2007; Raymond et al. 2013). The existing global and regional-scale estimates of GHG fluxes from aquatic systems, however, are poorly constrained by direct flux measurements and process-based understanding of the environmental factors, which regulate the magnitude and the spatial and temporal variability of the fluxes. Particularly the emission rates from abundant shallow and small aquatic systems, like headwater streams, wetlands and ponds have been observed to be most variable (Hotchkiss et al. 2015; Panneer Selvam et al. 2014; Teodoru et al. 2015), but are rarely included in regional-scale sampling. Therefore, quantifying CH_4 and CO_2 emissions from these aquatic systems using robust and replicable techniques are key for constraining aquatic GHG budgets.

Flux chambers have been used for measuring CH_4 and CO_2 emissions in various aquatic ecosystems (Beaulieu et al. 2014; DelSontro et al. 2011; Natchimuthu et al. 2014). Typically, flux chambers are deployed manually resulting a very low temporal resolution of the flux measurements. Often measurements are restricted to singular flux estimates at selected spots resolving neither diurnal, synoptic nor seasonal scales of variability. Few technical solutions of automated flux chambers have been proposed to provide continuous flux measurements over time periods of hours to months in terrestrial as well as in aquatic systems (Duc et al. 2013; Hoffmann et al. 2015a; Koskinen et al. 2014).

In existing approaches for automated flux chambers, the chamber headspace is vented periodically by lifting the chamber body up to replace the headspace with ambient air. The lifting of the chamber, however, is associated with enhanced deployment effort, high energy

consumption and high risk of mechanical failure. Alternatively, the headspace of the flux chambers can be replaced by ambient air using a vacuum pump. The practical performance of pump-operated chambers, particularly in combination with recently described chambers utilizing cheap CO_2 sensors for headspace concentration measurements (Bastviken et al. 2015), has not been assessed before. Pump-operated automated chambers potentially provide a very powerful and cost-efficient approach for continuous and easily replicable flux measurements from shallow aquatic systems. While the performance of the low-cost CO_2 sensors has been tested extensively under lab conditions and during short-term chamber deployment (Bastviken et al. 2015), the effects of the extended range of variability of the environmental conditions during continuous and automated chamber measurements on the sensor performance requires an additional assessment under field conditions.

Chamber-based flux estimates are commonly obtained from linear regression of the concentration change in the headspace of the flux chamber. Continuous concentration measurements in the headspace also allow for resolving the exponential behavior of its equilibration with the water surface (Bastviken et al. 2004; Silva et al. 2015). Because the exponential fit provides not only the actual flux, but also the gas exchange velocity and the dissolved gas concentration, it potentially provides a more detailed insight into the processes, which control the temporal flux dynamics.

While CO_2 exchanges between water and the atmosphere by diffusion, CH_4 may also be transferred via ebullition (Bastviken et al. 2004; Campeau and Del Giorgio 2014). CH_4 emission by ebullition has been observed to be the predominant emission pathway in many aquatic systems (Bastviken et al. 2004; Maeck et al. 2013; Teodoru et al. 2015). Quantifying CH_4 emission by ebullition possesses a significant challenge due to the episodic characteristic of

bubble release and its spatial heterogeneity. Measuring ebullition rates in shallow water systems is even more challenging due to the lack of a straightforward sampling technique and most of the ebullition measurements were conducted in aquatic systems with water depth exceeding 15 cm (Crawford et al. 2014b; Wilcock and Sorrell 2008).

Here we present two simple and cost efficient tools for quasi-continuous measurements of (i) the diffusive flux of CO_2, and (ii) the volumetric bubble release rate in shallow aquatic systems. We provide detailed instructions for building pump-controlled automated flux chambers (AFC) with built-in CO_2 loggers and an assessment of their performance during longer-term deployments in a small pond. Based on these measurements, we also tested the possibility to obtain time series of the concentration of dissolved CO_2 and the gas exchange velocity from AFC flux measurements using exponential curve fitting. Time-integrated estimates of the ebullition rate were measured with simple and cheap bubble traps (BT), for which we provide detailed do-it-yourself construction instructions. As a specific aspect of shallow-water measurements, we further assessed the effect of the transparency of the AFC and of the BT on the temperature below the instruments and the fluxes of CO_2 and CH_4.

4.2. Materials and procedures

4.2.1. Automated floating chamber (AFC)

4.2.1.1. Principle and specifications of AFC

The AFC is an automated version of the low-cost flux chamber described in Bastviken et al. (2015). It comprises a dome-shaped chamber body with an open bottom area of 0.066 m^2 and a total height of 0.13 m, which is closed at the top. Floats at the outside of the chamber can be adjusted in height to ensure a 0.025 m deep submergence of the chamber edges, resulting in a

closed headspace with a volume of 0.0068 m^3. The partial pressure of CO_2 (pCO_2), temperature and relative humidity in the headspace are measured at adjustable intervals by a low-cost, battery-powered infrared sensor with data logger (ELG, Senseair, Sweden, see Bastviken et al. (2015) for more information),

To automate the flux measurements, the headspace zone of the chamber is vented after a specified time by pumping ambient air into the headspace. The internal pressure is adjusted through a one-way valve, which is attached to the top of the chamber housing (Figure 4-1 A and B). For pumping the air, we used a small diaphragm vacuum pump with a flow rate of 1.2 l min^{-1}. The pump is controlled by a microcontroller (Arduino, USA), which switches the pump on and off at predefined time intervals. The microcontroller and the air pump are powered by a 12 VDC battery, which can be mounted on top of the chamber body, or connected by a cable from the shore. Detailed technical specifications and system assembly instructions using off-the shelf components are provided in Appendix B.

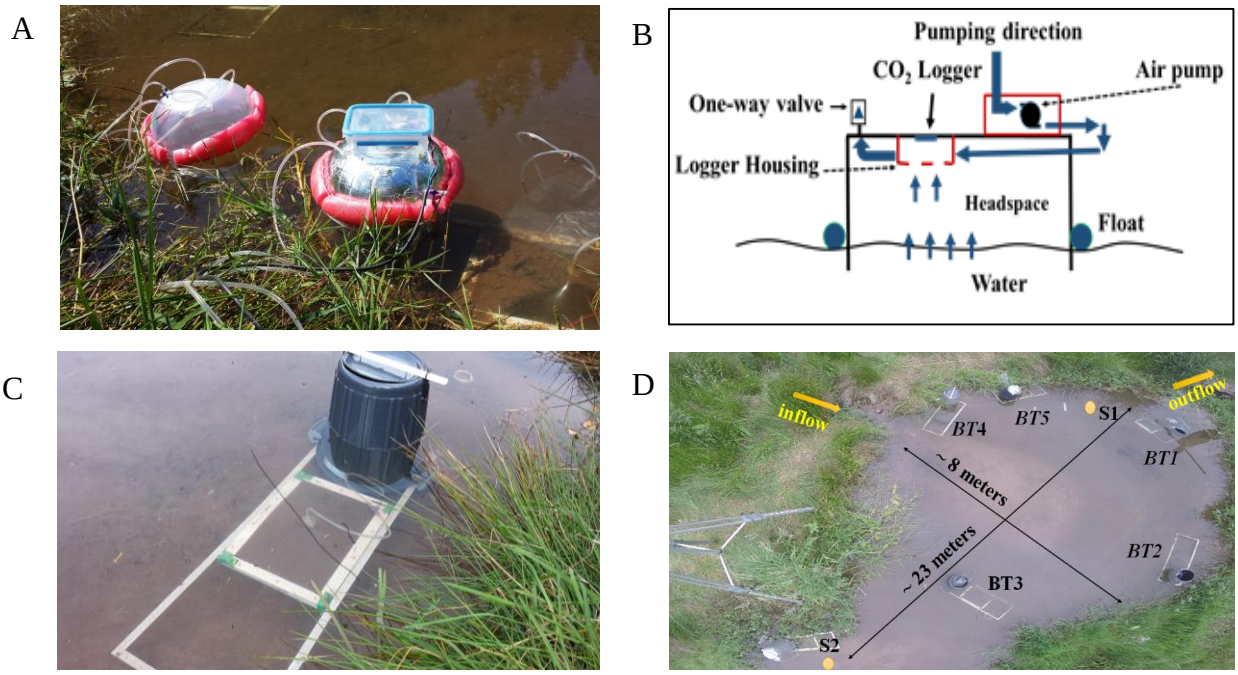

Figure 4-1: A) Pictures of the two AFC during deployment. The box on top of the right chamber contains the pump control unit. The tubes connect the chamber headspace with an external gas analyzer (not shown) B) Conceptual diagram of the main parts of the AFC. C) Picture of a deployed BT. The actual bubble trap is located in the center frame; the gasbag for gas collection is located below the dark-grey bucket in the upper part of the frame. D) Picture of the sampling site with the deployment locations of the AFC (S1 and S2) and of the BT (BT1-BT5). The black arrows indicate the dimensions of the pond.

4.2.1.2. Chamber flux estimates

The diffusive flux of CO_2 (fCO_2 in mmol CO_2 m^{-2} d^{-1}) can be calculated from the observed linear rate of change of pCO_2 in the chamber head space (S in ppm s^{-1}), the chamber

area covering water surface (A in m^2), and the chamber volume (V in m^3) (e.g., Campeau and Del Giorgio 2014):

$$fCO_2 = S\frac{V\,p}{A\,R\,T} \cdot 86400 \text{ s d}^{-1} \quad (4.1)$$

The number in the above equation is a conversion factor from seconds to days, T is temperature (K), p is the atmospheric pressure (kPa), and R is the universal gas constant (8.31 m^3 Pa mol^{-1} K^{-1}). Similarly, Eq. 4.1 can be used to estimate the flux of CH_4 (fCH_4) or that of other gases for which the linear increase of the mixing ratio in the chamber headspace was observed.

4.2.1.3. Gas exchange velocity

For a given difference between the headspace and the dissolved gas concentrations, the observed chamber flux can be related to the diffusive gas transfer velocity of (k_{CO2}) by inverting Fick's law of gas diffusion (Wanninkhof 1992):

$$fCO_2 = \alpha \cdot k_{CO2} \cdot k_H \cdot \left(pCO_{2,wat} - pCO_{2,HS}\right) \quad (4.2)$$

Where k_H is the Henry's constant adjusted for salinity and water temperature (Goldenfum 2011), and $pCO_{2,wat}$ and $pCO_{2,HS}$ are the CO_2 partial pressures of the dissolved gas in water and in the headspace, respectively. α is the chemical enhancement factor, which describes the enhancement of the diffusive transport by the conversion between carbonate or bicarbonate and CO_2 within the diffusive boundary layer at the air-water interface (Wanninkhof and Knox 1996). The magnitude of α depends on the carbonate equilibration kinetics, which is a function of pH, temperature and of the thickness of the water-side diffusive sublayer. α can be calculated using the formulas provided by Wanninkhof and Knox (1996). k_{CO2} is the specific gas exchange

velocity of CO_2, which is the quotient of the temperature-dependent diffusion coefficient of CO_2 in water and thickness of the water-side diffusive boundary layer (Lorke and Peeters 2006).

The dependence of the gas exchange velocity on the gas-specific diffusion coefficient and on temperature can be described by its dependence on the Schmidt number *Sc*, which is the ratio of the kinematic viscosity of water and the diffusion coefficient of the respective gas in water. Gas exchange velocities are typically standardized to *Sc*=600, which corresponds to the Schmidt number of CO_2 at 20°C. The standardized gas exchange velocity k_{600} can be estimated as:

$$k_{600} = k_{\mathrm{CO2}} \left(\frac{600}{Sc_{CO_2}}\right)^{-\mathrm{n}} \quad (4.3)$$

Sc_{CO2} is the Schmidt number of CO_2 at in-situ temperature and can be calculated using the empirical relationships provided by Wanninkhof (1992). Under moderately turbulent conditions, the exponent *n* was estimated to be 0.5 (Guérin et al. 2007; MacIntyre et al. 1995). The resulting standardized exchange velocity k_{600} is a function of boundary-layer turbulence (Lorke and Peeters 2006) and has been empirically related to wind speed, flow velocity and other bulk properties (Cole et al. 2010; Crusius and Wanninkhof 2003; Gålfalk et al. 2013).

Eq. 4.2 and 4.3 can also be applied to CH_4 and other gases, by using the corresponding values of the partial pressure, solubility and Schmidt number (α = 1 for CH_4 and other non-reactive gases). In particular, Eq. 4.3 can be rewritten to estimate the gas exchange velocity k_{CH4} from k_{CO2} or k_{600}:

$$k_{\mathrm{CH4}} = k_{\mathrm{CO2}} \left(\frac{\mathrm{Sc}_{CH_4}}{Sc_{CO_2}}\right)^{-\mathrm{n}} = k_{600} \left(\frac{Sc_{CH_4}}{600}\right)^{-\mathrm{n}} \quad (4.4)$$

This gas exchange velocity can be combined with measurements of $p\mathrm{CH}_{4,wat}$ to estimate the diffusive flux of CH_4 ($f\mathrm{CH}_4$, mmol CH_4 m^{-2} d^{-1}) using Eq. 4.2.

4.2.1.4. Chamber headspace equilibration

It is evident from Eq. 4.2, that the chamber flux, which is estimated from linear regression (Eq. 4.1), is equal to the gas flux at the free water surface, if the chamber headspace concentration is equal to the atmospheric gas concentration, and if the gas exchange velocity under the chamber is not affected by the presence of the chamber. In the closed chamber headspace, however, the CO_2 concentration is changing continuously with time and approaches the equilibrium concentration described by Henry's law (Figure 4-2), while the gas flux into the chamber is continuously decreasing towards zero. Application of Eq. 4.1 is therefore limited to short deployment times, where the effect of the changing gas concentration on the flux can be neglected.

An exact analytical solution for the temporal dynamics of the headspace gas concentration and corresponding partial pressure $pCO_{2,HS}$ can be obtained for a constant dissolved gas concentration (constant partial pressure $p\mathrm{CO}_{2,wat}$) and a constant exchange velocity k_{CO2} (Silva et al. 2015):

$$pCO_{2,HS}(t) = pCO_{2,wat} - \left(pCO_{2,wat} - pCO_{2,HS0}\right) e^{-Kt} \quad (4.5)$$

where $pCO_{2,HS0}$ is the initial CO_2 partial pressure in the headspace at the beginning of the chamber deployment (t=0) and the equilibration rate constant K is given by:

$$K = \alpha \cdot k_{CO2} \frac{k_H RTA}{V} \quad (4.6)$$

Fitting of measured time series of $p\mathrm{CO}_{2,HS}$ to Eq. 4.5 thus allows for estimating the enhanced gas exchange velocity $\alpha \cdot k_{\mathrm{CO2}}$ and the dissolved concentration in water (pCO_{2wat}) (Figure 4-2). Both parameters can then be combined to estimate the flux ($f\mathrm{CO}_2$) using Eq. 4.2.

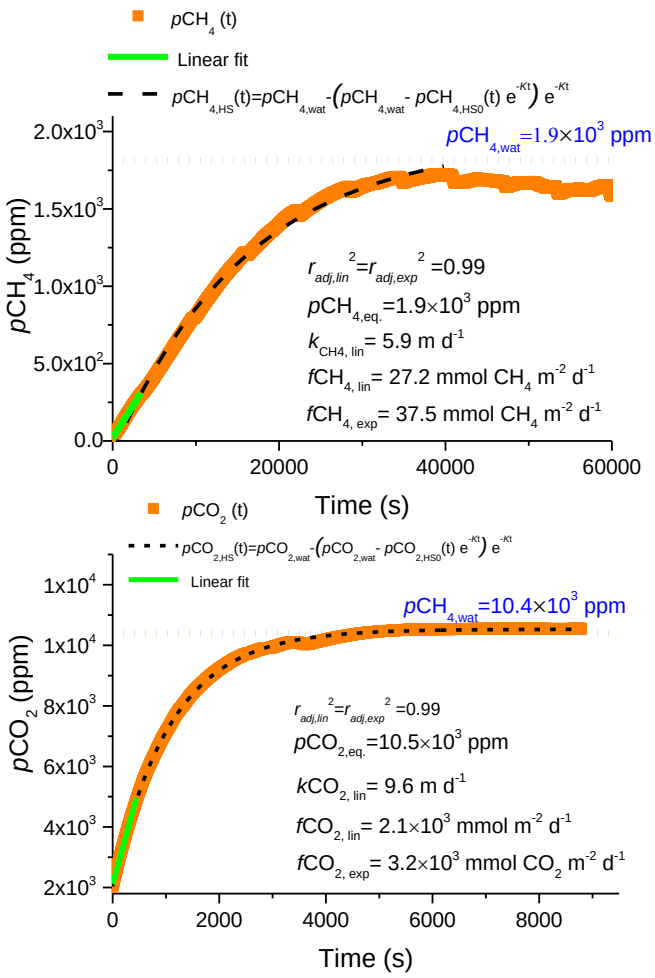

Figure 4-2. Example of measured pCH_4 (A) and pCO_2 (B) in the headspace of the chamber (orange) and the corresponding least-square fit to Eq. 14 (dashed black lines). The blue horizontal lines show the gas partial pressure estimated in a water sample using the headspace technique ($pCH_{4,wat}$ and $pCO_{2,wat}$) and the green lines show the linear fit for the data between 5 to 30 min after deployment start. The calculated fluxes using the linear ($fCH_{4,\ lin}$ and $fCO_{2,\ lin}$) and exponential regressions ($fCH_{4,\ exp}$ and $fCO_{2,\ exp}$) using Eq. 4.1 and Eq. 4.5, respectively, are shown. $kCH_{4,\ lin}$ and $kCO_{2,\ lin}$ were calculated from Eq. 4.2, and $r^2_{adj,lin}$ and $r^2_{adj,exp}$ are the adjusted coefficients of determination for the linear and exponential regression models, respectively.

4.2.2 Bubble traps for shallow waters

4.2.1. Design and specifications

When pCH_4 is measured continuously in the chamber headspace, the chamber-based flux estimates also include the flux contribution from ebullition (Bastviken et al. 2004; Duc et al. 2013). Unlike for CO_2, no suitable low-cost gas sensors are available for pCH_4. Therefore, the CH_4 fluxes cannot be measured directly with the AFC and the combination of a CO_2-based gas exchange velocity for CH_4 (Eq. 4.4) with discrete measurements of the dissolved CH_4 concentrations will underestimate the flux by neglecting ebullition. Measurements in various aquatic systems have shown, that at least at bubble emission hot spots, the diffusive flux can be of minor importance for the total emission rate (Maeck et al. 2014; Wik et al. 2013). Therefore, a low-cost and easily replicable method for measuring bubble fluxes in shallow water can help to constrain the currently very sparse measurements of methane emissions from inland waters.

Bubble fluxes can be estimated using inverted funnels as bubble traps, where the gas accumulation within the completely submerged funnel is observed either continuously (Maeck et al. 2014; Wilkinson et al. 2015) or by discrete sampling (Wik et al. 2013). In Appendix B we provide detailed descriptions and assembly instructions for low-profile bubble traps (BT), which are suitable for deployment in shallow waters with a minimum depth of 4 cm. A tube connector was mounted at the highest point of the dome-shaped BT, where it was connected via a 3-way stopcock to an inflatable gasbag with a maximum volume of 1.5 l. The stopcock was used for gas sampling and for avoiding gas collection during the BT deployment. The first BT design has a circular shape (0.096 m^2) and was made of non-transparent polyethylene material (NTBT). The

second BT was made of transparent acrylic sheets (TBT) with a rectangular shape (0.12 m^2). (See Appendix B for more information).

For sampling, the gasbag was removed and the captured gas volume was measured by emptying the gasbag with a graduated syringe. The ebullition rate (*ER* in mol CH_4 m^{-2} d^{-1}) can be calculated from the captured gas volume *V* (m^3), the bottom area of the BT *A* (m^2), and the length of the deployment period Δt (d).

$$ER = \frac{p\mathrm{CH_4}\, V\, p}{R\, T\, A\, \Delta t} \quad (4.7)$$

where pCH₄ is the mixing ratio of CH_4 in the collected gas, and *p* and *T* are atmospheric pressure and temperature at the time of the volume measurement, respectively.

4.3. Assessment

4.3.1. Objectives and overview

This study aimed to assess the following aspects related to the AFC and BT described above: (i) validate the performance of the AFC and of the build-in CO_2 logger during long-term automated chamber operation; (ii) compare linear-flux estimates with estimates of the gas exchange velocity and dissolved gas concentration obtained from continuous chamber headspace measurements using exponential curve-fitting; and (iii) test the effect of AFC and BT transparency on the measured fluxes.

Two different sets of field deployments of transparent and non-transparent AFC and BT were analyzed. At first, we monitored the AFC headspace concentration of CO_2 and CH_4 with a high accuracy using an external gas analyzer over a diurnal cycle. Subsequently, the AFC and BT were deployed autonomously for a period of 45 days of continuous flux observations. All

measurements were conducted in a small and shallow (12 to 44 cm water depth) pond, which receives its inflow from a spring (Figure 4-1) at Eusserthal Ecosystem Research Station (EERES, 49°15'03.5"N 7°57'06.1"E) near the city of Landau, in south-west Germany.

4.3.2. Measurements

4.3.2.1. Intensive short-term deployments

An intensive sampling campaign was conducted from 3 to 4 June 2015 using two AFC of different transparency, which were connected to two separate external gas analyzers (UGGA, Los Gatos Research Inc.). The AFC venting period was set to 5 min venting between 1-hour long flux measurement periods, resulting in 15 flux measurement cycles during the sampling period of 19 h. The first AFC is a non-transparent automated chamber (NTFAC), which was covered with aluminum tape. The chamber was equipped with a factory-calibrated internal CO_2 logger (log.1). The second AFC was made of transparent material (TAFC) and was not equipped with an internal CO_2 logger due to technical problems. Both chambers had five tube connectors attached to the top. Two of these connectors were used to circulate the chamber headspace through the gas analyzer, and one connector for the control unit (connected with the outlet of the air pump). While the remaining two connectors were used for a pressure adjustment (one-way valve) and a three-way stopcock for gas sampling, respectively.

The temperature of the sediment top layer was measured below the non-transparent material for three hours of deployment using a temperature sensor (TDIP15 PyroScience GmbH, Germany). The water temperature was measured continuously with a temperature logger (UTBI-001, Onset, USA) with an accuracy of ±0.2 ^{o}C and a sampling interval of 5 min.

Water samples collected from the pond were collected every six hours for estimating the partial pressures of dissolved CH_4 and CO_2 using the head space technique (Campeau and Del Giorgio 2014). The samples were collected near to the AFC, approximately 10 cm below the surface, and filled in a glass reagent bottle (borosilicate glass) of 1400 ml. The headspace was created in the bottle by replacing a volume of water by ambient air. The volume of the head space in the bottle was measured by measuring the volume of the replaced water using a graduated PVC cylinder (500±0.1 ml). The surface water concentrations of CH_4 and CO_2 values were then calculated based on the headspace ratio, using the in-situ measured ambient air CH_4 and CO_2 and water temperature at the sampling time and during equilibrium (Goldenfum 2011).

An additional comparison between the UGGA analyzer and a low-cost AFC CO_2 logger (log.2) was performed under lab conditions. The CO_2 logger was placed in a closed and gas tight chamber, which was connected with the gas analyzer in a closed loop. The gas in the chamber was continuously circulated and the CO_2 concentration was varied by injecting CO_2 standard gas.

Water temperature was also measured below two deployed BT (TBT and NTBT). The BT were sampled three times during the experiment for measuring the mixing ratio of CH_4 in the collected gas, and triplicate gas samples were transferred into crimped and brine-filled 12 ml borosilicate glass vials. The gas samples were analyzed by injecting them into the UGGA running in a closed gas-loop and the ebullition rate of CH_4 (ER) was calculated according to Eq. 4.7.

4.3.2.2. Long-term flux measurements and discrete sampling

We deployed two AFC (with internal CO_2 sensors log.1 and log.2) and five BT in the same pond between 16 April and 29 May 2015 (Figure 4-1). We used the same venting cycles for

AFC as in the intensive measurement campaign described above (5 min of headspace venting every 1 h of flux measurements), resulting in 213 and 413 flux measurements for the two chambers.

pCH_4 and pCO_2 of the pond water were measured weekly using the headspace method as described above. The BT were sampled approximately every week to measure volumetric bubble release rates according to the procedure described above.

4.3.2.3. CO_2 sensor performance

During the diurnal cycle, temperature and relative humidity in the chamber headspace varied from 10 to 32 °C and from 44 to 102 %, respectively. The CO_2 mixing ratios in the two AFC followed an identical diurnal pattern, with a difference of up 18 ppm (<4%) between the two chambers. The venting periods are clearly visible in the recorded time series and venting generally caused a reduction of temperature, *RH*, pCO_2, and pCH_4 in the headspace of the chambers (Figure 4-3).

In comparison to the UGGA gas analyzer, the low-cost CO_2 sensor consistently overestimated pCO_2 by up to 40% for log.1 and up to 30% for log.2. We used multiple linear regressions to relate pCO_2 measured by the gas analyzer (pCO_{2UGGA}) to that measured by the sensors (pCO_{2meas}), temperature (*T*) and relative humidity (*RH*) in the chamber headspace:

$$pCO_{2,\mathrm{UGGA}} = A + B \cdot pCO_{2,meas} + C \cdot T + D \cdot RH \quad (4.8).$$

Consistent, but sensor-specific regression coefficients were observed for *RH*<99% (Figure 4-4, Table 4-1), while the slope varied for *RH*>99%. Because the nominal operating conditions of the sensors are specified as non-condensing, we excluded all data for which *RH*≥99 % from the analysis and we corrected the remaining sensor readings according to Eq. 4.8. The

residual difference between the corrected sensor readings and the gas analyzer measurements ranged between -16 and 13 % and from -1 to 0.7 % for log.1 and log.2, respectively (Figure 4-3 and Figure 4-4).

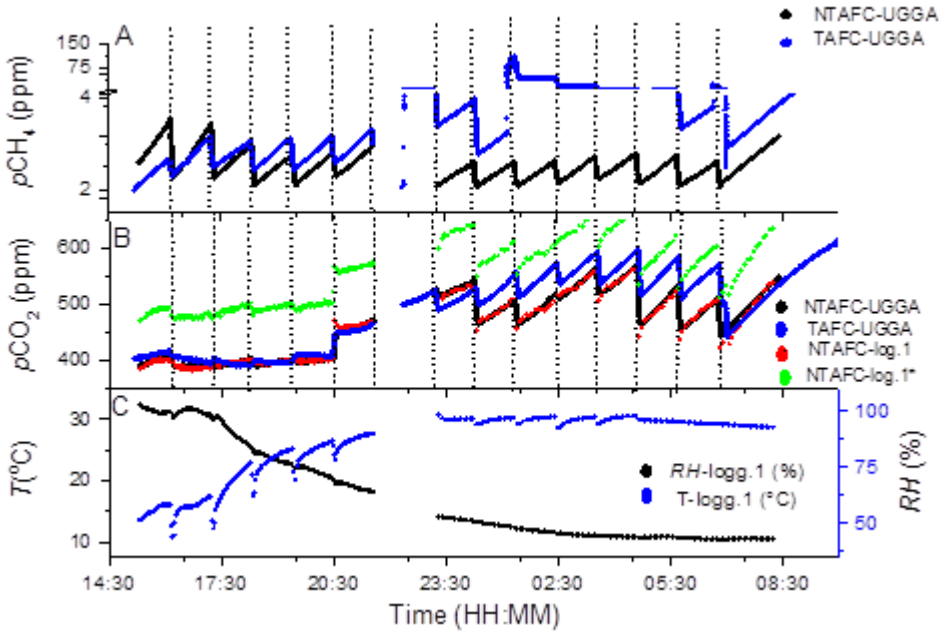

Figure 4-3. Measured pCH_4 and pCO_2 in the headspace of the TAFC (blue) and NTAFC (black) during the intensive short-term deployment. A) NTAFC-UGGA and TAFC-UGGA denote to continuous measurement of pCH_4 in the headspace of the NTAFC and TAFC with the gas analyzer. B) Continuous measurements of pCO_2 in the headspace of the NTAFC and the TAFC measured by the gas analyzer (NTAFC-UGGA and TAFC-UGGA), and by the internal CO_2 logger (NTAFC-log.1*). The logger data were corrected using Eq. 4.8 (NTAFC-log.1). C) Simultaneous measurements of temperature (black) and RH (blue) in the headspace of NTAFC. The dotted vertical lines in A) and B) indicate venting times of the chamber headspace.

Table 4-1. Coefficients for multiple linear regression of pCO_2 measured by two different CO_2 loggers as a function of temperature and RH (see Eq. 4.8). *n* denotes to number of pCO_2 measurements with RH<99 %, and Upper-95 % represents the upper limit of the data range.

		A (ppm)	*B (-)*	*C (ppm (°C)$^{-1}$)*	*D (ppm)*
log.1	*Value*	*69.48*	*0.92*	*-2.01*	*-1.01*
r^2=0.99	*p-value*	*<0.05*	*<0.05*	*<0.05*	*<0.05*
n=271	*Upper-95%*	*92.5*	*0.9*	*-1.6*	*-0.9*
log.2	*Value*	*-34.35*	*0.83*	*-0.04*	*-0.27*
r^2=0.99	*p-value*	*0.4*	*<0.05*	*0.9*	*0.4*
n=63	*Upper-95%*	*50*	*0.8*	*2.1*	*0.4*

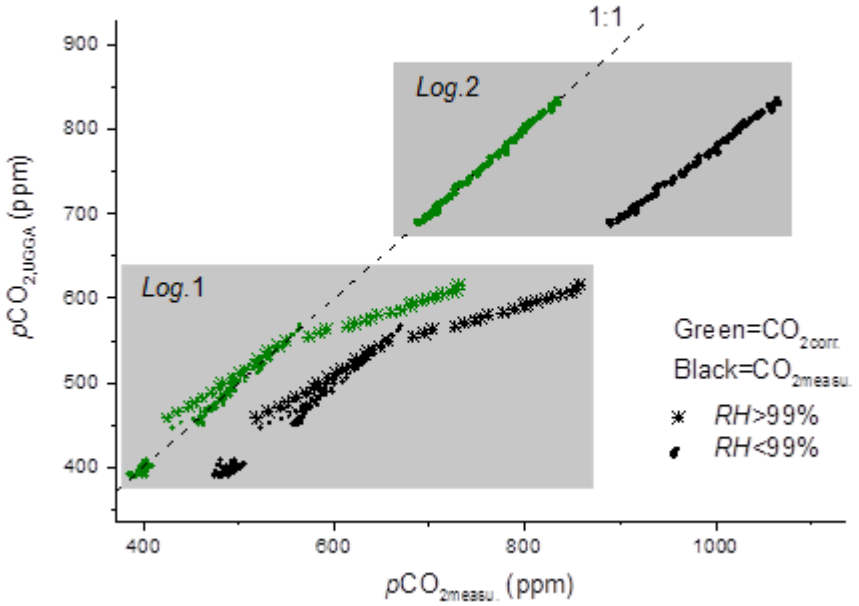

Figure 4-4. Comparison of pCO_2 in the AFC measured by the gas analyzer ($CO_{2,\ UGGA}$) (black) and by the internal CO_2 loggers ($CO_{2,measu.}$): log.1 (during the intensive field measurement, lower gray box) and log.2 (lab experiment, upper gray box). The corrected values of $pCO_{2,measu.}$ using Eq. 4.8 are shown in green; stars denoted values for which RH was >99 %.

4.3.3. AFC flux measurements

We obtained continuous time series of the chamber headspace CO_2 mixing ratios during automated chamber operation for two AFC for partially overlapping periods of 21 and 23 days, respectively (Figure 4-5). The removal of all samples with *RH*>99 % resulted in 213 (47 %) and 413 (59 %) valid CO_2 flux measurement intervals. Time series of hourly CO_2 flux estimates were obtained by linear regression of the temporal change of pCO_{2HS} using Eq. 4.1 (Figure 4-6) and all of regression of variation (r^2) are higher than 0.93. The first 5 min of each flux measurements interval were excluded from the regression to allow for headspace pressure adjustment after each venting period (Figure 4-5).

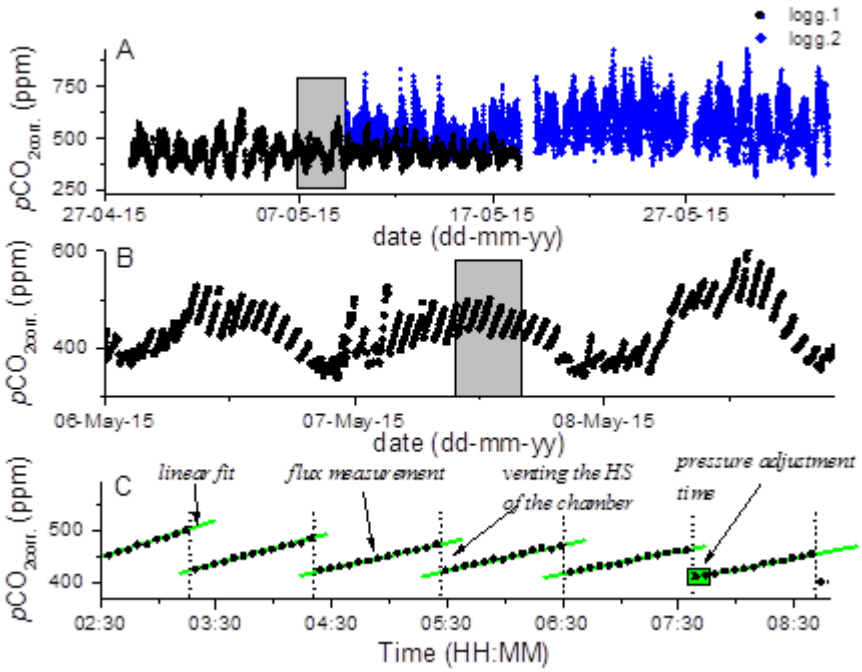

Figure 4-5. A) Continuous measurements of pCO_2 in the chamber headspace of two AFC (log.1 and log.2). The grey box shows the data range which is shown in B) at greater detail. C) Same as B) for the range indicated by the grey box. The vertical dashed

lines indicate the venting times of the chamber headspace; green lines show linear fits of the data during the individual flux measurement periods.

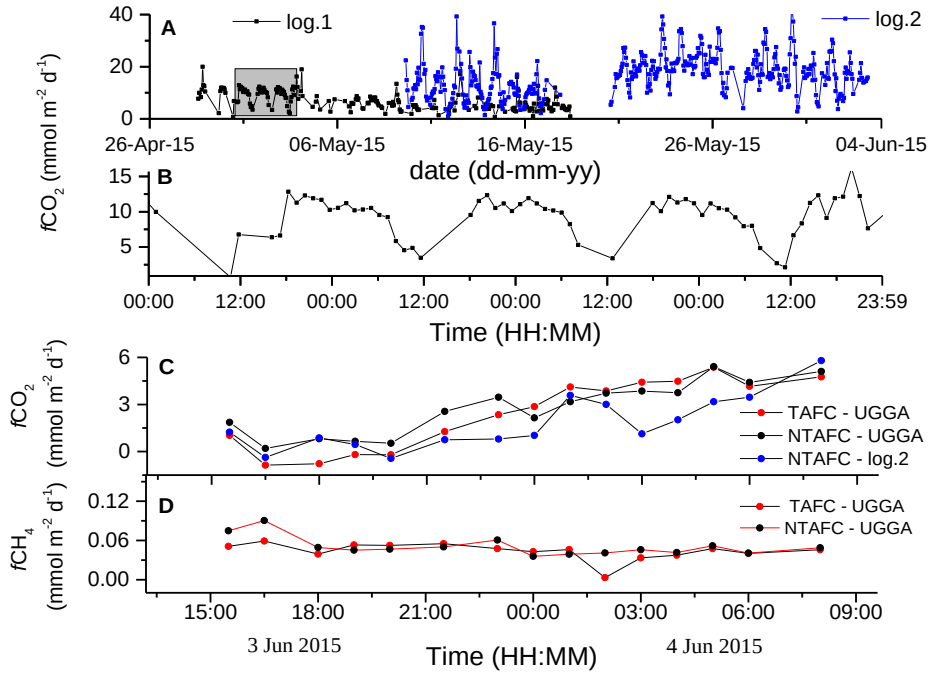

Figure 4-6. A) Time series of CO_2 fluxes (fCO_2) estimated from two AFC (log.1 and log.2) during the long-term deployment (cf. Figure 4-5). B) Example of diurnal variation of fCO_2. The time period shown here corresponds to the grey box in A). C) fCO_2 measured by gas analyzer in a TFAC (red) and NTAFC (black) and by log.1 in TAFC (blue) during the intensive short-term deployment. D) fCH_4 measured by UGGA in a NTAFC (black) and TAFC (red) during the intensive short-term deployment.

All water samples were saturated with respect to atmospheric CH_4 and CO_2 and the measured concentrations of dissolved CH_4 and CO_2 were highly variable within the sampling area (Table 4-2). Mean dissolved CO_2 varied over more than three order of magnitude across the

system, while dissolved CH_4 varied over two orders of magnitude. Dissolved CH_4 and CO_2 were statistically different between the sampling points (ANOVA, $p<0.05$). CO_2 was significantly correlated to CH_4 (*slope*=0.005 µM CO_2 (µM CH_4)$^{-1}$, $p<0.05$). This relationship between CH_4 and CO_2 has been observed at various aquatic ecosystems (Billett and Harvey 2013; Billett and Moore 2008; Campeau and Del Giorgio 2014; Richey et al. 1988). We observed a significant relationship between water temperature and CO_2 (*slope*=3.5 µM CH_4 (^{o}C)$^{-1}$, r^2=0.7, $p<0.05$) and CH_4 (*slope*=0.04 µM CO_2 (^{o}C)$^{-1}$, r^2=0.73, $p<0.05$) (Appendix C). A temperature dependence of the concentration of both gases has been observed in various aquatic environments (Dinsmore et al. 2013a; Dinsmore et al. 2013b; Roehm et al. 2009) and CH_4 (Campeau and Del Giorgio 2014; Huttunen et al. 2003).

Table 4-2. Summary of the continuous CH_4 and CO_2 flux measurement (fCH_4 and fCO_2), water temperature (T) and partial pressure of dissolved gases (pCH_4 and pCO_2). log.1 and log.2 refer to the two AFC during the long-term flux measurement (16 April and 29 May 2015). The data measured during the intensive short-term flux measurement are listed separately for the gas analyzer (UGGA) and the build-in CO_2 sensors (log.1) for transparent (TAFC) and non-transparent (NTAFC) chambers. All data are represented as mean±SD and values in parentheses indicate to the range of observations.

	***f* CH$_4$**	***f*CO$_2$**	***T***	***p*CH$_4$**	***p*CO$_2$**
	mmol m^{-2}d^{-1}	**mmol m^{-2} d^{-1}**	**(^{o}C)**	**ppm**	**ppm**
log.1 (16-29 April 15)		7.0±3.6 (0.7 - 20)	10.7±1.8 (7 - 24)	133±76 (46-246)	9200±200) (600 – 12000)
log.2 (16-29 May 15)		15±7.6 (0.8- 41)	17.8±5 (12.8-24.5)	354±28 (326-392)	2600±1500 (1200 – 4200)
TAFC-UGGA (3-4 June 15)	0.04±0.01 (0.003 -0.06)	2.4±2.2 (-0.86 - 5.4)			
NTAFC-UGGA (3-4 June 15)	0.05±0.01 (0.04 - 0.09)	2.8±1.7 (0.2 - 5.4)	17±3 (14.4 -20.2)	340±6 (336-345)	2500±27 (2400 - 2500)
NTAFC-*log.1* (3-4 June 15)	0.06±0.05 (-0.01-0.14)	1.8±1.7 (-0.4 - 5.8)			

All flux estimates were positive, i.e. the water surface was a persistent source for atmospheric CO_2 during the entire deployment period (Figure 4-6 A) with a consistent diurnal pattern during most of sampling days with higher fluxes at night (Figure 4-6 B). The diffusive CO_2 flux differed significantly between the two AFC (ANOVA, $p<0.05$). The mean diffusive CO_2 flux that measured by the two chambers differed by a factor of two (Table 4-2). We observed a significant relationship between water temperature and CO_2 flux. During the intensive measurements campaign, the fluxes estimated using pCO_2 measurements from the gas analyzer did not differ significantly from those estimated from the CO_2 logger data (Table 4-2).

4.3.4. Exponential curve fitting

Least-square fitting of the AFC headspace concentration to Eq. 4.5 resulted in equilibration times $1/K$ (Eq. 15) between 3.5 and 12 hours. $pCO_{2,wat}$ estimated from exponential curve fitting showed only weak agreement with the dissolved concentration measured in discrete water samples during the weekly sampling (Figure 4-7 A), with differences between both estimates of up to 53 %. Similarly, also the gas exchange velocities k_{600} derived from Eq. 4.6 ($k_{600,\ exp}$) and from Eq. 4.2 ($k_{600,\ lin}$) differed strongly (Figure 4-7 B). The differences were not systematic and can most likely be attributed to the short measurement period (1 and 1.5 h) in comparison to the relatively long equilibration time of the chamber. Due to the short flux measurement period of AFC, the increase of the gas partial pressure in the chamber headspace was mostly linear. The accuracy could probably be enhanced by prolonging the flux measurement intervals in between the venting periods of the AFC. However, this would have resulted in increasing humidity in the chamber headspace and therewith in the potential removal of data for which $RH>99$ %.

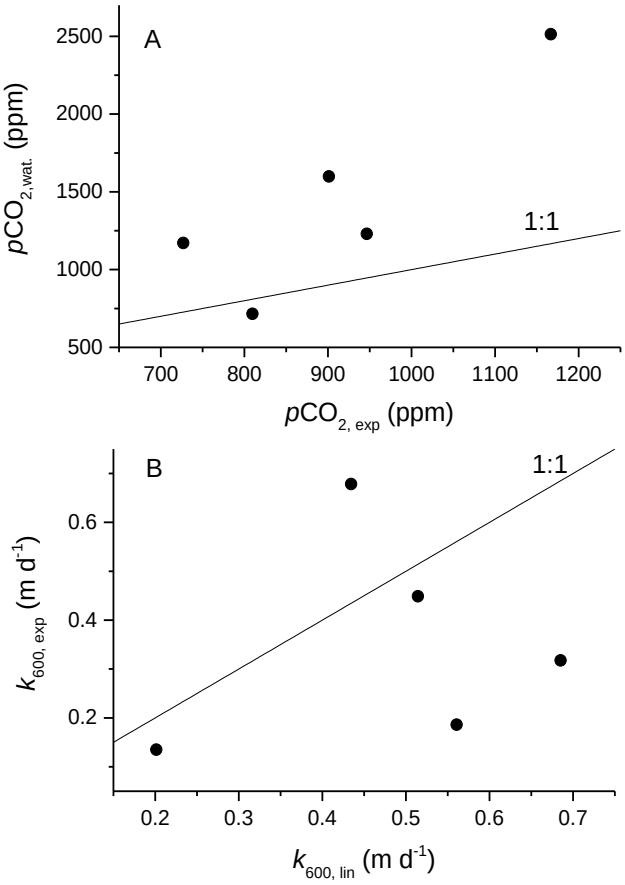

Figure 4-7. A) Comparison between $pCO_{2,wat}$ estimated from exponential curve fitting (Eq. 4.5) and the measured partial pressure in water samples. B) Comparison of standardized gas exchange velocities estimated from measured fluxes and water samples (k_{600_lin}) and that obtained from exponential curve fitting ($k_{600,\ exp}$). The solid black lines indicate a 1:1 relationship between both estimates.

Disagreement between linear and exponential regressions of measured gas partial pressures in chamber headspaces for short measurement periods has been observed in several studies (Forbrich et al. 2010; Kutzbach et al. 2007; Nakano et al. 2004; Pirk et al. 2015; Riederer et al. 2014). Using statistical criteria, Forbrich et al. (2010) found that the linear regression

model is preferable under these conditions. For long-term chamber deployment (3 to 24 h), however, Bastviken et al. (2015) have found good agreement between chambers-based estimates and directly measured pCO_2 in water.

4.3.5. Ebullition rates

The gas volumes, which were collected at the weekly sampling intervals of the bubble traps (BT1-BT5, Figure 4-1) varied strongly in time and among sites and ranged between 0 and 840 ml. The CH_4 mixing ratio was measured in naturally released bubbles and varied between 30 to 39 % with a mean value of 33.9±3.2 %. The corresponding ebullition rates (Eq. 4.7) ranged between 0 and 32.5 mmol CH_4 m^{-2} d^{-1} with a mean value 3.7±7.2 mmol CH_4 m^{-2} d^{-1} (Figure 4-8). Ebullition rates exceeded the diffusive gas flux measured in the two AFC during the intensive campaign by a factor of 80 (Figure 4-8). We observed ebullition events also during the intensive short-term deployment of TAFC, which are discussed below.

Strong temporal variability of ebullition rates has been observed in various aquatic systems (Crawford et al. 2014b; Varadharajan et al. 2010; Wilkinson et al. 2015) and has been related to variations in hydrostatic pressure and other physical forcing mechanisms, which trigger the formation and the release of gas bubbles from the sediment (Deshmukh et al. 2014; Maeck et al. 2014; Wik et al. 2014). The strong spatial heterogeneity of methane ebullition, which was observed in the same pond at the meter-scale, can most likely be attributed to spatial variations of the deposition of fine sediments (cf. the photograph shown in Figure 4-1D), which has been shown to be a primary driver for methane ebullition at larger scales (Maeck et al. 2013; Natchimuthu et al. 2015). The simple BT design described in the Appendix B could be approved to be practicable for measuring time-integrated ebullition rates in shallow aquatic systems. Our

findings further demonstrate the need for low-cost, and therewith easily replicable instruments, which allow for simultaneous measurements at various sampling sites.

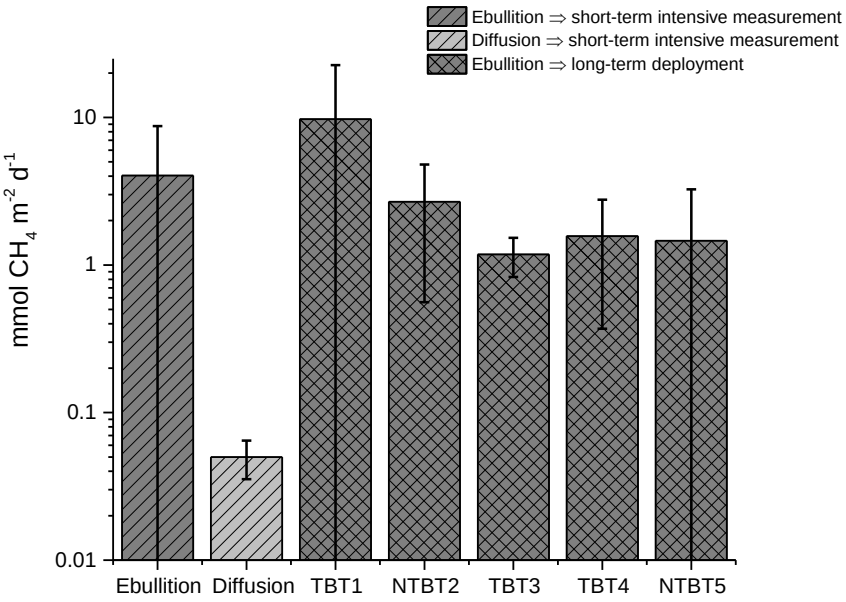

Figure 4-8. Measured CH_4 flux by diffusion and by ebullition for different deployment intervals. Dark-gray columns denote to the CH_4 ebullition rates and white-gray columns represent the diffusive CH_4 flux data during the intensive campaign. The columns labeled as BT1-BT5 represent CH_4 ebullition rates measured during the long-term deployments of transparent (TBT) and non-transparent (NTBT) bubble traps (cf. Figure 4-1 for deployment information).

4.3.6. Effects of AFC and BT transparency

We observed no significant difference between the temperature in the headspace of the TAFC (13.2±3.4 ºC) and the NTAFC (13.9±3.8 ºC) (Table 4-2). There was also no statistical difference between the water temperatures below the TBT and NTBT (ANOVA, p>0.0.5). However, the temperature of the sediment top layer was affected by the transparency of both chambers and bubble traps. The temperature difference between the sediment under the transparent material and under the non-transparent material of AFC and BT increased with the deployment time and reached ~1 °C after three hours of deployment. There was no significant difference between the CH_4 and CO_2 diffusive fluxes measured by TAFC and NTAFC (ANOVA, p>0.0.5) (Table 4.2). In addition, the ebullition rates measured by the TBT and the NTBT did not differ significantly. The lack of statistical significance, however, could be related to the small sample size and the large spatial heterogeneity of the observed fluxes (Figure 4-8). Although, without statistical significance, three CH_4 ebullition events were observed in the TAFC, while no ebullition was observed in the NTAFC during the intensive campaign (Figure 4-3).

CH_4 production rates in aquatic sediments are temperature dependent and radiative energy input and sediment temperature have been demonstrated to be primary drivers for methane ebullition (Natchimuthu et al. 2014; Wik et al. 2014; Wilkinson et al. 2015). Our results suggest that chamber and bubble trap transparency have negligible effects on the measurement of diffusive fluxes of CH_4 and CO_2, but potentially have an effect on ebullition rates and therewith on the total flux of CH_4 in shallow aquatic systems.

4.4. Comments and recommendations

Simultaneous deployment of AFC and BT provided quasi-continuous estimates of diffusive fluxes of CO_2 and ebullition rates of CH_4 in a shallow pond. The current design of the pump-operated AFC was applicable only for anchored chamber deployments because we used an external power source. Anchored chambers can generate additional turbulence if they are deployed in running waters, which can significantly overestimate the resulting fluxes (Lorke et al. 2015). Application of the AFC is therefore restricted to lentic ecosystems. In principle, the AFC can be modified to allow for freely drifting deployments, e.g. on lakes or larger ponds, by using a light-weight rechargeable LiPo battery. For instance, the battery proposed by Duc et al. (2013), can power the AFC for about two days of continuous flux measurements.

In the current application, the flux measurement periods were limited by the increasing relative humidity in the chamber headspace, which impeded the use of the CO_2 sensor for continuous concentration measurements. The short measurement periods and frequent venting of the chamber headspace resulted in a large uncertainty of the estimates of dissolved gas concentration and gas exchange velocity from exponential curve fitting. The AFC could be modified for faster equilibration times by increasing the surface area to volume ratio of the chamber body. This can be accomplished by changing the chamber geometric shape to a more conical body.

In shallow waters, the solar radiation can reach the sediment surface and non-transparent chambers and bubble traps potentially modify the physical conditions and the gas fluxes. The main purposes of using non-transparent materials for the chambers is the avoidance of overheating, and chambers are typically covered with reflecting aluminum foil. However, we did not observe a significant difference between the temperature in the chamber headspace of TAFC

and NTAFC. Although, we did not observe significant differences between the measured diffusive fluxes of CH_4 and CO_2 in TAFC and NTAFC, the observed change of sediment temperature suggests a potential bias of CH_4 ebullition rates estimated using non-transparent materials.

Acknowledgement

This study was financially supported by the Sustainable Water Management Program (NaWaM) of the German Academic Exchange Service (grant number: A/12/91768) and by the German Research Foundation (grant number: LO 1150/9).

Supporting Information

Appendix B provides further detail on methods and assembly instructions for the AFC and the BT. appendix C provides additional results.

Chapter 5 : Continuous Seasonal River Ebullition Measurements Linked to Sediment Methane Formation

Jeremy Wilkinson,,† Andreas Maeck,‡ Zeyad Alshboul,† and Andreas Lorke†*

* wilkinson@uni-landau.de.

†University of Koblenz-Landau, Institute for Environmental Sciences, Fortstr. 7, 76829 Landau, Germany

‡Senect GmbH & Co. KG, An 44 - No. 11, 76829 Landau, Germany

Published in **Environmental Science and Technology,** 2015,
DOI: 10.1021/acs.est.5b01525

This chapter is based on the following journal publication (Wilkinson et al. 2015).

Wilkinson, J., A. Maeck, Z. Alshboul, and A. Lorke. 2015. Continuous Seasonal River Ebullition Measurements Linked to Sediment Methane Formation. Environ. Sci. Technol. **49:** 13121-13129.

Author contribution

Alshboul, Zeyad: Sediment incubation experiment

The readers are kindly asked to read the published paper following this link:

http://pubs.acs.org/doi/full/10.1021/acs.est.5b01525

Summary and discussion

Our study of the three water reservoirs in Jordan presents estimates of CO_2 in a region where few biogeochemical studies exist and provides rare snapshot of how reservoirs in arid and semi-arid regions act in terms of CO_2 emission. This study show that the reservoirs were supersaturated and acted as net sources of CO_2 to the atmosphere, and the highest emissions were registered for a newly established reservoir (Al-Wihdeh Dam). Dissolved partial pressure of CO_2 was continuously increasing with time at the newly established reservoir (established in 2006), and we observed continuous decreasing in dissolved partial pressure of CO_2 for the old reservoirs King Talal Dam and Wadi Al-Arab Dam (>20 years). This long-term decrease in CO_2 was associated with decreasing in water alkalinity. However, we found significant relationship between water alkalinity and salinity that can be linked to the removal of freshwater, e.g. the decreasing contribution of spring water, which is reflected by salinity changes (Jiang et al. 2014; Lee et al. 2006).

CO_2 flux was chemically enhanced and varied widely among reservoirs. The highest mean CO_2 flux was registered for the newly established reservoir and negative fluxes were observed during the initial filling of this reservoir. Mean CO_2 flux for the two old reservoirs are comparable to the global-mean estimate for lentic ecosystems of 1 g CO_2 m^{-2} d^{-1} (Raymond et al. 2013), while mean CO_2 flux of the newly established reservoir exceeded this value more than 5 times. This was higher than the global mean flux of reservoirs younger than 20 years, and it was comparable to the new established reservoirs in tropical and boreal zones (Barros et al. 2011). In contrast to these reservoirs, we did not observe continuous decrease in CO_2 flux in the newly established reservoir during the first year of operation. This because the newly established reservoir did not reach its first year of filling and the biomass is still flooding. CO_2 flux from the

old reservoirs decreased during the observation period and this can potentially be caused by the declining availability of degradable carbon in the flooded biomass and soil organic matter. Water retention time and salinity decreased in these reservoirs indicate that also changes in water management and water quality may contribute to the observed decline in CO_2 flux. The surface area changes are caused by the hydrological characteristics of the three reservoirs and is strongly linked to the water management practice by changing the balance between water inflow and outflow.

Not only reservoir age, eutrophication and primary production can have strong effects on the carbon budget. This suggest a strong diurnal variation of CO_2 flux that can bias the annual estimated flux. However, our estimates are based on monthly sampling restricted to day time and based on monthly sampling routine. High sedimentation rates are expected to be exist for the three reservoirs and this was apparent from the reported sedimentation rates for one of these reservoirs. High sedimentation rate is expected to yield high CH_4 emission rates. Our flux estimates are subject to uncertainty arising from uncertainties of the measured input data, limited spatial and temporal resolution of these data as well as the uncertainty related to the gas exchange velocity. One of the studied reservoirs received large portion of its inflow from effluent of WWTPs. Effluent of WWTPs can export organic and inorganic carbon to receiving water systems, and can change the physical and chemical properties of these systems.

Our results show that the effluents of WWTPs export an additional CH_4 and CO_2 load to the receiving streams and have higher concentrations than that of upstream sites through most of the monitoring period at nine WWTPs in Germany (Figure 3-1). The exported CH_4 load to the surrounding streams accounts for only a small fraction (0.02%) of the total estimated CH_4 emissions of the WWTPs. However, the results show that this small fraction is strongly

enhancing CH_4 and CO_2 in the receiving stream waters. Based on the total number of the WWTPs in Germany and total length of the rivers and streams, the average density of WWTPs has been estimated to be one treatment plant every 12.7 km. Based on the estimated decay length of CH_4 and CO_2, rivers and streams in highly populated areas can be anthropogenically influenced by the inputs of WWTPs in terms of CH_4 and CO_2 emissions. Our results show the importance of include effluents waters for any future attempts to estimate regional and global CH_4 and CO_2 for inland water systems. We found that CH_4 concentrations in effluents are related to the organic load of the wastewater inflows (Figure 3-4), this provides an empirical basis for future estimates of carbon fluxes from inland waters. We found an exceptional high specific export rate of CH_4 at Bellheim WWTP, which receives about ~20% of its inflow from surrounding breweries. We were not able to investigate the exact factors and processes that cause this exceptional high values, and further studies should aim at explaining the drivers for this high rates of exported CH_4 from this plant. High uncertainty is related to the estimated CH_4 emission from WWTPs, and there are no previous studies measured gross CH_4 emission from WWTPs in Germany.

Moreover, the results are based on monthly measurements and may have missed large emission events. CH_4 emission by ebullition is not included in this study for stream sampling points, and this can lead to a large uncertainty for our CH_4 emission estimates. Moreover, the diel variation of dissolved CH_4 and CO_2 and their fluxes of effluents and their receiving streams have not been covered. The diel variation has not been included for estimating CO_2 flux at water reservoirs in Jordan either, and we expect a significant uncertainty related to the input parameters and the gas exchange velocity. We don't have direct measurements of dissolved CO_2 and flux for these reservoirs and this can lead to a large uncertainty in our estimates.

Producing direct flux measurements with high spatial and temporal resolution of CH_4 and CO_2 is an urgent need for future attempts to constrain contribution of carbon sources and sinks. Higher temporal resolution flux measurements can boost the understanding of interactions between emissions and controlling factors. Simple and cost-efficient tools have been modified for measuring continuous diffusive CO_2 fluxes and bubble release rate for shallow water systems. The results showed that the automated flux chamber can cover the diurnal variation of CO_2 flux and suitable for long deployment times. We tested and validated the CO_2 logger and the automated chamber by the gas analyzer. We also observed spatiotemporal variability of CO_2 flux within a small area. This indicates that spatial and temporal variation may also exist in the Jordan's water reservoirs and further studies may consider this variability. High spatial variability of CH_4 ebullition rates measured by the bubble traps was observed, and the mean CH_4 flux by ebullition exceeded that by diffusion. However, CH_4 emission by ebullition is very important in any attempt to estimates CH_4 emission from shallow waters.

We have tested the effect of the material transparency used for the automated chamber and the bubble traps. The results revealed a considerable effect from material transparency on the temperature of the sediment top layer in shallow waters due to prevention of solar irradiance reaching the sediments surface beneath the instrument. Non-transparent material can reduce the gained energy at the sediment-water interface. We observed a temperature reduction by one degree at the sediment top layer after three hours of deployment of non-transparent bubble trap. Temperature change may significantly modify CH_4 production rate. This was apparent from the significant relationship between temperature and CH_4 production for the incubated River Saar sediment samples, and this relationship has also been observed at various aquatic ecosystems (Duc et al. 2010; Wik et al. 2014; Yvon-Durocher et al. 2014). However, based on the obtained

correlation between temperature and CH_4 formation from the Saar sediment cores incubation experiment, a reduction in sediment temperature by one degree can reduce CH_4 formation ~13%. Based on the temperature dependency of methane formation, high methane formation rate is expected in warm climates, e.g. subtropics. However, reservoirs in Jordan are located in the subtropical zone and expected to yield large amount of CH_4.

Within this study, we presented new examples of spatial and temporal variation of CH_4 and CO_2 fluxes from inland waters. However, CH_4 and CO_2 fluxes can spatially vary within a water system (e.g. the observed spatial variation of fluxes for both gases in the shallow pond at Eusserthal research station) and among different water systems (e.g. the observed spatial variation of flux among the three water reservoirs in Jordan and among the receiving streams of the nine WWTPs). The spatial variation of CH_4 and CO_2 fluxes in inland waters can be caused by physical, chemical and hydrological conditions (e.g. CO_2 flux variation among the three water reservoirs in Jordan), but it can also be caused by the anthropogenic sources of both gases (e.g. downstream of the receiving streams of effluents at the nine WWTPs). However, temporal variation of CH_4 and CO_2 flux has been noticed for different time scales, e.g. diel variation that observed in the shallow pond at Eusserthal Research Station and the monthly variation that observed in the receiving streams and the three water reservoirs in Jordan. We presented two simple and low-cost models of measuring bubble release rate and continuous CO_2 flux from shallow waters. The affordable cost of these tools bring the opportunity of using these tools for large spatial scale and high resolution CO_2 flux measurements. This in role will reduce the uncertainty related to the discrete and single-point sampling strategies.

Outlook

This study discussed several topics related to emission patterns of CH_4 and CO_2 from inland waters and several issues, which relate to current global emission estimates. For instance, the study provided CO_2 emission estimates for surface waters in a semi-arid region and showed how these systems are affected by water management practices. We highlighted the importance of including such freshwater systems in future emission estimates. The study showed the role of WWTPs in transferring a substantial amount of CH_4 and CO_2 into the receiving streams, which has not been considered in any previous global or regional study concerning the emissions of both gases from inland waters. By studying the status of these water systems (semi-arid reservoirs and receiving streams at the nine WWTPs), we have discussed the uncertainty margin that is related to their variability in time and space. However, several knowledge gaps remain and need to be studied such as:

(i) CO_2 flux values from the three drinking water reservoirs in Jordan are not based on direct measurements and did not include high spatial and temporal resolution data. In addition, CH_4 flux was not included for these reservoirs and is expected to be high. Further studies which aim at a complete greenhouse gas budget of these reservoirs should cover large spatial and temporal measurements of dissolved CH_4 and CO_2 and their fluxes as well as the processes, which regulate the variability of the physico-chemical characteristics of these reservoirs. Our proposed tools e.g. the automated flux chamber can be used for continuous flux measurements and the automated bubble trap, presented by (Maeck et al. (2014)) can be also used. The effect of WWTPs discharge should be taken into account for further studies aiming to identify carbon sources for these reservoirs.

(ii) The organic load of the inflow wastewater varied among the nine WWTPs during the study period. Further, dissolved CH_4 in the effluents also varied among the plants and the period of observation. However, we still don't know the exact causes of this variability, especially the high range of organic load at Edenkoben WWTP and the exceptionally high values of dissolved CH_4 of the effluent of Bellehim WWTP. Our hypothesis that the spatiotemporal variability of organic load for inflow wastewater might refer to the domestic consumption patterns and to the amount of industrial wastewater included with the domestic wastewater. However, future studies should seek to identify the sources of wastewater for these plants. Further, the variability of dissolved CH_4 in effluents can be linked to the treatment conditions and operation practices as well as the amount of CH_4 in the inflow wastewater. The reasons for the variability of dissolved CH_4 in the effluents have not been studied, and further studies might seek to identify their causes to improve our understanding of the impact of WWTPs on CH_4 emissions

References

NOAA, 2015. National Centers for Environmental Information, State of the Climate: Global Analysis for September 2015, published online October 2015, retrieved on October 26, 2015 from http://www.ncdc.noaa.gov/sotc/global/201509.

Abril, G. and others 2015. Technical Note: Large overestimation of pCO2 calculated from pH and alkalinity in acidic, organic-rich freshwaters. Biogeosciences **12:** 67-78.

Abril, G. and others 2005. Carbon dioxide and methane emissions and the carbon budget of a 10-year old tropical reservoir (Petit Saut, French Guiana). Global Biogeochem. Cycles. **19:** GB4007.

Al-Ghazawi, Z., and F. Abdulla. 2008. Mitigation of methane emissions from sanitary landfills and sewage treatment plants in Jordan. Clean Techn Environ Policy **10:** 341-350.

Al-Sheriadeh, M. S., and A. Z. Al-Hamdan. 1999. Erosion risk assessment and sediment yield production of the King Talal Watershed, Jordan. Environmental Geology **37:** 234-242.

Al-Taani, A. 2013. Seasonal variations in water quality of Al-Wehda Dam north of Jordan and water suitability for irrigation in summer. Arab J Geosci **6:** 1131-1140.

Alshboul, Z., and A. Lorke. 2015. Carbon Dioxide Emissions from Reservoirs in the Lower Jordan Watershed. PLoS One **10:** e0143381.

Aufdenkampe, A. K. and others 2011. Riverine coupling of biogeochemical cycles between land, oceans, and atmosphere. Front. Ecol. Environ. **9:** 53-60.

Bade, D. L., and J. J. Cole. 2006. Impact of chemically enhanced diffusion on dissolved inorganic carbon stable isotopes in a fertilized lake. J. Geophys. Res. Oceans. **111:** C01014.

Barros, N. and others 2011. Carbon emission from hydroelectric reservoirs linked to reservoir age and latitude. Nature Geoscience **4:** 593-596.

Bastviken, D., J. Cole, M. Pace, and L. Tranvik. 2004. Methane emissions from lakes: Dependence of lake characteristics, two regional assessments, and a global estimate. Global Biogeochem. Cycles. **18:** GB4009.

Bastviken, D., I. Sundgren, S. Natchimuthu, H. Reyier, and M. Gålfalk. 2015. Technical Note: Cost-efficient approaches to measure carbon dioxide (CO2) fluxes and concentrations in terrestrial and aquatic environments using mini loggers. Biogeosciences **12:** 3849-3859.

Bastviken, D., L. J. Tranvik, J. A. Downing, P. M. Crill, and A. Enrich-Prast. 2011. Freshwater Methane Emissions Offset the Continental Carbon Sink. Science **331:** 50.

Battin, T. J., S. Luyssaert, L. A. Kaplan, A. K. Aufdenkampe, A. Richter, and L. J. Tranvik. 2009. The boundless carbon cycle. Nature Geosci **2:** 598-600.

Baulch, H. M., P. J. Dillon, R. Maranger, and S. L. Schiff. 2011. Diffusive and ebullitive transport of methane and nitrous oxide from streams: Are bubble-mediated fluxes important? J. Geophys. Res. Biogeosci. **116:** G04028.

Beaulieu, J. J., R. L. Smolenski, C. T. Nietch, A. Townsend-Small, and M. S. Elovitz. 2014. High Methane Emissions from a Midlatitude Reservoir Draining an Agricultural Watershed. Environ. Sci. Technol. **48:** 11100-11108.

Billett, M. F., and F. H. Harvey. 2013. Measurements of CO2 and CH4 evasion from UK peatland headwater streams. Biogeochemistry **114:** 165-181.

Billett, M. F., and T. R. Moore. 2008. Supersaturation and evasion of CO2 and CH4 in surface waters at Mer Bleue peatland, Canada. Hydrological Processes **22:** 2044-2054.

Borges, A. V. and others 2015. Globally significant greenhouse-gas emissions from African inland waters. Nature Geosci **8:** 637-642.

Boylen, C. W., and T. D. Brock. 1973. Bacterial decomposition processes in Lake Wingra sediments during winter. Limnol. Oceanogr. **18:** 628-634.

Butman, D., and P. A. Raymond. 2011. Significant efflux of carbon dioxide from streams and rivers in the United States. Nature Geoscience **4:** 839-842.

Campeau, A., and P. A. Del Giorgio. 2014. Patterns in CH4 and CO2 concentrations across boreal rivers: Major drivers and implications for fluvial greenhouse emissions under climate change scenarios. Glob Chang Biol **20:** 1075-1088.

Casper, P., S. Maberly, G. Hall, and B. Finlay. 2000. Fluxes of methane and carbon dioxide from a small productive lake to the atmosphere. Biogeochemistry **49:** 1-19.

Cole, J. J., D. L. Bade, D. Bastviken, M. L. Pace, and M. V. D. Bogert. 2010. Multiple approaches to estimating air-water gas exchange in small lakes. Limnology and Oceanography-methods **8:** 285-293.

Cole, J. J., N. F. Caraco, G. W. Kling, and T. K. Kratz. 1994. Carbon dioxide supersaturation in the surface waters of lakes. Science **265:** 1568-1570.

Cole, J. J., J. J. Cole, N. F. Caraco, and N. F. Caraco. 2001. Carbon in catchments: connecting terrestrial carbon losses with aquatic metabolism. Marine and Freshwater Research **52:** 101-110.

Cole, J. J. and others 2007. Plumbing the Global Carbon Cycle: Integrating Inland Waters into the Terrestrial Carbon Budget. Ecosystems **10:** 172-185.

Crawford, J. T. and others 2014a. CO2 and CH4 emissions from streams in a lake-rich landscape: Patterns, controls, and regional significance. Global Biogeochem. Cycles. **28:** 197-210.

Crawford, J. T., E. H. Stanley, S. A. Spawn, J. C. Finlay, L. C. Loken, and R. G. Striegl. 2014b. Ebullitive methane emissions from oxygenated wetland streams. Global Change Biol. **20:** 3408-3422.

Crusius, J., and R. Wanninkhof. 2003. Gas transfer velocities measured at low wind speed over a lake. Limnol. Oceanogr. **48:** 1010-1017.

Curry, C. L. 2007. Modeling the soil consumption of atmospheric methane at the global scale. Global Biogeochem. Cycles. **21:** n/a-n/a.

Czepiel, P., P. Crill, and R. Harriss. 1995. Nitrous Oxide Emissions from Municipal Wastewater Treatment. Environ. Sci. Technol. **29:** 2352-2356.

Czepiel, P. M., P. M. Crill, and R. C. Harriss. 1993. Methane emissions from municipal wastewater treatment processes. Environ. Sci. Technol. **27:** 2472-2477.

Daelman, M. R. J., E. M. Van Voorthuizen, U. G. J. M. Van Dongen, E. I. P. Volcke, and M. C. M. Van Loosdrecht. 2012. Methane emission during municipal wastewater treatment. Water Res. **46:** 3657-3670.

Delsontro, T., M. J. Kunz, T. Kempter, A. Wüest, B. Wehrli, and D. B. Senn. 2011. Spatial Heterogeneity of Methane Ebullition in a Large Tropical Reservoir. Environ. Sci. Technol. **45:** 9866-9873.

Deshmukh, C. and others 2014. Physical controls on CH4 emissions from a newly flooded subtropical freshwater hydroelectric reservoir: Nam Theun 2. Biogeosciences **11:** 4251-4269.

Dickson, A. G., and F. J. Millero. 1987. A comparison of the equilibrium constants for the dissociation of carbonic acid in seawater media. Deep Sea Research Part A. Oceanographic Research Papers **34:** 1733-1743.

Dinsmore, K. and others 2013a. Contrasting CO2 concentration discharge dynamics in headwater streams: A multi-catchment comparison. J. Geophys. Res. Biogeosci. **118:** 445-461.

Dinsmore, K. J., M. F. Billett, and K. E. Dyson. 2013b. Temperature and precipitation drive temporal variability in aquatic carbon and GHG concentrations and fluxes in a peatland catchment. Glob Chang Biol **19:** 2133-2148.

Downing, J. A. and others 2006. The global abundance and size distribution of lakes, ponds, and impoundments. Limnol. Oceanogr. **51:** 2388-2397.

Duarte, C. M. and others 2008. CO2emissions from saline lakes: A global estimate of a surprisingly large flux. J. Geophys. Res. **113**.

Duc, N., P. Crill, and D. Bastviken. 2010. Implications of temperature and sediment characteristics on methane formation and oxidation in lake sediments. Biogeochemistry **100:** 185-196.

Duc, N. T., S. Silverstein, L. Lundmark, H. Reyier, P. Crill, and D. Bastviken. 2013. Automated flux chamber for investigating gas flux at water-air interfaces. Environ. Sci. Technol. **47:** 968-975.

El-Fadel, M., and M. Massoud. 2001. Methane emissions from wastewater management. Environ. Pollut. **114:** 177-185.

Evans, J. P. 2009. 21st century climate change in the Middle East. Clim. Change. **92:** 417-432.

Farber, E. and others 2004. The origin and mechanisms of salinization of the lower Jordan river. Geochim. Cosmochim. Acta **68:** 1989-2006.

Forbrich, I., L. Kutzbach, A. Hormann, and M. Wilmking. 2010. A comparison of linear and exponential regression for estimating diffusive CH4 fluxes by closed-chambers in peatlands. Soil Biol. Biochem. **42:** 507-515.

Forster, P., V. Ramaswamy, P. Artaxo, P. Artaxo, and Et Al. 2007. Changes in Atmospheric Constituents and in Radiative Forcing. *In* S. Solomon, D. Qin and M. Manning [eds.]. Cambridge University Press.

Gålfalk, M., D. Bastviken, S. Fredriksson, and L. Arneborg. 2013. Determination of the piston velocity for water-air interfaces using flux chambers, acoustic Doppler velocimetry, and IR imaging of the water surface. J. Geophys. Res.-Biogeo. **118:** 770-782.

Goldenfum, J. A. 2011. GHG measurement guidelines for freshwater reservoirs. UNESCO/IHA, London, UK.

Gudasz, C., D. Bastviken, K. Steger, K. Premke, S. Sobek, and L. J. Tranvik. 2010. Temperature-controlled organic carbon mineralization in lake sediments. Nature **466:** 478-481.

Guérin, F. and others 2007. Gas transfer velocities of CO2 and CH4 in a tropical reservoir and its river downstream. J. Mar. Syst. **66:** 161-172.

Guisasola, A., D. De Haas, J. Keller, and Z. Yuan. 2008. Methane formation in sewer systems. Water Res. **42:** 1421-1430.

Gunkel, A., and J. Lange. 2012. New Insights Into The Natural Variability of Water Resources in The Lower Jordan River Basin. Water Resour. Manage. **26:** 963-980.

Heimann, M., and M. Reichstein. 2008. Terrestrial ecosystem carbon dynamics and climate feedbacks. Nature **451:** 289-292.

Ho, D. T., F. Veron, E. Harrison, L. F. Bliven, N. Scott, and W. R. Mcgillis. 2007. The combined effect of rain and wind on air–water gas exchange: A feasibility study. J. Mar. Syst. **66:** 150-160.

Hoffmann, M. and others 2015a. Automated modeling of ecosystem CO2 fluxes based on periodic closed chamber measurements: A standardized conceptual and practical approach. Agricultural and Forest Meteorology **200:** 30-45.

Hoffmann, M. and others 2015b. Technical Note: A simple calculation algorithm to separate high-resolution CH4 flux measurements into ebullition and diffusion-derived components. Biogeosciences Discuss. **12:** 12923-12945.

Hoover, T. E., and D. C. Berkshire. 1969. Effects of hydration on carbon dioxide exchange across an air-water interface. J. Geophys. Res. **74:** 456-464.

Hope, D., S. M. Palmer, M. F. Billett, and J. J. C. Dawson. 2001. Carbon dioxide and methane evasion from a temperate peatland stream. Limnol. Oceanogr. **46:** 847-857.

Hotchkiss, E. R. and others 2015. Sources of and processes controlling CO2 emissions change with the size of streams and rivers. Nature Geosci **8:** 696-699.

Houser, J. N. 2006. Water color affects the stratification, surface temperature, heat content, and mean epilimnetic irradiance of small lakes. Can. J. Fish. Aquat. Sci. **63:** 2447-2455.

Humborg, C. and others 2010. CO2 supersaturation along the aquatic conduit in Swedish watersheds as constrained by terrestrial respiration, aquatic respiration and weathering. Global Change Biol. **16:** 1966-1978.

Huttunen, J. T. and others 2003. Fluxes of methane, carbon dioxide and nitrous oxide in boreal lakes and potential anthropogenic effects on the aquatic greenhouse gas emissions. Chemosphere **52:** 609-621.

Ipcc. 2007. The Physical Science Basis. Contribution of Working Group I to the Fourth Assessment Report of the Intergovernmental Panel on Climate Change [Solomon, S., D. Qin, M. Manning, Z. Chen, M. Marquis, K. B. Averyt, M. Tignor and H. L. Miller (eds.)]. Cambridge University Press, Cambridge, United Kingdom and New York, NY, USA, 996 pp.

---. 2013. Climate Change 2013: The Physical Science Basis. Contribution of Working Group I to the Fifth Assessment Report of the Intergovernmental Panel on Climate Change. Cambridge University Press.

Jiang, Z.-P., T. Tyrrell, D. J. Hydes, M. Dai, and S. E. Hartman. 2014. Variability of alkalinity and the alkalinity-salinity relationship in the tropical and subtropical surface ocean. Global Biogeochem. Cycles. **28:** 729-742.

Johnson, K. S. 1982. Carbon dioxide hydration and dehydration kinetics in seawater. Limnol. Oceanogr. **27:** 849-855.

Kirschke, S. and others 2013. Three decades of global methane sources and sinks. Nature Geosci **6:** 813-823.

Koskinen, M., K. Minkkinen, P. Ojanen, M. Kämäräinen, T. Laurila, and A. Lohila. 2014. Measurements of CO2 exchange with an automated chamber system throughout the year: challenges in measuring night-time respiration on porous peat soil. Biogeosciences **11:** 347-363.

Kutzbach, L. and others 2007. CO2 flux determination by closed-chamber methods can be seriously biased by inappropriate application of linear regression. Biogeosciences **4:** 1005-1025.

Lauerwald, R., G. G. Laruelle, J. Hartmann, P. Ciais, and P. a. G. Regnier. 2015. Spatial patterns in CO2 evasion from the global river network. Global Biogeochem. Cycles. **29:** 534-554.

Law, Y., G. E. Jacobsen, A. M. Smith, Z. Yuan, and P. Lant. 2013. Fossil organic carbon in wastewater and its fate in treatment plants. Water Res. **47:** 5270-5281.

Law, Y., L. Ye, Y. Pan, and Z. Yuan. 2012. Nitrous oxide emissions from wastewater treatment processes. Philosophical Transactions of the Royal Society B-Biological Sciences **367:** 1265-1277.

Lee, K. and others 2006. Global relationships of total alkalinity with salinity and temperature in surface waters of the world's oceans. Geophys. Res. Lett. **33:** L19605.

López, P., R. Marcé, and J. Armengol. 2011. Net heterotrophy and CO2 evasion from a productive calcareous reservoir: Adding complexity to the metabolism-CO2 evasion issue. J. Geophys. Res. Biogeosci. **116**.

Lorke, A. and others 2015. Technical note: drifting versus anchored flux chambers for measuring greenhouse gas emissions from running waters. Biogeosciences **12:** 7013-7024.

Lorke, A., and F. Peeters. 2006. Toward a unified scaling relation for interfacial fluxes. J. Phys. Oceanogr. **36:** 955-961.

Macintyre, S., R. Wanninkhof, and J. P. Chanton. 1995. Trace gas exchange across the air-water interface in freshwater and coastal marine environments. *In* P. A. Matson and R. C. Harriss [eds.], Measuring Emissions from Soil and Water. Blackwell Science Ltd.

Maeck, A. and others 2013. Sediment trapping by dams creates methane emission hot spots. Environ. Sci. Technol. **47:** 8130-8137.

Maeck, A., H. Hofmann, and A. Lorke. 2014. Pumping methane out of aquatic sediments – ebullition forcing mechanisms in an impounded river. Biogeosciences **11:** 2925-2938.

Mcdonald, C. P., E. G. Stets, R. G. Striegl, and D. Butman. 2013. Inorganic carbon loading as a primary driver of dissolved carbon dioxide concentrations in the lakes and reservoirs of the contiguous United States. Global Biogeochem. Cycles.**:** 1-11.

Millero, F. J., K. Lee, and M. Roche. 1998. Distribution of alkalinity in the surface waters of the major oceans. Mar. Chem. **60:** 111-130.

Mitchell, J. F. B. 1989. The “Greenhouse” effect and climate change. Rev. Geophys. **27:** 115-139.

Morales-Pineda, M., A. Cózar, I. Laiz, B. Úbeda, and J. Á. Gálvez. 2014. Daily, biweekly, and seasonal temporal scales of pCO2 variability in two stratified Mediterranean reservoirs. J. Geophys. Res. Biogeosci. **119:** 509-520.

Nakano, T., T. Sawamoto, T. Morishita, G. Inoue, and R. Hatano. 2004. A comparison of regression methods for estimating soil–atmosphere diffusion gas fluxes by a closed-chamber technique. Soil Biol. Biochem. **36:** 107-113.

Natchimuthu, S., B. Panneer Selvam, and D. Bastviken. 2014. Influence of weather variables on methane and carbon dioxide flux from a shallow pond. Biogeochemistry **119:** 403-413.

Natchimuthu, S. and others 2015. Spatio-temporal variability of lake CH_4 fluxes and its influence on annual whole lake emission estimates. Limnol. Oceanogr.**:** n/a-n/a.

Panneer Selvam, B., S. Natchimuthu, L. Arunachalam, and D. Bastviken. 2014. Methane and carbon dioxide emissions from inland waters in India – implications for large scale greenhouse gas balances. Global Change Biol.**:** n/a-n/a.

Parkhurst, D. L., and C. Appelo. 2013. Description of input and examples for PHREEQC version 3—A computer program for speciation, batch-reaction, one-dimensional transport, and inverse geochemical calculations. U.S. Geological Survey Techniques and Methods.

Pirk, N., M. Mastepanov, F. J. W. Parmentier, M. Lund, P. Crill, and T. R. Christensen. 2015. Calculations of automatic chamber flux measurements of methane and carbon dioxide using short time series of concentrations. Biogeosciences Discuss. **12:** 14593-14617.

Prairie, Y. T., and P. A. Del Giorgio. 2013. A new pathway of freshwater methane emissions and the putative importance of microbubbles. Inland Waters **3:** 311-320.

Raymond, P. A. and others 2013. Global carbon dioxide emissions from inland waters. Nature **503:** 355-359.

Raymond, P. A. and others 2012. Scaling the gas transfer velocity and hydraulic geometry in streams and small rivers. Limnology & Oceanography: Fluids & Environments **2:** 41-53.

Read, J. S. and others 2012. Lake-size dependency of wind shear and convection as controls on gas exchange. Geophys. Res. Lett. **39:** L09405.

Regnier, P. and others 2013. Anthropogenic perturbation of the carbon fluxes from land to ocean. Nature Geosci **6:** 597-607.

Richey, J. E., A. H. Devol, S. C. Wofsy, R. Victoria, and M. N. G. Riberio. 1988. Biogenic gases and the oxidation and reduction of carbon in Amazon River and floodplain waters. Limnol. Oceanogr. **33:** 551-561.

Riederer, M., A. Serafimovich, and T. Foken. 2014. Net ecosystem CO2 exchange measurements by the closed chamber method and the eddy covariance technique and their dependence on atmospheric conditions. Atmos. Meas. Tech. **7:** 1057-1064.

Roehm, C. L., Y. T. Prairie, and P. A. Del Giorgio. 2009. The pCO2 dynamics in lakes in the boreal region of northern Québec, Canada. Global Biogeochem. Cycles. **23:** GB3013.

Saadoun, I., E. Bataineh, and I. Al-Handal, Y,. 2008a. The Primary Production Conditions of Wadi Al-Arab Dam (Reservoir). Jordan J. Biol. Sci. **1:** 67-72.

Saadoun, I., E. Bataineh, and A. Alhandal. 2008b. Phytoplankton Species Composition and Seasonal Variation at Wadi Al-Arab Dam Lake, Jordan. Turkish J. Biol. **32:** 291-298.

Saadoun, I., E. Batayneh, A. Alhandal, and M. Hindieh. 2010. Physicochemical features of Wadi Al-Arab Dam (reservoir), Jordan. Oceanol. Hydrobiol. Stud. **39:** 189-203.

Sarmiento, J. L., and E. T. Sundquist. 1992. Revised budget for the oceanic uptake of anthropogenic carbon dioxide. Nature **356:** 589-593.

Schladow, S. G., M. Lee, B. E. Hürzeler, and P. B. Kelly. 2002. Oxygen transfer across the air-water interface by natural convection in lakes. Limnol. Oceanogr. **47:** 1394-1404.

Shatanawi, M., and M. Fayyad. 1996. Effect of Khirbet As-Samra treated effluent on the quality of irrigation water in the Central Jordan Valley. Water Res. **30:** 2915-2920.

Silva, J. P., A. Lasso, H. J. Lubberding, M. R. Peña, and H. J. Gijzen. 2015. Biases in greenhouse gases static chambers measurements in stabilization ponds: Comparison of flux estimation using linear and non-linear models. Atmos. Environ. **109:** 130-138.

St. Louis, V. L., C. A. Kelly, É. Duchemin, J. W. M. Rudd, and D. M. Rosenberg. 2000. Reservoir Surfaces as Sources of Greenhouse Gases to the Atmosphere: A Global Estimate. Bioscience **50:** 766-775.

Teodoru, C., Y. Prairie, and P. Del Giorgio. 2011. Spatial Heterogeneity of Surface CO2 Fluxes in a Newly Created Eastmain-1 Reservoir in Northern Quebec, Canada. Ecosystems **14:** 28-46.

Teodoru, C. R. and others 2012. The net carbon footprint of a newly created boreal hydroelectric reservoir. Global Biogeochem. Cycles. **26**.

Teodoru, C. R., F. C. Nyoni, A. V. Borges, F. Darchambeau, I. Nyambe, and S. Bouillon. 2015. Dynamics of greenhouse gases (CO2, CH4, N2O) along the Zambezi River and major tributaries, and their importance in the riverine carbon budget. Biogeosciences **12:** 2431-2453.

Tortajada, C., D. Altinbilek, and A. K. Biswas. 2012. Impacts of Large Dams: A Global Assessment, 1 ed. Springer.

Tranvik, L. J. and others 2009. Lakes and reservoirs as regulators of carbon cycling and climate. Limnol. Oceanogr. **54:** 2298-2314.

Vachon, D., Y. T. Prairie, and J. J. Cole. 2010. The relationship between near-surface turbulence and gas transfer velocity in freshwater systems and its implications for floating chamber measurements of gas exchange. Limnol. Oceanogr. **55:** 1723-1732.

Varadharajan, C., R. Hermosillo, and H. F. Hemond. 2010. A low-cost automated trap to measure bubbling gas fluxes. Limnol. Oceanogr. Meth. **8:** 363-375.

Von Schiller, D. and others 2014. Carbon dioxide emissions from dry watercourses. Inland Waters **4:** 377-382.

Wanninkhof, and L. F. Bliven. 1991. Relationship between gas exchange, wind speed, and radar backscatter in a large wind-wave tank. J. Geophys. Res. Oceans. **96:** 2785-2796.

Wanninkhof, and M. Knox. 1996. Chemical enhancement of CO2 exchange in natural waters. Limnol. Oceanogr. **41:** 689-697.

Wanninkhof, R. 1992. Relationship between wind speed and gas exchange over the ocean. J. Geophys. Res. **97:** 7373.

Wanninkhof, R., and W. R. Mcgillis. 1999. A cubic relationship between air-sea CO2 exchange and wind speed. Geophys. Res. Lett. **26:** 1889-1892.

Wik, M., P. M. Crill, R. K. Varner, and D. Bastviken. 2013. Multiyear measurements of ebullitive methane flux from three subarctic lakes. J. Geophys. Res. Biogeosci. **118:** 1307-1321.

Wik, M., B. F. Thornton, D. Bastviken, S. Macintyre, R. K. Varner, and P. M. Crill. 2014. Energy input is primary controller of methane bubbling in subarctic lakes. Geophys. Res. Lett.**:** 2013GL058510.

Wilcock, R., and B. Sorrell. 2008. Emissions of Greenhouse Gases CH4 and N2O from Low-gradient Streams in Agriculturally Developed Catchments. Water, Air, Soil Pollut. **188:** 155-170.

Wilkinson, J., A. Maeck, Z. Alshboul, and A. Lorke. 2015. Continuous Seasonal River Ebullition Measurements Linked to Sediment Methane Formation. Environ. Sci. Technol. **49:** 13121-13129.

Williamson, C. E., W. Dodds, T. K. Kratz, and M. A. Palmer. 2008. Lakes and streams as sentinels of environmental change in terrestrial and atmospheric processes. Front. Ecol. Environ. **6:** 247-254.

Yvon-Durocher, G. and others 2014. Methane fluxes show consistent temperature dependence across microbial to ecosystem scales. Nature **507:** 488-491.

Zappa, C. J., P. A. Raymond, E. A. Terray, and W. R. Mcgillis. 2003. Variation in Surface Turbulence and the Gas Transfer Velocity over a Tidal Cycle in a Macro-Tidal Estuary. Estuaries **26:** 1401-1415.

Zeikus, J. G., and M. R. Winfrey. 1976. Temperature limitation of methanogenesis in aquatic sediments. Appl. Environ. Microbiol. **31:** 99-107.

Zhuang, Q. and others 2004. Methane fluxes between terrestrial ecosystems and the atmosphere at northern high latitudes during the past century: A retrospective analysis with a process-based biogeochemistry model. Global Biogeochem. Cycles. **18:** GB3010.

Resume

ZEYAD ALSHBOUL

Oct. 1982 Irbid-Jordan

Zeyad@uni-landau.de

Education

2012-2015

PhD candidate: Environmental physics - Institute for Environmental Sciences - University of Koblenz-Landau - Germany

2011-2012

Research fellowship - Water Resources and Environment - TU-Braunschweig- Germany

2008-2011

M.Sc. of Water Resources and Environment: Institute of Earth and Environmental Sciences -Al al-Bayt University - Jordan.

2001-2005

B.Sc. of Physics: Department of physics – Faculty of Science - Al al-Bayt University - Jordan

1990-2001

Alshajara high school – Irbid – Jordan

Carriers

2006-2010

Operator and Supervisor (water and wastewater treatment plants - Ministry of Water and Irrigation - Jordan

2010-2011

Desalination and water treatment unit assistant - Ministry of Water and Irrigation – Jordan

List of publications

Alshboul, Z., and A. Lorke. 2015. Carbon Dioxide Emissions from Reservoirs in the Lower Jordan Watershed. PLoS One 10: e0143381. (Published in **Plos One**)

Alshboul, Zeyad, Fernández, Jorge, Hofmann, Hilmar, Lorke, Andreas, Export of dissolved methane and carbon dioxide with effluents from municipal wastewater treatment plants, Environmental science and technology, 2015. (Under review in **Environmental Science and Technology**)

Alshboul, Zeyad, Celia Somlai-Haase, Christoph Bors, Andreas Lorke, Simple approaches to measure the diffusive flux of carbon dioxide and the rate of bubble release in shallow aquatic systems, Limnology and Oceanography, 2015. (Submitted in **Limnology and Oceanography-Methods**)

Lorke, A., Bodmer, P., Noss, C., **Alshboul, Z.,** Koschorreck, M., Somlai, C., Bastviken, D., Flury, S., McGinnis, D. F., Maeck, A., Müller, D., and Premke, K.: Technical Note: Drifting vs. anchored flux chambers for measuring greenhouse gas

emissions from running waters, Biogeosciences Discuss., 12, 14619-14645, doi:10.5194/bgd-12-14619-2015, 2015. (Published in journal of **Biogeoscince**)

Jeremy Wilkinson, Andreas Maeck, **Zeyad Alshboul**, and Andreas Lorke, Continuous Seasonal River Ebullition Measurements Linked to Sediment Methane Formation, *Environmental Science & Technology*, DOI: 10.1021/acs.est.5b01525. (Published in **Environmental Science and Technology**)

Selected talks

Alshboul, Z; Celia Somlai; Christoph Bors; Lorke, A; Methane ebullition from small streams affected by the effluent of municipal wastewater treatment plants, Symposium for European Freshwater Sciences 2015, 5-10 July; Geneva, Switzerland.

Alshboul, Z; Lorke,A; Carbon dioxide and methane exported to streams from municipal wastewater treatment plants, ASLO 2015, 22-27 Feb., Granada, Spain.

Poster presentations

Alshboul, Z; Noss, C; Lorke, A; Drifting versus static chambers for measuring air-water gas fluxes in running waters, 18th workshop on physical processes in natural waters (PPNW 2015), 2015, 24-28 Aug., Landau, Germany.

Acknowledgement

First and foremost, I have to thank God for being my strength and guide in handling the PhD. Without the support of God I would not have the wisdom and the physical ability to do so. I would like to take this opportunity to thank my parents, sisters and brothers for their support.

I would like to gratefully acknowledge the guidance, support and encouragement of my doctoral advisor, Andreas Lorke. I am grateful for the trust you put in me and the freedom you granted me. I am grateful for your patience, motivation and enthusiasm; you have been a tremendous mentor for me.

I thank Prof. Hermann Jungkunst for his support during the investigation of nitrous oxide emissions from wastewater treatment plants. I thank him for his patience since the data are still not analyzed. But I promise him to procced with the analysis soon!. Andreas Mäck, you were a friend and teacher at the same time, and I would like to thank you for the support during the first months of my PhD. I would like to thank you that you directed me to Andreas Lorke, this has changed my life totally. I will forever be thankful to my former colleague Celia for her support, I have learned a lot from her. I will not forget her and her husband when they saved my life when I stuck in an elevator. I thank Christian Noss for his support and help. He helped me a lot during the fund extension applications and helped strongly to procced with the manuscript of '' Static vs. anchored……''. I would like also to thank Angelika Holderle for her help while staying in Landau and for her administrative support.

I would like to thank Christoph Bors for his help during the field campaigns and technical support. He did a great job during the instrumentation development and we were able to measure CO_2 flux in a continuous time series. This was big job and he prepared a professional

instrumentation manual, which set the basis for the third manuscript. I would also like to thank Lalith for his support during the difficult times of my PhD. For their support during the data analysis for the manuscript '' Export of methane…'', I would like to thank Hilmar Hofmann and Jorge Fernández. I would like to thank the Ministry of Water and Irrigation - Jordan for providing data and information.

I would like to thank Martin Schulte and Valerie Münch for their support. They were as a brother and sister and I can't imagine Landau without them. Many thanks to Azzaya, Bruno, Erni, Florian, Jeremy Wilkinson, Kaan Koca, Liu Liu, Lorenz Fahse, Julika Kreling, Pavel Ondruch and Sebastian Geissler. They were my colleagues and friends in the same time. Our working group was a big family and we had a great time together. Thank you all! I would like to thank the people in the Environmental and Soil Chemistry Group for their help during samples analysis.

At the end, I would like to thank the German Academic Exchange Service (DAAD) and the Sustainable Water Management Program (NaWaM) for the Fund (Grant number: A/12/91768).

Appendixes

Table of content

Table of Contents

Appendix A - Chapter 4

Simple approaches to measure the diffusive flux of carbon dioxide and the rate of bubble release in shallow aquatic systems.

Zeyad Alshboul,,[⊥] Celia Somlai-Haase,[⊥] Christoph Bors,[⊥] Andreas Lorke*[⊥]

*zeyad@uni-landau.de

[⊥]University of Koblenz-Landau, Institute for Environmental Sciences, Fortstr.7, 76829 Landau, Germany

Author contribution

Alshboul, Zeyad: Data analysis – Experimental part and field measurement – Writing the manuscript

Submitted to Limnology and Oceanography - Methods, 2016, under review.

A.1. Automated flux chamber

A.1.1. Hardware

The chamber consisted of three main parts: control unit, floating chamber and CO_2 logger ((Bastviken et al. 2015) , Figure A-1). The control unit consisted of an air pump, a battery and microcontroller board (MB) (Figure A-2). An additional tube connector was attached to the top of the chamber body and connected to the outlet of the air pump (Figure A-3). The air was pumped through the tube and vented the headspace zone of the chamber using Tygon® tube (R-3603, inner diameter 3.2 mm, outer diameter 6.4 mm). The housings of the CO_2 logger and the battery were fixed beneath the chamber body using two plastic screws sealed with a rubber.

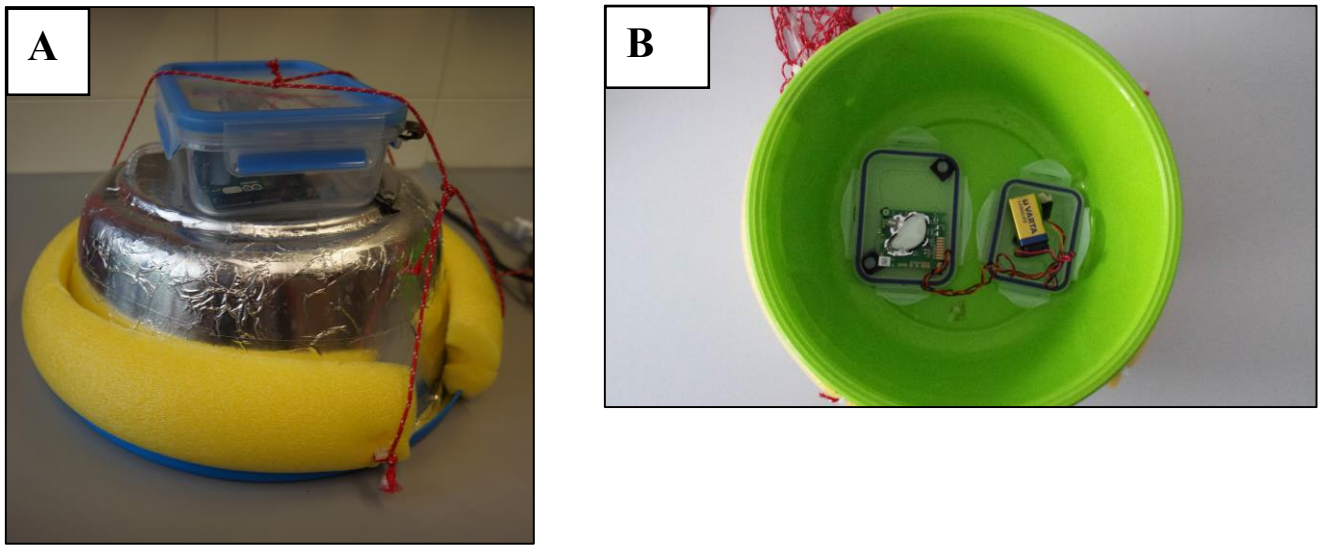

Figure A-1. A) Floating chamber with the attached control unit on the top of the chamber body, B). CO_2 logger and the battery are attached to the chamber body.

A.1.2. Housing

Three different waterproof plastic housings were used for the CO_2 logger, the battery and the control unit housing (more information on the battery and the CO_2 logger assembly can be found in Bastviken et al. (2015)). The housing of the control unit was attached to the top of the chamber body by using the opposite site of the same screws that has been used for CO_2 logger. Two separate holes were drilled in the housing walls, and tube connectors were attached to and glued in the holes. The attached connectors were used for the inlet and the outlet ports of the air pump and connected through two separate tygon tubes.

A.1.3. Energy

Two alkaline batteries (9V, 6LR61) were connected to the CO_2 logger, which provide sufficient energy to operate the logger for seven days. All other electric parts (Arduino microcontroller and the air pump) were powered with a 12 V lead battery (68 Ah at 20 °C, GIVC 12-65, Banner batteries). The whole pump-setup used 1.4 A current with the pump running, 0.6A without running (5 minutes venting and 60 minutes measuring intervals provide a duty-cycle of a week).

A.1.4. Microcontroller Board

A digital input/output port (IO 13) of the "*Arduino Uno R*3" microcontroller board (produced by Arduino) was used to switch the pump (Figure A-2).

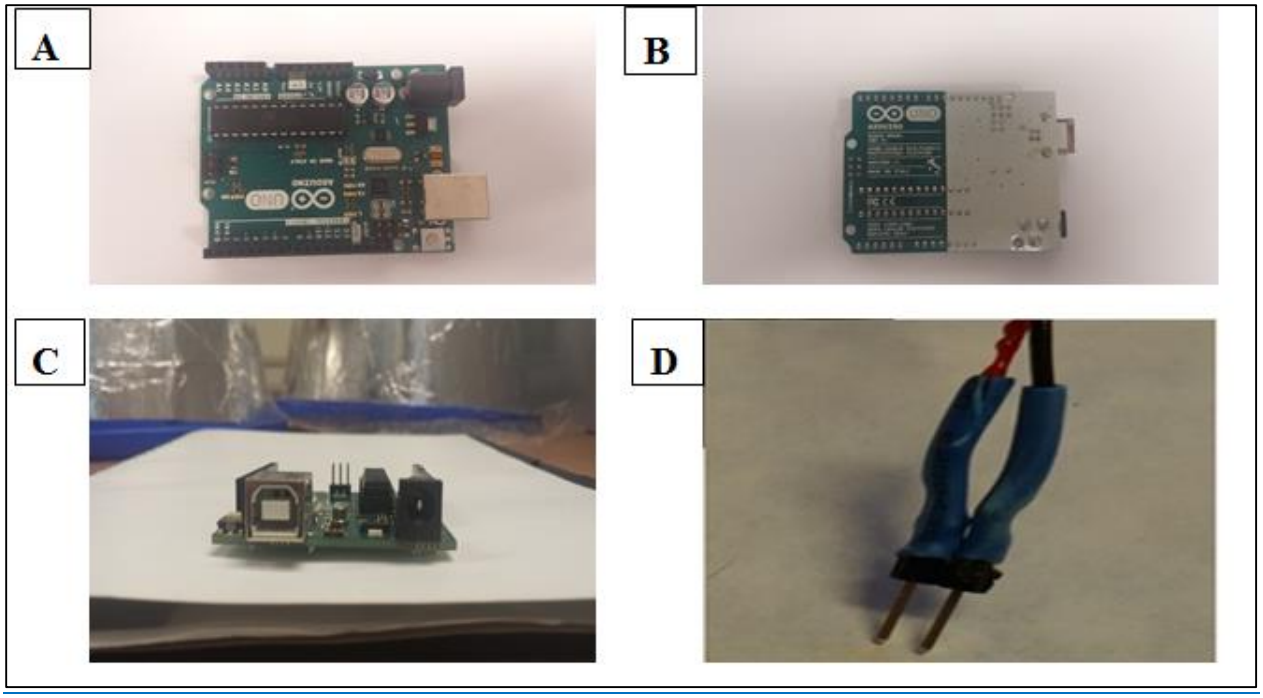

Figure A-2. A-C) the MB *"Arduino Uno R3",* D) Plug connecting pump to Arduino.

A.1.5. Air Pump

The air pump is a diaphragm pump (Thomas Membrane pump Serie 3013) of 1.2 l min^{-1} and it can be operated with a 12 V battery. The approximate time interval of the venting process for the specific headspace volume of the chamber (~6 l) was 5 minutes. A print relay (Print-Relais 5VDC, Series 36, Finder) connected the air pump to the MB.

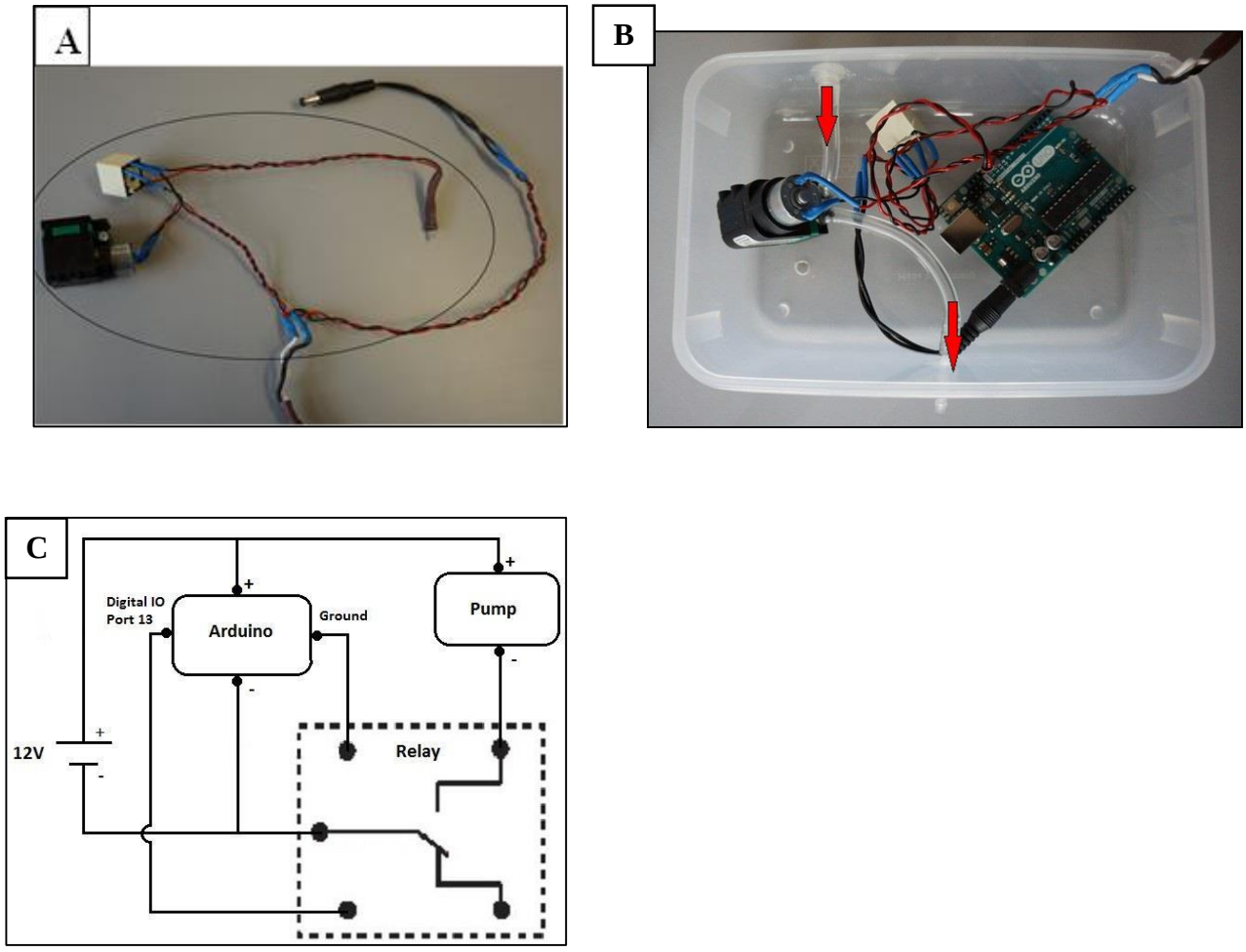

Figure A-3. A) Relay, pump and cable header of the AFC. B) All parts shown in A, the Arduino board and tubes arranged in the water –proof housing. The red arrows represent the flow directions of the air, C) Wiring diagram of the connected pins with the MB, dashed box showing the relay.

Table. A-1. List of parts, which are used for the AFC construction. The table shows the specification of the parts, recommended assembly procedures and the expected price range (2015).

Part	Specification	Assembly	price
Pump housing	17.5 cm x 11.5 cm x 5 cm	Drilling, Gluing	~5 €
Air pump	Thomas diaphragm pump 1.2 l min^{-1} with 12 V, 3.6 W	Soldering	~75 €
Microcontroller model	Arduino Uno R3, 13.2 W pumping, 0.6 W not pumping	Soldering a plug as shown in Figure A-2	~25 €
Relay (Print-Relais 5VDC, Series 36, Finder)	5 V print-relay	Soldering as shown in Figure A-3	~0.90 €
Tube	~0.5m, tygon (ID:3.2, OD: 6.2)	Pushing on connectors	~1.5 €
DC-Plug	2.1 mm ID, 5.5 mm OD	Soldering	~0.50 €
Tube connectors	3.2-4.2 mm/3.2-4.2 mm	Gluing in	~0.5 €
One-way Valve	Tetra CV 4 Rückschlagventil	Pushing on connector	~3 €

A1.6. Software

Two separated types of user interface software were used to operate the CO_2 logger and the MB. The CO_2 logger was operated and programed using the free software UIP5, which is available on the website of the manufacturer (www.senseair.se). The software was updated immediately after installation from **Help/check for updates** menu. The serial port was selected from **Meter/connection configuration** menu (this is likely to be COM3 or higher) and the **Modbus** box was checked. (See detailed information in Bastviken et al. (2015)). The start sleep and log period were fixed from the **logger** menu to be 5 s and 300 s, respectively. The UIP5 allows the users to start and stop the CO_2 logger, as well as export the data to the connected

Laptop. The data are stored in a text file, which includes date/time, status, type, CO_2 (ppm), temperature (^oC) and relative humidity (%). The UIP5 allows the user to reset the date/time and synchronize the CO_2 logger with the connected computer.

The MB was programmed and operated with the open-source software (*ARDUINO* 1.6.5), which can be downloaded from the manufacturer website (https://www.arduino.cc/en/Main/Software). The software was updated immediately after installation and the Arduino board model was selected from **Tools/Board** menu. The standard USB cable (A plug to B plug) was provided by the manufactures and was used to connect the computer with the MB. The USB cable can also be used as an external power supply. The drivers of the MB and the USB cable were installed by following the manufacture guideline (https://www.arduino.cc/en/Guide/Windows). The serial port of the Arduino was selected from **Tools/port** menu, and this is likely to be COM3 or higher (Figure A-4 and Figure A-5). The script to the MB was uploaded from the **upload** button of the Arduino 1.6.5 and the RX/TX LEDs on the board was flushing. The Arduino 1.6.5 provides the status of the board and ‘’*uploading message*’’ appears in the status bar after a successful upload process. (See also Table A-1),

The following script was used to operate the AFC:

```
%setting the venting interval in ms
const int vent = 300000;
%setting the measurement interval in ms
const int measure = 3600000;
void setup() {
pinMode(13, OUTPUT);
%switch pump with pin13
digitalWrite( 13, LOW );
}
void loop() {
digitalWrite( 13, High );
%pump on
delay(vent);
digitalWrite( 13, LOW );
%pump off
delay(measure);
}
    }
```

The venting-time (ms) (Figure A-5 A) is set by the integer constant “vent”; the duration of the flux measurement period by the constant “measure” (ms). The script was compiled, approved and uploaded by the software to the board (Figure A-5 B). The storage capacity information appeared on the software interface. To start the program on the board, you can either connect the battery, or press the reset button. You will then see the ON LED is on and the L LED blinking 3 times. This L LED stays on, if the pump is running.

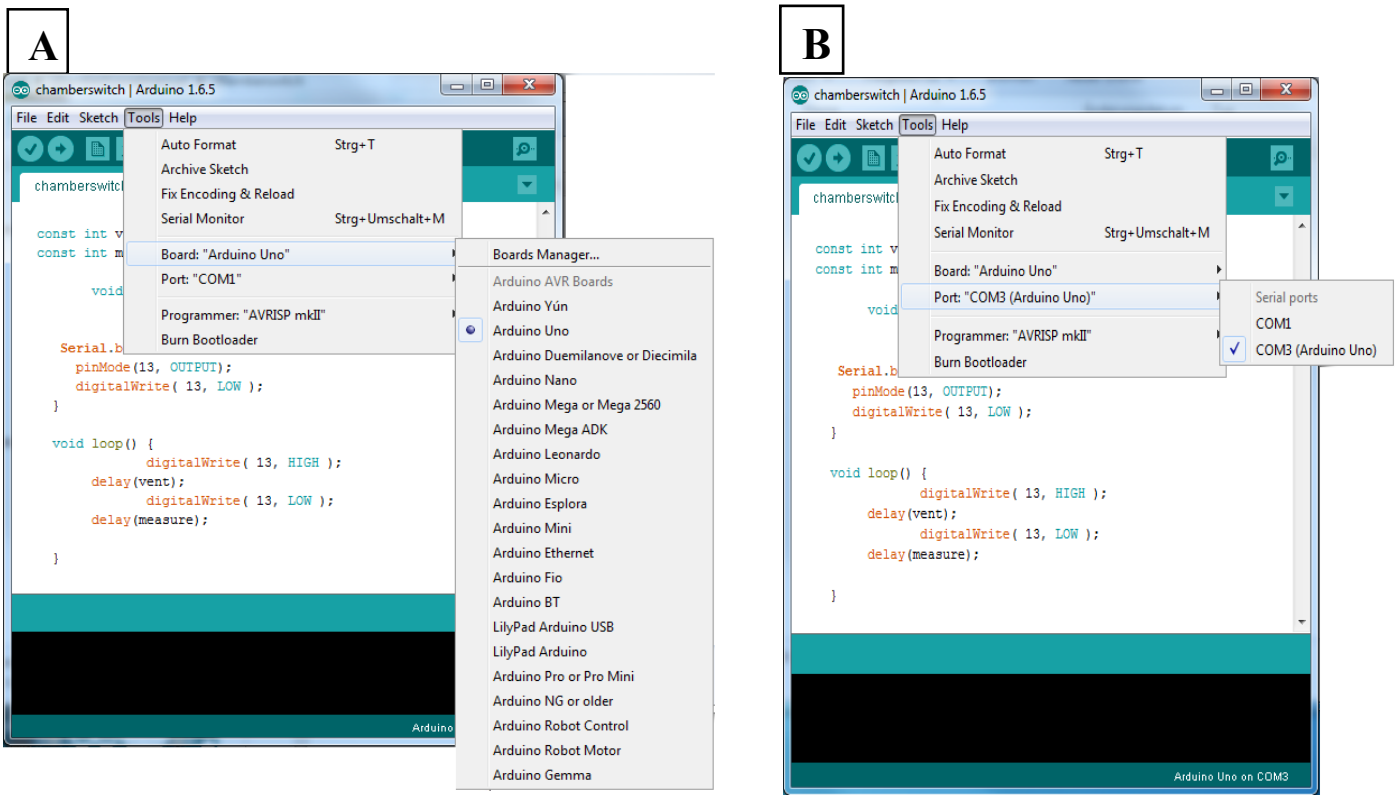

Figure A-4. A) Changing the used board: Tools->Board, B) Changing the COM-Port: Tools->Port.

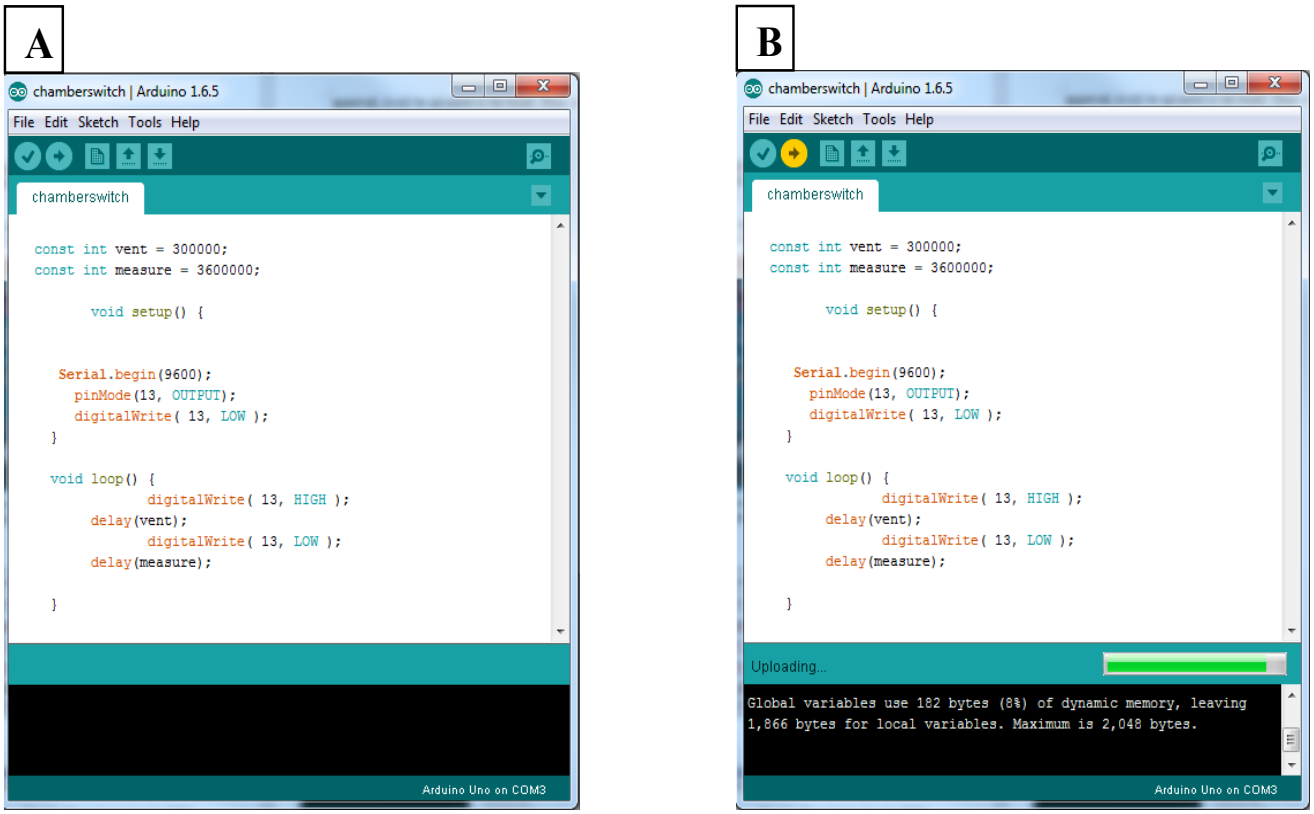

Figure A-5. A) You can set any time for flushing in milliseconds. Here 5 minutes venting time and 60 minutes measuring time is used. B) uploading the script: Upload.

A.2. Bubble traps: design and assembly

A.2.1. Design and assembly

Two designs were used for the bubble traps (BT), which differed by the transparency of the material that was used (Figure A-6). Both of the designs were narrowed at the top, and a tube connector was attached to the top of the BT body. The bottom surface areas of both designs were geometrically identical. Both designs were attached to a plastic/metal frame and a gasbag, which were protected by a plastic bucket (23 l). The frames of both designs were attached with cable ties to weights, in order to pound the BT into the substrate of the pond.

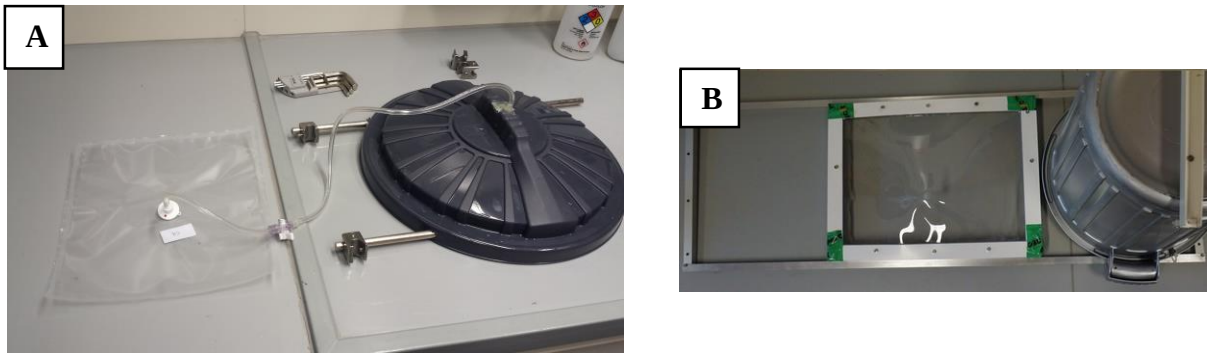

***Figure* A-6.** *Assembled A) Non-transparent bubble trap and B) Transparent bubble trap.*

A.2.2. Non-transparent bubble trap (NTBT)

The NTBT is made of polypropylene material that is available on the market, and the gas bag was attached and covered by the bucket in order to avoid overheating (Figure A-7 A). The gas bag was attached to the BT body through the tube connector (Figure A-7 B). The tube connector was attached and secured with the BT body using glue, and the test of the resistance of the glue against water and the tension during the deployment is recommended.

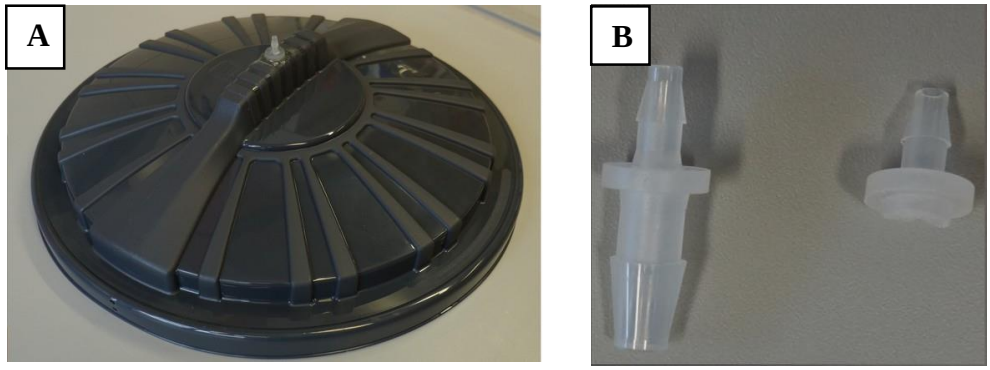

Figure A-7. A) NTF. B) Original connector (left) and connector cut to be glued in (right).

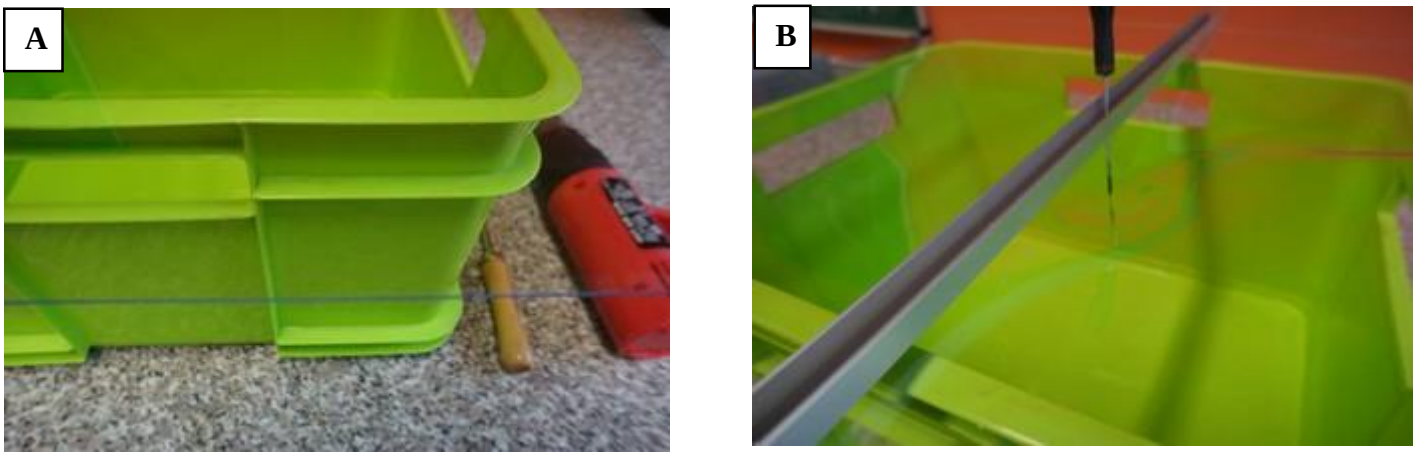

Figure A-8. A) Placement of the acrylic sheet. B) Measuring the funnel height during the heating process.

Figure A-9. Assembled TBT, edges are sealed with gas-tight tape

A.2.3. Transparent bubble trap (TBT)

The TBT was made of acrylic glass. Hot air gun, a rectangular-box plastic mold, an acrylic sheet and plastic L-profile frames to create the edges, were used. The acrylic-sheet was placed on the mold (the green box), so that 10 cm on each side were overlapping (Figure A-8). The acrylic sheet was heated using hot air and pressed down into the middle until there was a funnel shape with 3 cm height.

The BT body of (width 30 mm× length 3 0 mm) was cut out using an electric saw, and the cut residues was eliminated using sand papers. This process was performed after several minutes of cooling. A plastic L-Profile frame (30 mm×30 mm) was attached to the side of the TBT (Figure A-9). The edges were welded and sealed off with a gas-tight and waterproof tape, and the gaps between the profiles and the acrylic-sheet were filled with acrylic glue (Acrifix).

A.2.4. Frame and accessories

Four aluminum/plastic-profiles were used for frame formation and were attached to the squared bottom of BT of 1 m×0.3 m. The NTBT was connected to a similar frame. The plastic body of the BT was fixed in the middle of the frame aligned to the frame for preventing any movement during the deployment period resulted from external pressure e.g. water flow.

A.2.5. Tubing/gasbag

The gasbag of 1.5 l (Gallendrainagebeutel, pfm medical) equipped with male Luer-Lock was connected to the BT through a Tygon tube. The bag was placed in the bucket, so it was floating on the water surface, and therefore was always above the highest point of the BT.

A.2.6. Bucket

The gasbag was positioned and protected using a plastic bucket, which was attached to the BT frame. The plastic was coated with aluminum paint to avoid overheating of the trapped gas. The gas bag was accessible from the bottom of the bucket that was opened and equipped with a plastic handle. The plastic handle was fixed to the bucket body using two screws and cable ties (Figure A-10).

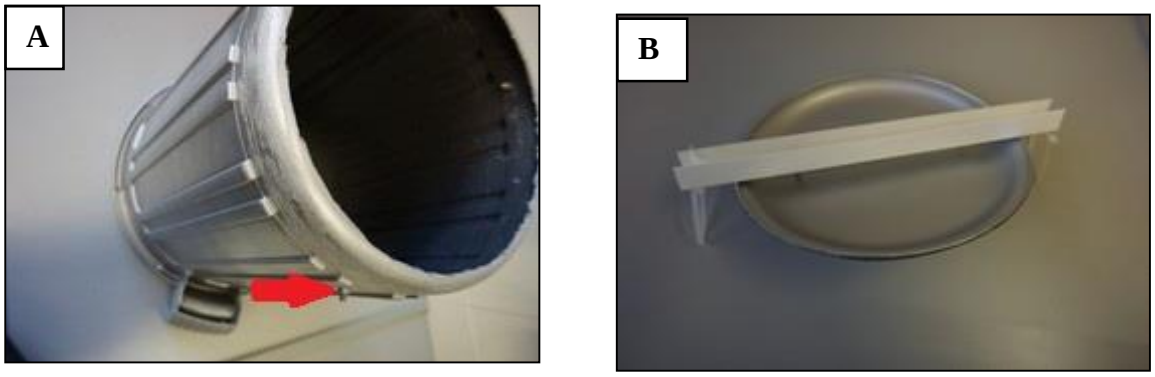

Figure A-10. A) bucket, bottom cut open and spray-painted. Pointed is one of the screws, to hold the lid. B) Assembled lid of the bucket. Note the handle with holes for cable ties.

Table A-2. The part specifications of the BT (2015).

Part	**Specification**	**Assembly**	**Price**
bucket	23 l	Cut the bottom with a multi-tools set	~10 €
frame		Screw to a square	~10 €
screws	M4	Save with a nut	~1 €
Polystyrene sheet	500 x 400 x 2 mm	Process as shown above	~10 €
Tube	~0.5 m, gas tight	Push over connector	~1.5 €
Connector	3.2-4.2 mm/ 6.4-7.4 mm	Cut, glue in place	~0.50 €
gasbag	1.5 l, gas tight	Connect to BT	~5 €

B.2.7. Installation and deployment

The BT was gently pounded into the substrate by attaching them with two weights, which were attached at ends of the frame. The evacuated gasbag was connected to the BT and was placed under plastic bucket. The plastic bucket was closed and secured.

Appendix B – Chapter 4

Simple approaches to measure the diffusive flux of carbon dioxide and the rate of bubble release in shallow aquatic systems.

Zeyad Alshboul,,[⊥] Celia Somlai-Haase,[⊥] Christoph Bors,[⊥] Andreas Lorke*[⊥]

*zeyad@uni-landau.de

[⊥]University of Koblenz-Landau, Institute for Environmental Sciences, Fortstr.7, 76829 Landau, Germany

Author contribution

Alshboul, Zeyad: Data analysis – Experimental part and field measurement – Writing the manuscript

Submitted to Limnology and Oceanography - Methods, 2016, under review.

B.1. Figures and supplement subsections

B.1.1 Dissolved CH_4 and CO_2 versus temperature

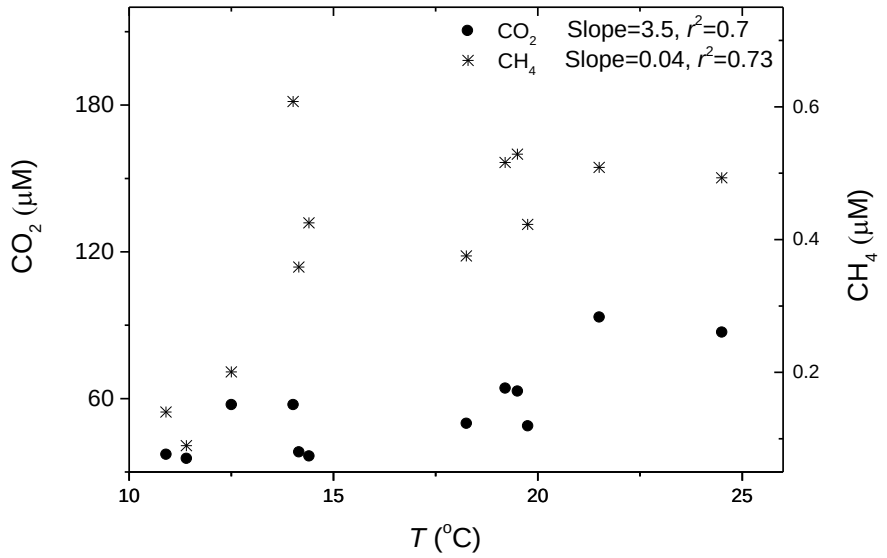

Figure B-1. Relationship between water temperature and the dissolved concentrations of CH_4 (stars) and CO_2 (black) of Log.1 and Log.2.

B.1.2. Transparency and water temperature

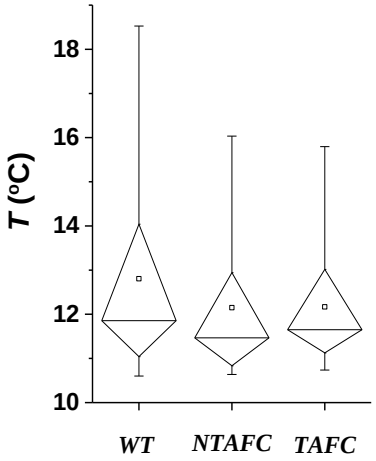

Figure B-2. Comparison of water temperature measured below the unobstructed water surface (WT) with measured water temperature beneath the non-transparent chamber (NTAFC) and beneath the transparent chamber (TAFC). Diamond-shaped boxes show the 25 and 75 percentile range and the whiskers extend this range by a factor of 1.5.

References

Bastviken, D., I. Sundgren, S. Natchimuthu, H. Reyier, and M. Gålfalk. 2015. Technical Note: Cost-efficient approaches to measure carbon dioxide (CO2) fluxes and concentrations in terrestrial and aquatic environments using mini loggers. Biogeosciences **12:** 3849-3859.